FINAL REPORT FOR THE PERIOD

3-1-96 to 8-31-99

AN ULTRASONIC TECHNIQUE TO DETERMINE
THE RESIDUAL STRENGTH OF ADHESIVE BONDS

GRANT NUMBER NAG 1 1813

Prepared by J. D. Achenbach and Z. Tang

Center for Quality Engineering and Failure Prevention
Northwestern University
2137 N. Sheridan Road
Evanston, IL 60208-3020

Telephone: 847-491-5527
Fax: 847-491-5227
e-mail: achenbach@nwu.edu

Submitted to
NASA Langley
Dr. W. P. Winfree, LaRC Technical Officer

April 4, 2000

Page intentionally left blank

ABSTRACT

An Ultrasonic Technique to determine the Residual Strength of Adhesive Bonds

J. D. Achenbach and Zhenzeng Tang

In this work, ultrasonic techniques to nondestructively evaluate adhesive bond degradation have been studied. The key to the present approach is the introduction of an external factor which pulls the adhesive bond in the nonlinear range, simultaneously with the application of an ultrasonic technique.

With the aid of an external static tensile loading, a superimposed longitudinal wave has been used to obtain the slopes of the stress-strain curve of an adhesive bond at a series of load levels. The critical load, at which a reduction of the slope is detected by the superimposed longitudinal wave, is an indication of the onset of nonlinear behavior of the adhesive bond, and therefore of bond degradation. This approach has been applied to the detection of adhesive bond degradation induced by cyclic fatigue loading.

Analogously to the longitudinal wave case, a superimposed shear wave has been used to obtain the effective shear modulus of adhesive layers at different shear load levels. The onset of the nonlinear behavior of an adhesive bond under shear loading has been detected by the use of a superimposed shear wave. Experiments show that a longitudinal wave can also detect the nonlinear behavior when an adhesive bond is subjected to shear loading. An optimal combination of ultrasonic testing and mechanical loading methods for the detection of degradation related nonlinear

behavior of adhesive bonds has been discussed.

For the purpose of a practical application, an ultrasonic technique that uses a temperature increase as an alternative to static loading has also been investigated. A general strain-temperature correspondence principle that relates a mechanical strain to a temperature has been presented. Explicit strain-temperature correspondence relations for both the tension and shear cases have been derived. An important parameter which quantifies the relation between the wave velocity and temperature has been defined. This parameter, which is indicative of adhesive bond nonlinearity and which can be conveniently obtained by an ultrasonic measurement, has been used as an indication of adhesive bond degradation. Experimental results have shown that the temperature increase method is a convenient and productive alternative to static loading.

A technique which uses the reflected waveform data to obtain the fundamental ultrasonic parameters (transit time, reflection coefficient and attenuation coefficient) of an adhesive bond has also been presented.

Multiple Pages Intentionally Left Blank

Contents

List of Tables

List of Figures

xvi

Chapter 1

Introduction

Adhesive bonding offers many important advantages over other joining methods such as welding, riveting, and mechanical fastening [1-4]. Some of these advantages are that adhesive bonds can 1) distributes stress more uniformly and minimizes areas of high stress concentration and, therefore permit fabrication of lighter and stronger structures, 2) reduce the fabrication cost of a structure. Thus, adhesive bonds are increasingly being used by industry to obtain stronger, lighter weight, and more durable structures. Because of these excellent qualities many adhesively bonded structures are used under critical conditions and therefore are subjected to tremendous environmental weathering and service stresses. As a consequence, some advantages turn into disadvantages. Since adhesive bonds degrade, quality control and quality assurance become more than an important issue.

This dissertation is exclusively concerned with the adhesive bond quality control issue, more specifically with ultrasonic nondestructive evaluation (NDE) of adhesive bond degradation.

1

It is well known that the strength of an adhesive bond can seriously deteriorate under in-service conditions. Such deterioration can be a consequence of adverse environmental conditions such as infiltration of moisture, or of thermal and/or cyclic loading conditions. It has proven to be difficult to obtain information on the deterioration of adhesive bond strength from NDE test results. Inadequate NDE techniques for the detection of adhesive bond degradation has somewhat limited the more widespread use of adhesive bonds in primary structures.

The nondestructive evaluation of adhesive bonds is a very old and difficult problem of long-standing importance. Indeed, the nondestructive evaluation of adhesive bond has been an issue for well over 40 years. Almost at the same time that Fokker initially applied metal bonding in its primary aircraft structures in the early 50s, the Fokker Bond Tester was introduced for measuring and quantifying the quality of bonded structures in the manufacturing process as well as for maintenance inspection. Over the last 30 years, an increasing assortment of equipment based on a variety of principles has been developed for the NDE of adhesive bonds. In 1972, a special case for a fundamental approach to NDE of adhesively bonded structures was made at a workshop held at the North American Rockwell Science Center (NARSC), Thousand Oaks, California. Based on the deliberations at the workshop, a panel from the Air Force Materials Laboratory (AFML), the National Science Foundations (NSF) and NARSC made some recommendations for fundamental approaches. Those recommendations were presented in Ref. [5]. As stated in that article, if the panel would be reconvened today, the conclusions might not be too different, since many of those recommendations are still being addressed in current research programs. Indeed, within the recent five years, an average of about 5-10

papers solely dealing with adhesive bond evaluation has been presented at the annual Review of Progress in Quantitative Nondestructive Evaluation Conference. At this meeting researchers from all over the world present their newest findings and ideas in the nondestructive evaluation area. That the NDE of adhesive bonds has continued to receive extensive attention shows that there are still many problems remained to be solved.

A fairly systematic presentation of the adhesive bond quality control concerns and currently available NDE techniques can be found in Refs. [6-7]. A more recent review of the progress in the NDE of adhesive bonds up to the early 90s has been presented in Ref. [8]. It is evident that there are still several adhesive bond imperfections that need to be nondestructively evaluated. Typical adhesive bond defects are disbonds, voids, ill-cured bonds, poor cohesion and adhesion, and strength reduction. The available NDE methods include a variety of techniques such as sonics, ultrasonics, acoustic emission, nuclear magnetic resonance, x-ray and radiography, optical holography, and thermography. Different methods have achieved different degrees of success. Ultrasonics is one of the most active and productive approaches. However, it remains a real and largely unanswered challenge to obtain information on adhesive bond strength from ultrasonic test results. It is not certain that this challenge can be met. Indeed, it is often questioned whether it is really possible to define a single parameter or a set of parameters which determines the adhesive bond strength and which can be measured by an ultrasonic technique.

A substantial amount of laboratory work has been dedicated to searching for a method that can answer this challenge. Much work has been carried out using such ultrasonic techniques as amplitude domain reflection/transmission [9-11], spectral

domain reflection/transmission [12-17], low frequency testing [18], interface waves [19-21], Lamb waves [22] leaky Lamb waves [23-25], the stress-wave factor method [26], horizontally polarized transverse waves [27], oblique incident ultrasound [28-29] and guided waves [30-31]. In these papers, it was attempted to correlate the ultrasonic results with the strength of the adhesive bond, where the latter was obtained by a destructive testing method.

To the best of our knowledge, it has, however, so far not been possible to establish a consistent correlation between ultrasonic measurement results and the adhesive bond strength. This is not surprising because ultrasonic methods generally yield stiffness and dimensional parameters. In some cases, low stiffness happens to coincide with low strength and hence ultrasonic results can be correlated with strength. This is, however, not a generally valid result, and exceptions have been found (see Chapter 4).

Generally, ultrasonic signals are very small in amplitude and they interact with a solid only in the very initial linear regime of stress-strain behavior. Thus an ultrasonic measurement basically yields the initial slope of the stress-strain curve which characterizes the material. For three stress-strain curves given in Figure 1.1, (a) represents a good bond with no deterioration, (b) and (c) represent deteriorated bonds with an increasing severity of degradation. The initial slopes of these three curves are basically the same. Therefore, without introducing an external factor which pushes the bond to a nonlinear regime, an ultrasonic measurement cannot distinguish between these three bonds which have three distinct stress-strain relations. Until now, no methods can determine the degradation for the case when the initial slope of the stress-strain curve does not characterize the bond properties.
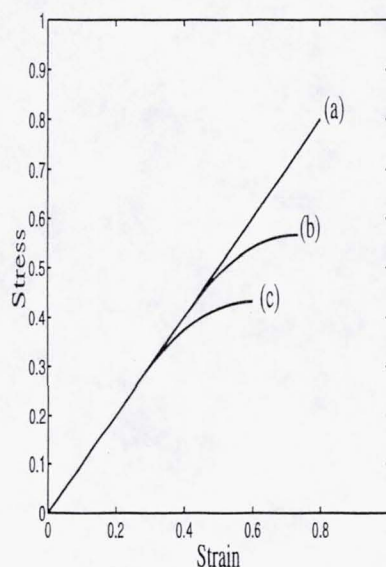
Figure 1.1: Stress-strain relation for different severities of degradation. (a), no degradation, (b), some degradation, (c), severe degradation.

The purpose of the present research was to develop a new technique which has more general applicability.

The theoretical investigations in Refs. [32,33] have shown considerable potential to attack the bond strength problem. With emphasis on the experimental aspects, the present research extends the efforts of Refs. [32,33]. The key to the current approach is the introduction of an external factor which pulls the bond in the non-linear range. A simultaneous ultrasonic test can then obtain an ultrasonic parameter which can be related to adhesive bond strength.

Chapter 2 is an extension of theoretical investigation of Ref. [32]. An external static tensile loading is introduced as the external factor. The static load is used to initiate the nonlinear response of the adhesive bonds. An ultrasonic parameter that is directly related to the local slope of the stress-strain curve of an adhesive

bond is defined. This parameter can be obtained by comparing the measured signal reflected from the adhesive bond and the simulated signal using a theoretical model developed in this chapter. The so obtained parameter is used to calculate the effective modulus of the bond at a given load. By varying the load, effective moduli can be obtained at different load levels using the ultrasonic tests. The critical load, at which a reduction of the effective modulus can be detected by an ultrasonic test, serves as an indication of the onset of the nonlinear stress-strain behavior of the adhesive bond, and therefore of bond degradation. This approach has been used to detect adhesive bond degradation induced by cyclic fatigue loading.

As an extension of Chapter 2, Chapter 3 implements an external shear loading as the external factor. A superimposed shear wave is used to obtain the effective shear modulus at a given shear load. The reduction of the effective shear modulus is an indication of nonlinear behavior of adhesive bonds under shear loading, and therefore of bond degradation. For practical reasons, a longitudinal wave approach is also explored to detect the stress-strain nonlinearity when the adhesive bond is subjected to shear loading. A comparison is given for shear wave and longitudinal wave inspection results. Results for shear and tensile loading are compared. An optimal combination of ultrasonic testing and mechanical loading method for the detection of nonlinear behavior of adhesive bonds is suggested.

After it has been experimentally verified by Chapters 2 and 3 that applying an external factor is a feasible and promising approach, Chapter 4 takes another step forward. It is shown that a temperature change can be used as the external factor to provide a convenient alternative to static loading. A strain-temperature correspondence principle is presented. This principle relates the initial slope of the

stress-strain curve at a higher temperature to the slope at a higher strain and at a reference temperature. Ultrasonic measurements at different temperatures and at small strains are used to predict the behavior of the adhesive bonds at the reference temperature and at larger strains. The stress-strain behavior in the full strain range of an adhesive bond is reconstructed, hence the strength of the adhesive bond can be obtained. By assuming explicit forms of the stress-strain relations for the tension and shear cases, the strain-temperature correspondences for tension and shear are established. Experiments have been carried out for the tension case. Results of the application of the strain-temperature correspondence principle for the tension case to the nondestructive evaluation of adhesive bond degradation generated by three-point-bending fatigue are presented.

Chapter 5 discusses a method that can accurately determine the fundamental ultrasonic parameters (transit time, reflection coefficient and attenuation coefficient) of an adhesive bond using reflected waveform data.

A brief summary of conclusions is presented in Chapter 6.

Chapter 2

Ultrasonic Evaluation of Adhesive Bond Degradation by Detection of the Onset of Nonlinear Behavior

2.1   Introduction

Reviews of progress in the nondestructive evaluation of adhesive bonds up to the early 90s can be found in Refs. [5,8]. In recent years, techniques to detect nonlinear effects related to bond degradation have received increasing attention [32-34]. Most work done so far has been of a theoretical nature. Several models have been suggested and theoretically investigated by Baik and Thompson [34]. A theoretical investigation using a spring model has been performed by Achenbach and Parikh [32]. The studies mentioned above have shown promise that the strength of adhesive bonds can be evaluated by detecting nonlinear behavior.

In some cases the strength degradation of an adhesive bond correlates with a reduction of the effective modulus of the bond, i.e., a reduction of the slope of the

8

stress-strain ($\sigma - \epsilon$) curve of the bond, where σ is the stress normal to the adhesive-adherend interface, averaged over the thickness of the adhesive layer, and ϵ is the change of the bond thickness divided by the thickness in the unloaded state. In other cases, the degradation gives rise to an early onset of the nonlinear portion of that curve with no change in slope of the linear part. The work presented here is for a class of adhesive bonds for which degradation is indicated by a reduction of the linear part of the $\sigma - \epsilon$ curve.

The reduction in the modulus is generally easier to detect since it usually results in a change of acoustic impedance contrast between adherend and adhesive. However, the adhesive layer is usually a very thin layer, around $100 \mu m$ thick, and separation of the reflected signals from the top and bottom adherend/adhesive interfaces is extremely difficult [13, 36-37]. Very high frequencies have to be used [36-37] for this separation. In order to avoid this difficulty, we view the reflected signals as a single signal replacing the thin adhesive layer by a layer of springs. The reduction of the linear part of the $\sigma - \epsilon$ curve is even more difficult to detect because direct ultrasonic measurements may not result in any distinguishable difference between a bond with this kind of degradation and one without any degradation. To bring out the presence of nonlinear behavior due to bond degradation, an external factor is introduced in this chapter.

In this chapter the external factor is a static tensile load, applied to the bond to move the bond response to the nonlinear portion of the $\sigma - \epsilon$ curve while the ultrasonic test is carried out. A theoretical model which relates the signal reflected from the bond interface to the properties of that interface has been established.

For a given load, the effective modulus of the bond can be determined using

this approach. By varying the load, effective moduli can be obtained at different load levels using the ultrasonic test results. Within the linear range, the effective modulus is a constant. Once nonlinear behavior begins, a change of the effective modulus is detected. Thus the onset of the nonlinear behavior in the stress-strain relation of the bond under investigation can be detected by the ultrasonic test. The results provide quantitative information about the degradation of the bond.

2.2   Experimental

2.2.1   Experimental setup and specimen

The configuration for the pulse-echo experiment is shown in Fig. 2.1. A Panametrics ultrasonic Pulser/Receiver (Model 5055PR) was used to excite the ultrasonic transducer and to receive the ultrasonic signals. An ultrasonic transducer with a central frequency of 5 MHz was used. The diameter of the transducer is $0.5in$. A Digital Oscilloscope (Tektronix TDS520) was employed for data acquisition. The data from the oscilloscope were acquired by a computer through a General Purpose Interface Bus (GPIB). The sampling frequency was 500 MHz.

Figure 2.2 shows the specimen for the experiments. Both adherends were aluminum cylinders with a thickness of $1.0in$. The bonding area was selected as a region with a diameter of $0.75in$. The adhesive layer was made of an epoxy resin supplied by the Dow Chemical Company. Two different kinds of adhesive layers were prepared. One kind of layer consisted of 70% DER 331, 30% DER 732. The curing agent was DEH 24, 13% in weight. The second kind was 50% DER 331, 50% DER 732 with 13% DEH24 curing agent in weight. An aluminum tube was used
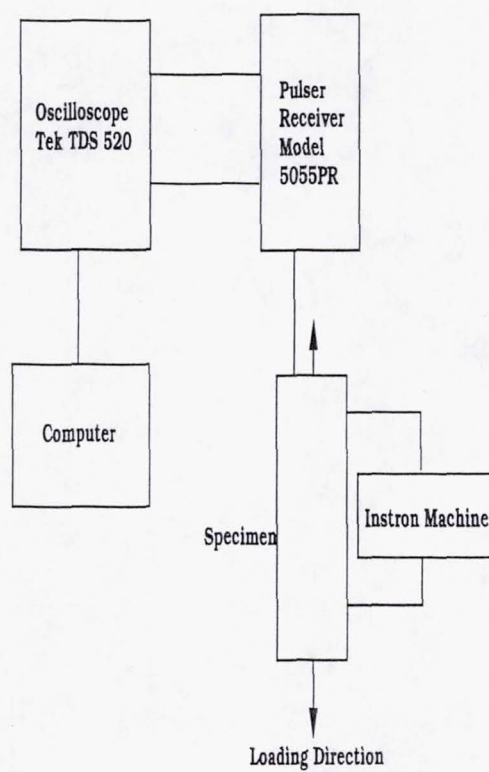
Figure 2.1: Setup of the experiment for the measurement of ultrasonic reflected signal from the adhesive bond while a static load is applied to the specimen

as a water tank and to hold the transducer. The transducer was placed inside the water-filled tube. Three evenly spaced screws were used to align the transducer to guarantee normal incidence of a longitudinal wave. The aluminum tube was connected to the bond specimen by an adhesive layer. In order to achieve acceptable interface strength for adhesive bonds, surface preparation of the adherends is required. Sulfuric acid dichromate etch [38] was used for the preparation of the bond surfaces. After assembly, the adhesive bonds were cured in vacuum. The gas released during curing was removed to eliminate debonds and porosities in the bond. The vacuum was kept at 29.5 $in \ Hg$. The layer thickness was maintained by maintaining a uniform gap between the two adherends. For all the adhesive layers that were used , the thickness was $80 \mu m$.

The purpose of the experiment was to determine the ultrasonic responses for different severities of degradation. Degradation was generated by applying increasing numbers of fatigue cycles to the specimens. The cyclic fatigue loading was applied using an Instron machine. For this study, three groups of specimens were prepared for each kind of adhesive layer. For the first group, no fatigue cycles were applied. The second group was subjected to $50k$ fatigue cycles. The third group was subjected to $100k$ cycles. The different fatigue cycles were applied to generate different severities of deterioration in the adhesive layer. The waveform for the cyclic fatigue was a sinewave centered at $-200lbs$ with an amplitude of $100lbs$ ($i.e.$ $100 - 300lbs$ compression). The frequency of the sine waveform was $2.0Hz$.

1. Adhesive
   (connection)
2. Adhesive
   (test layer)
3. Al Block
   (adherend 2)
4. Al Tube
5. Screw
6. Al Block
   (adherend 1)
7. Transducer
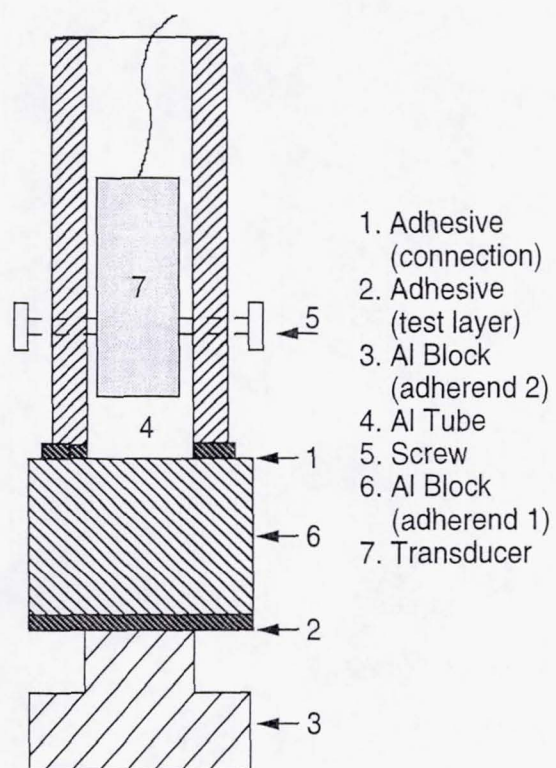
Figure 2.2: Specimen for the measurement of ultrasonic reflected signal from the adhesive bond while a static load is applied

2.2.2 Some experimental observations

Influence of degradation on the reflected signals

It has often been assumed that the degradation of the adhesive layer introduces a reduction of the modulus of the layer and therefore the reflected ultrasonic signal changes (increases) due to the acoustic impedance reduction of the layer. It has been shown that this assumption is valid for some cases. However, the experiment conducted here, revealed that this assumption does not apply for the adhesive considered in this chapter.

Ultrasonic measurements of the reflected signals were carried out for the three groups of specimens with different severities of fatigue degradation. The signals reflected from the thin adhesive bond were recorded. The experimental setup was kept strictly the same during these measurements. No detectable differences of the reflected signals were observed for these three groups of the same kind of epoxy specimen. This means that the degradation of this kind cannot be detected by an ultrasonic test without introducing loading of the specimen. Figure 2.3 is a typical comparison of the reflected signals from a fatigued specimen and a non-fatigued specimen. The specimens were 70-30 epoxy specimens. The fatigued specimen was subjected to $100k$ cycles fatigue loading. From the figure, little difference can be seen.

Influence of the static load on the reflected signals

The experiment clearly shows that a static load influences the reflected signals. For all specimens, there is a loading range in which the reflected signal remains unchanged (of course, small fluctuation may be expected). There also exists a
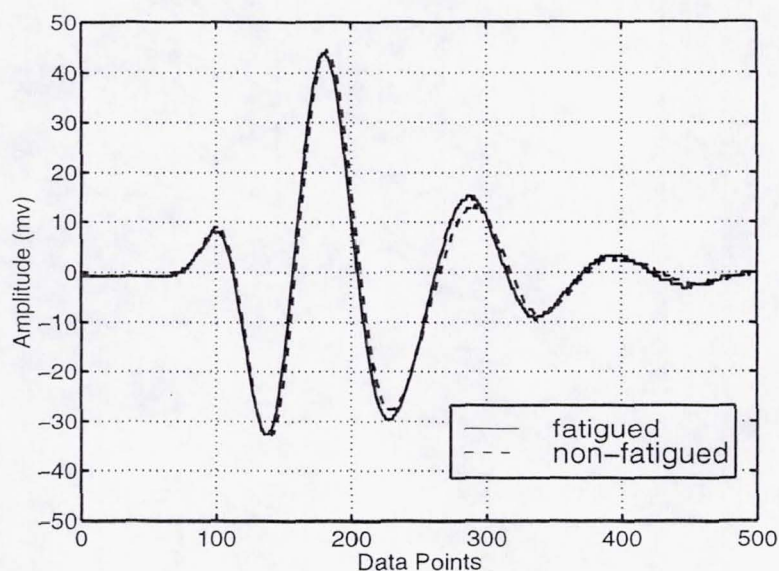
Figure 2.3: Comparison of reflected signals for fatigued and non-fatigued specimens (70-30 epoxy layer) without application of static load

critical loading point. Once the loading exceeds this point, the reflected signal shows changes. Figure 2.4 is for a 70-30 epoxy layer specimen that was not subjected to fatigue loading. It can be clearly seen that up to 1000 *lbs* load, the reflected signals are the same. For all other fatigued specimens, the situation is the same except that the critical points vary from one specimen to another (See Table 2.1). Figure 2.5 is for a 50-50 epoxy layer specimen with $100k$ fatigue cycles. It shows that the reflected signals change when the loading is increased over 200 *lbs*. As seen from this figure, at loads of 215 *lbs* and 247 *lbs*, the signals show differences from the earlier one.
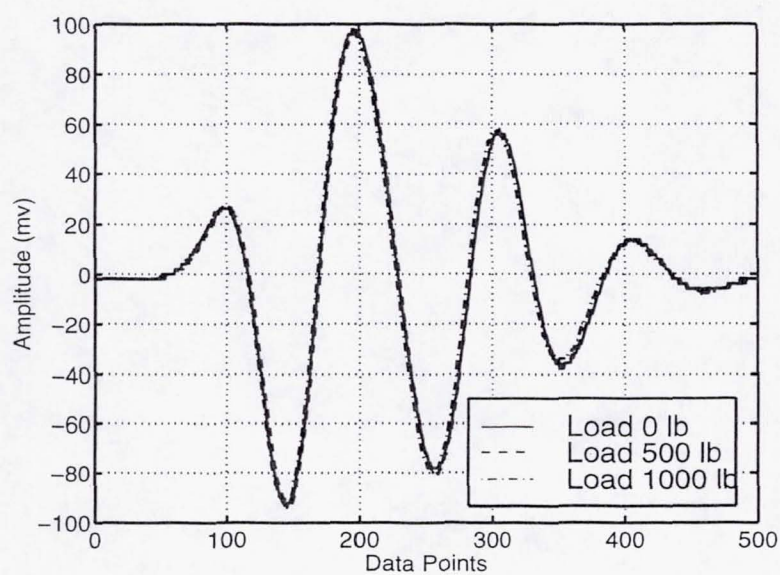
Figure 2.4: Reflected signals as the static load increases, for a specimen that has not been subjected to fatigue loading
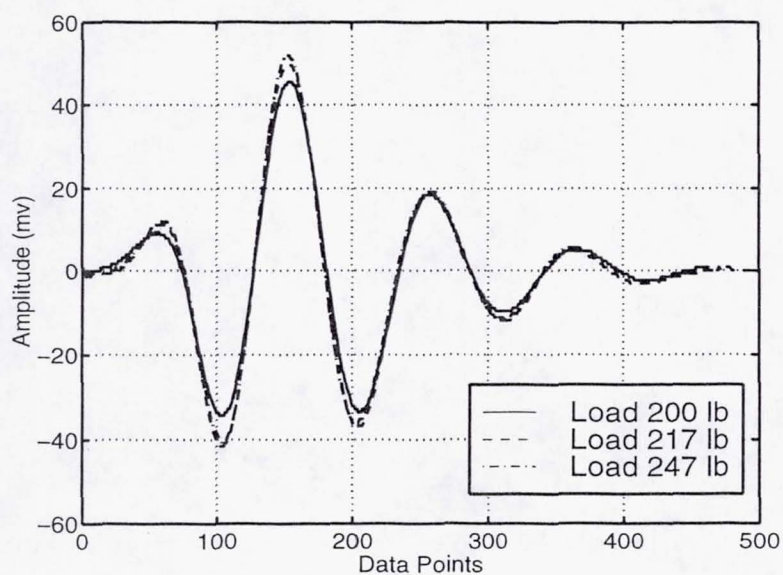
Figure 2.5: Reflected signal changes as load increases for the 50-50 epoxy bond that has been subjected to fatigue loading

Table 2.1: Critical load levels for different specimens

Epoxy Composition (DER331-DER732)	Group number	Fatigue History (k cycles)	Critical Load Level (lbs)
50-50	1	0	> 1000
	2	50	535
	3	100	215
70-30	1	0	> 1000
	2	50	853
	3	100	458

2.3   Interpretation of the experiments

2.3.1   Nonlinear behavior

The mechanical behavior of the adhesive bond is represented by a spring layer, i.e., a relation between the traction, Q, and the displacement, Δ, corresponding to the change of thickness of the adhesive layer. Figure 2.6 shows four typical $Q - \Delta$ curves with their associated failure points. Figure 2.6(a) represents a brittle bond with a linear relation between Q and Δ. When Q reaches a critical value the bond breaks in a brittle fashion. Deterioration of the bond gives rise to a lower critical value. Figure 2.6(b) shows a bond with nonlinear elastic behavior typical of rubbery adhesives. The failure point is reached for $dQ/d\Delta = 0$. Deterioration of this bond maybe described by the curves shown in figures 2.6(c) and 2.6(d). Note that in Fig. 2.6(c) the slope remains the same at $Q = 0$, while in Fig. 2.6(d) this slope changes. For the case of Fig. 2.6(d) the slope at $Q = 0$ which can be measured by traditional ultrasonic methods can be correlated with residual bond strength. This has been done by many investigators [8]. The case of Fig. 2.6(c) is more difficult

because this slope does not change at the origin.

We consider the case that the deterioration of adhesive bonds is indicated by nonlinear behavior. In this section, we will give a brief discussion on how the static load is useful in this investigation and how the ultrasonic test is involved in the nonlinear behavior study.

The application of a prestress, in the form of a traction, Q, to the bond yields a gross displacement Δ across the bond thickness. The ultrasonic signal is a stress pulse of small amplitude. Consider the traction due to the ultrasound as q and the displacement across the adhesive layer due to ultrasound as δ, the loaded specimen has a total normal stress of $Q + q$ and a total displacement of $\Delta + \delta$. Let us define a function $Q(\Delta)$ for the nonlinear elastic relation between the traction and displacement across an adhesive layer. The general behavior of the $Q(\Delta)$ curve is as shown in Fig. 2.6. The degradation of the adhesive layer can be defined as the reduction of the slope of the $Q - \Delta$ curve (Case d) or as the reduction of the linear part of the $Q - \Delta$ curve before the onset of nonlinearity (Case c).

At any local point, the slope of a $Q - \Delta$ curve is defined as $dQ/d\Delta$. Because the small disturbance generated by an ultrasonic wave produces a small stress field and a small displacement, it is possible to obtain this slope at any local point. At a local point, we can make the following linear approximation

$$\frac{dQ}{d\Delta} \approx \frac{q}{\delta} = \beta \tag{2.1}$$

In a later section, it will be shown that the parameter β can be obtained from the ultrasonic measurements. Thus, the introduction of the external load and the
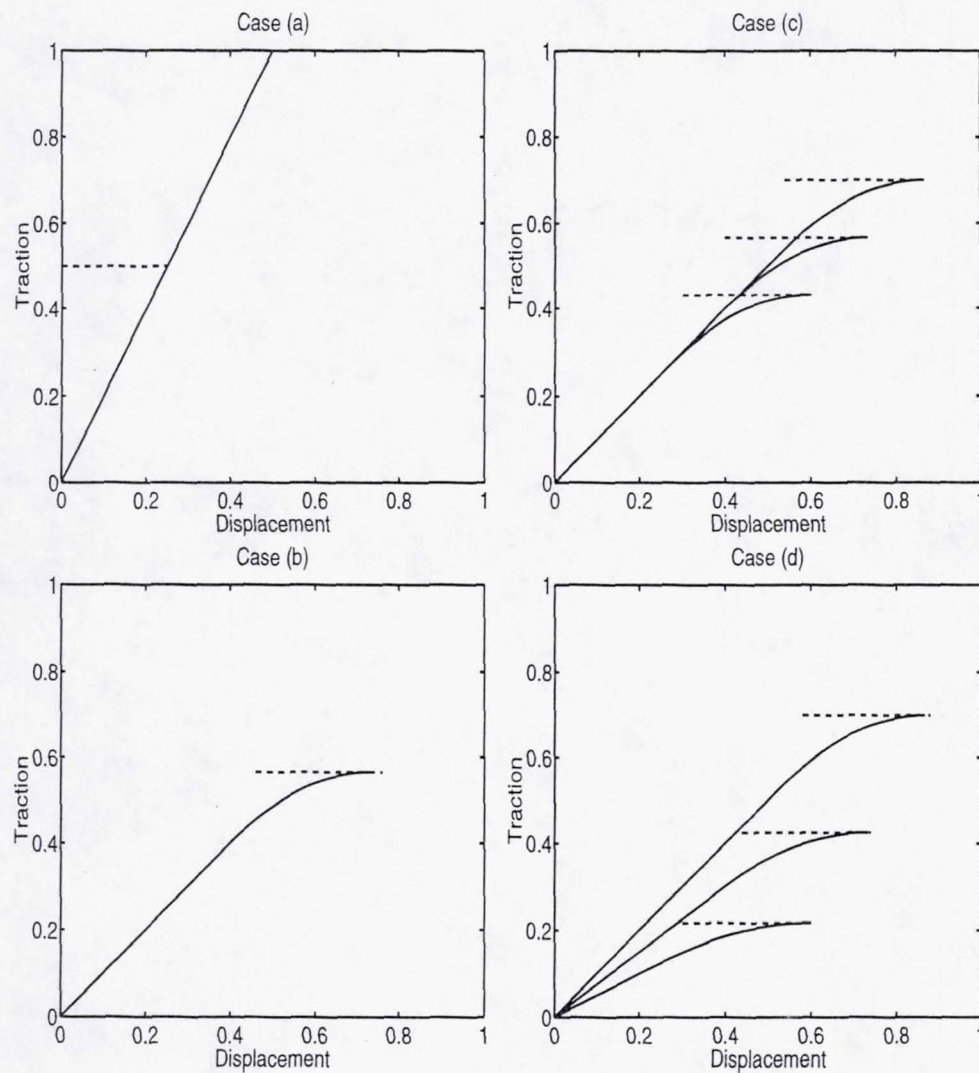
Figure 2.6: Traction-displacement curves and associated failure points (dashed lines are associated with failure points). Case (a): A brittle bond with linear elastic relation. Case (b): Nonlinear elastic behavior typical of rubbery adhesive. Case (c): The same slope at origin. Case (d): Different slopes at origin (all units are in normalized relative units)
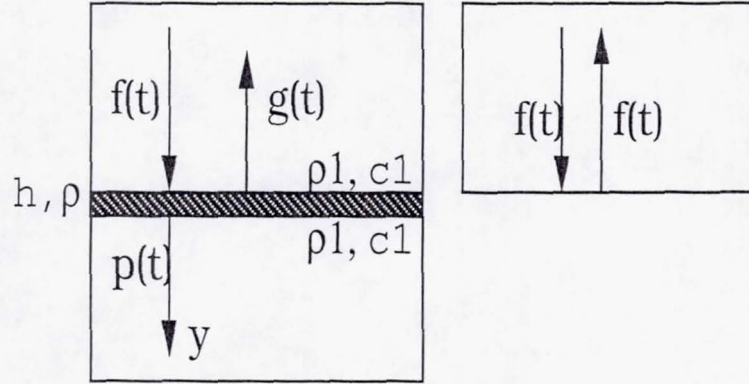
Figure 2.7: Illustration of incident and reflected wave motions (Left: incident wave $f(t)$, reflected wave $g(t)$, transmitted wave $p(t)$. Right: incident wave $f(t)$ is totally reflected at a free interface)

small ultrasonic disturbance can yield the information of the local slope of the $Q - \Delta$ curve.

2.3.2 Correlating the incident signal with the reflected signal

The theoretical investigation of Ref. [32], which assumes that the adhesive bond has been pulled in the nonlinear range by a static prestress, uses a spring model to relate the incident signal and the reflected signal.

Let us consider a special case for the spring model (Fig. 2.7), in which the adherends are the same material. At the bond surface, $y = 0$, the following conditions are satisfied

$$\sigma_y|_{y=0+} - \sigma_y|_{y=0-} = \frac{1}{2}\rho h[\ddot{v}|_{y=0+} + \ddot{v}|_{y=0-}] \tag{2.2}$$

$$\sigma_y^0 = \frac{1}{2}[\sigma_y|_{y=0+} + \sigma_y|_{y=0-}] \tag{2.3}$$

$$\delta = v|_{y=0+} - v|_{y=0-} \tag{2.4}$$

where ρ, h are the mass density and thickness of the layer, σ_y is the normal stress, v is the displacement in the y direction, σ_y^0 is the average stress across the layer and δ is the gross displacement across the layer.

It is assumed that the bond is prestressed and that for a small perturbation introduced by an ultrasonic signal, a linear elastic equation holds between the superposed traction and the superposed displacement across the adhesive layer, $i.e.$,

$$\sigma_y^0 = q = \beta\delta \tag{2.5}$$

where β is a constant, namely the local slope of the nonlinear elastic relation.

If a plane harmonic longitudinal wave is incident from $y < 0$, we can write the general forms of the incident $[v^I(y,t)]$, reflected $[v^R(y,t)]$ and transmitted $[v^T(y,t)]$ displacement signals as follows

$$v^I(y,t) = f(t - y/c_1) = Fe^{i(\omega t - ky)} \tag{2.6}$$

$$v^R(y,t) = g(t + y/c_1) = Ge^{i(\omega t + ky)} \tag{2.7}$$

$$v^T(y,t) = p(t - y/c_1) = Pe^{i(\omega t - ky)} \tag{2.8}$$

where c_1 is the wave velocity of the adherends, ω is the angular frequency of the harmonic wave, k is the wavenumber.

In terms of above defined displacement expressions, the interface conditions in the displacements and stresses follow from Eqs. 2.2-2.8 as

$$v|_{y=0+} = p(t) = Pe^{i\omega t} \tag{2.9}$$

$$v|_{y=0-} = f(t) + g(t) = (F + G)e^{i\omega t} \tag{2.10}$$

$$\sigma_y|_{y=0+} = -\rho_1 c_1 \dot{p}(t) = -\rho_1 c_1 i\omega Pe^{i\omega t} \tag{2.11}$$

$$\sigma_y|_{y=0^-} = -\rho_1 c_1 [\dot{f}(t) - \dot{g}(t)] = -\rho_1 c_1 i\omega [F - G]e^{i\omega t} \tag{2.12}$$

$$\delta = (P - F - G)e^{i\omega t} \tag{2.13}$$

By using the above relations, and equation 2.2, we find

$$\rho_1 c_1 i\omega [P - F + G] = \frac{1}{2}\rho h \omega^2 [P + F + G] \tag{2.14}$$

By using Eqs. 2.3 and 2.5, we can obtain

$$-\rho_1 c_1 i\omega [P + F - G] = 2\beta(P - F - G) \tag{2.15}$$

In order to simplify the expressions, we define

$$\beta_0 = \frac{\rho_1^2 c_1^2}{\frac{1}{2}\rho h}; \tag{2.16}$$

$$\omega_0 = \frac{\rho_1 c_1}{\frac{1}{2}\rho h} \tag{2.17}$$

where

$$\beta = \gamma \beta_0 \tag{2.18}$$

$$\omega = \bar{\omega}\omega_0 \tag{2.19}$$

By using the above simplifications, we obtain from Eqs.2.14 and 2.15

$$\rho_1 c_1 i(P - F + G) = \frac{1}{2}\rho h \bar{\omega}\frac{\rho_1 c_1}{\frac{1}{2}\rho h}(P + F + G) \tag{2.20}$$

$$-\rho_1 c_1 i\bar{\omega}\frac{\rho_1 c_1}{\frac{1}{2}\rho h}(P + F - G) = 2\gamma\frac{2\rho_1^2 c_1^2}{\rho h}(P - F + G) \tag{2.21}$$

Eqs. 2.20 and 2.21 can be further simplified as

$$P - F + G = -i\bar{\omega}(P + F + G) \tag{2.22}$$

$$-i\bar{\omega}(P + F - G) = 2\gamma(P - F - G) \tag{2.23}$$

The elimination of P in the previous system of equations yields

$$G = H(\omega)F = (\frac{i\bar{\omega}}{i\bar{\omega} + 2\gamma} - \frac{i\bar{\omega}}{i\bar{\omega} + 1})F \qquad (2.24)$$

where $H(\omega)$ can be viewed as the transfer function relating input F and output G.

If we define the Fourier Transform of $f(t)$ as $F(\omega)$, the simulated reflected signal g^s can be written as

$$g^s(t) = \int_{-\infty}^{\infty} H(\omega)F(\omega)e^{-i\omega t}d\omega \qquad (2.25)$$

2.3.3 Inverse problem formulation

The desired parameter γ, defined by Eq. 2.18, is the solution of an inverse problem. The inverse problem is as follows: For a known incident signal $f(t)$, Equation 2.25 can be used to simulate a reflected signal $g^s(t)$ for a fixed parameter γ. If we define an error function as

$$Error(\gamma) = \sum_{t=0}^{t=T}(g(t) - g^s(t,\gamma))^2 \qquad (2.26)$$

where T is the duration of the measured reflected signal $g(t)$, we can determine the best value of the parameter γ by minimizing the error function. The parameter γ represents the adhesive layer property that is to be determined.

To simulate $g^s(t)$, we need to know the incident signal $f(t)$. By virtue of near 100% reflection at an aluminum-air interface, the reflected signal from the aluminum-air interface was used as incident signal $f(t)$. The measured signal $g(t)$ was the actual signal reflected from the bond (Fig. 2.7). The measured signals can be directly used for the calculation. An identical specimen without the adhesive layer and the bottom adherend was prepared for the incident signal measurement.
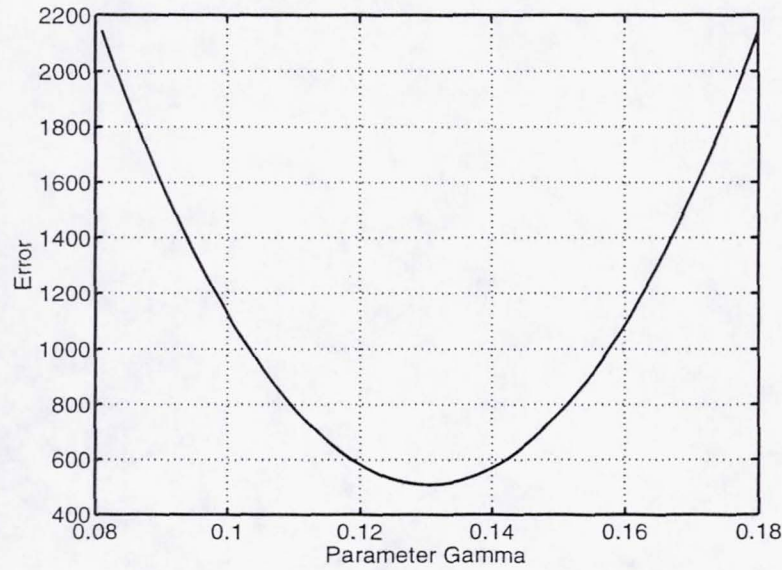
Figure 2.8: Error function for the 50-50 epoxy layer simulation (Parameter γ is defined in Eq. 2.18. Error function is defined in Eq. 2.26)

In order to verify the theoretical model and the inverse problem, some tests were done on the bonded specimen without external load. The model was tested on the two different adhesive layers mentioned above. The parameter γ was obtained as 0.0129 and 0.0156 for the 50-50 and the 70-30 epoxy layers, respectively. Figure 2.8 shows the error function vs. the parameter γ for the $50-50$ adhesive layer. Figure 2.9 shows the simulated signal $g^s(t)$ and the measured signal $g(t)$ for the best parameter γ for the $50-50$ adhesive bond. From Fig. 2.8, it can be seen that the error increases as the parameter deviates from the best fit parameter. From the comparison of the simulated and measured signals (Fig. 2.9), it is noted that good agreement between these measured and simulated signals has been achieved.

From Eq. 2.5, it is straightforward to define an effective modulus M_{eff} as

$$M_{eff} = \beta h = \gamma \beta_0 h = 2\rho_1^2 c_1^2 \gamma / \rho \tag{2.27}$$
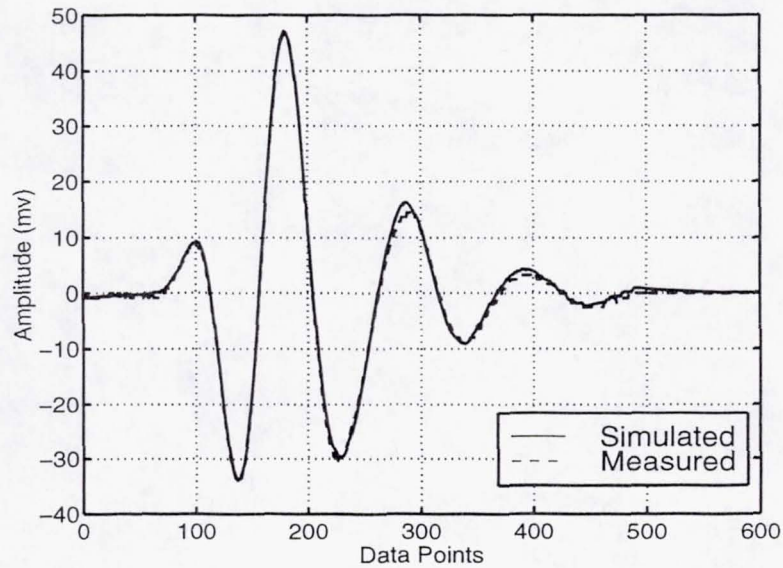
Figure 2.9: Comparison of simulated and measured signals for the 50-50 epoxy layer

In this manner, the inverse scheme yields effective moduli of 6.83 GPa and 8.04 GPa for the 50-50 and the 70-30 epoxy layers, respectively.

The velocities and densities of these two different layers were also measured using samples of the adhesive materials. The velocities were obtained as $2.42km/s$ and $2.65km/s$ for the 50-50 and the 70-30 epoxy layers, respectively. The densities were obtained as $1.11g/cm^3$ and $1.14g/cm^3$ for the 50-50 and the 70-30 epoxy layers, respectively. Using the standard relation $\lambda + 2\mu = \rho c^2$, the elastic constant $\lambda + 2\mu$, where λ and μ are Lame's elastic constants, was obtained as $6.50GPa$ and $8.01GPa$ respectively, which are values very close to the measured results. Table 2.2 shows the comparison.

Even though we have obtained very good results for calculating the effective modulus of the adhesive layer using our model, it should be pointed out that in Equation 2.2 h has to be very small for this equation to hold. This point has also

Table 2.2: Comparisons of Lame's elastic constant $(\lambda + 2\mu)$ and the calculated effective modulus (M_{eff})

Epoxy Composition (DER331-DER732)	Density (g/cm^3)	Velocity (km/s)	$\lambda + 2\mu$ (GPa)	M_{eff} (GPa)
50-50	1.11	2.42	6.50	6.83
70-30	1.14	2.65	8.01	8.04

been discussed in [34]. For our case, the thickness of the adhesive was $80\mu m$ while the wavelength λ was roughly $500\mu m$. Our approach did not account for propagation of the signal in the adhesive layer, and the actual time separation of signals reflected from the front and back interfaces of the adhesive layer was neglected. To do this we should have $\lambda/h > 6$ or even larger.

From this section it can concluded that the theoretical model can reliably calculate the effective modulus.

2.3.4 Results and discussion

To study the nonlinear behavior, a tensile load was applied to the bonded specimen. The loading direction is specified in Fig. 2.1. The static tensile loading was applied through an Instron machine just prior to ultrasonic testing. The ends of the specimen shown in Fig. 2.2 were clamped in the machine.

For the $50 - 50$ epoxy bond, the reflected signal kept very steady except for a
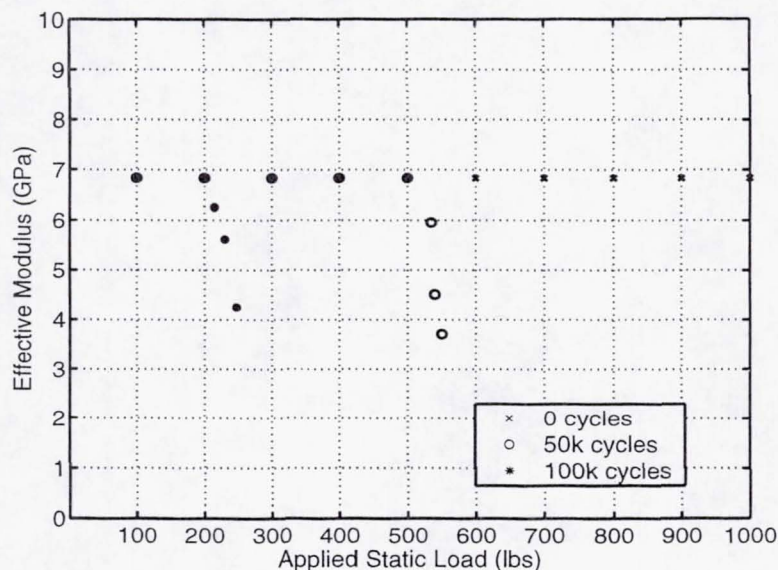
Figure 2.10: Effective modulus vs. applied static load for the 50-50 Epoxy Layer

very small fluctuation, less than 1%, when a static load up to 1000 lbs was applied to the non-fatigued specimen. This means that the effective modulus has not changed because the $\sigma - \epsilon$ curve is still in the linear range. However, for the $50k$ cycles fatigued specimen, a clearly detectable change in the reflected signal can be seen once the load exceed 500 lbs. This means that the nonlinear part has been reached. For the $100k$ cycles fatigued specimen, the nonlinearity happens earlier, namely, at 200 lbs.

Figure 2.10 shows the calculated effective moduli vs. the applied load. Figure 2.11 is the reconstruction of the stress-strain relation for the $50 - 50$ epoxy bonds.

For the $70 - 30$ epoxy bond, the results are of the same form as the $50 - 50$ epoxy bond, but the critical load level where nonlinear behavior starts is higher. Figure 2.12 shows the effective moduli vs. the applied load. Figure 2.13 is the
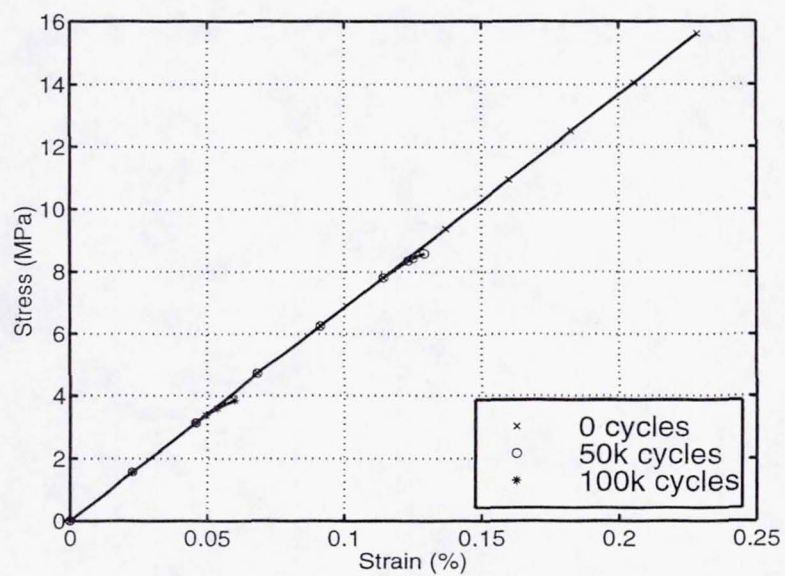
Figure 2.11: Reconstructed stress-strain relation for the 50-50 epoxy layer
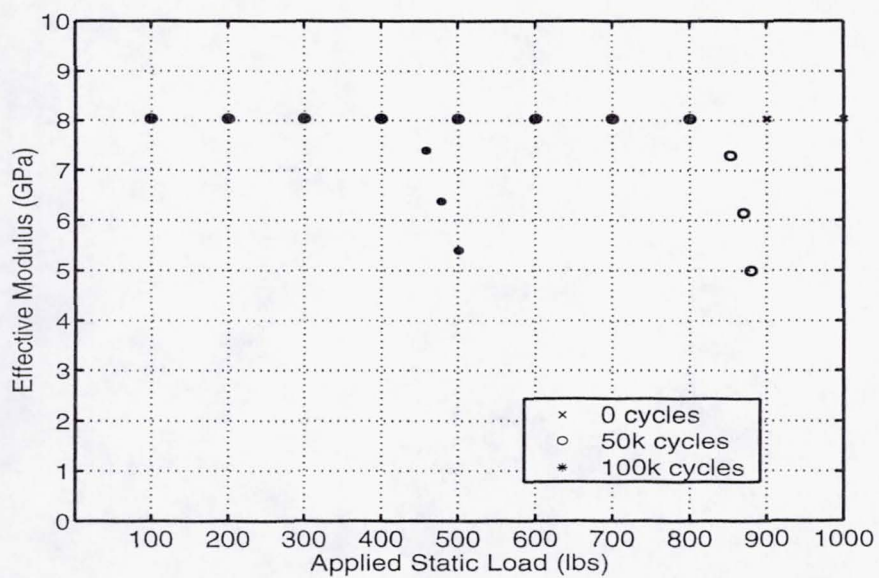
Figure 2.12: Effective modulus vs. applied static load for the 70-30 epoxy layer
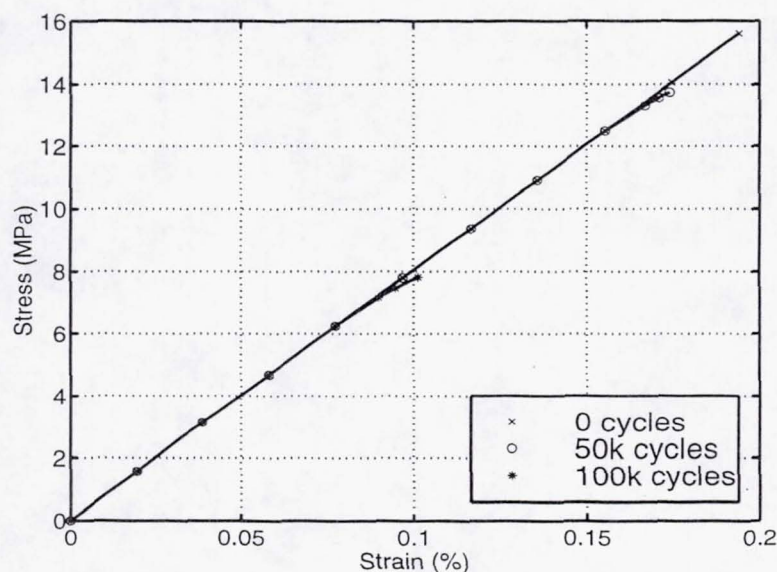
Figure 2.13: Reconstructed stress-strain relation for the 70-30 epoxy layer

reconstruction of the stress-strain relation for the $70 - 30$ epoxy bond.

From Figures 2.10 to 2.13, it can be seen that for an epoxy bond of the type considered here, $50k$ fatigue cycles clearly reduce the load at which nonlinearity starts while $100k$ fatigue cycles reduce this load further. However, for both cases, the deteriorated bonds did not show any difference in modulus in the linear range as compared to the bond that had not been subjected to cyclic loading.

From the results of this section it may be concluded that the degradation of the adhesive can be detected by the reduction of the linear portion of the traction-displacement or stress-strain curve.

The consistency of the experimental results depends on the accuracy of the measurements of incident and reflected signals. In order to obtain repeatable results, every potentially variable factor in the setup was kept unchanged. One important factor is the water path distance. It was attempted to keep the distance the same

for every measurement by monitoring the time of the first reflection from the water/aluminum interface. The water distance had a slight change during the loading process because of the elongation of the aluminum tube and the connection layer. However, the slight change in the water path distance does not cause a detectable change in the shape and magnitude of the signal, but the arrival of the reflected signal has an extra delay. This delay was manually adjusted for the convenience of subsequent calculations. Normal incidence of ultrasound to the interface, which is also an important factor, was achieved by adjusting the three screws on the tube. Another important factor is the pulser setup. During this investigation, the setup for the pulser remained unchanged.

The adhesive layer is elongated when a load is applied to the specimen. However, for our study, the strain is well under 0.5%. The corresponding change in thickness has a negligible effect on the inverse results. Similarly, the density variation of the layer is also negligible.

2.4   Conclusions

A comparison of experimental and simulated results was used to obtain the effective modulus of an adhesive layer. The onset of nonlinear behavior of adhesive bonds was detected. The results show that degradation due to cyclic fatigue can be detected by the reduction of the linear portion of the stress-strain curve without any change in slope in the linear range.

The use of a superimposed shear wave to detect the onset of nonlinear behavior induced by a static shear loading will be discussed in next chapter.

Chapter 3

Use of Shear Waves to Detect the Onset of Nonlinear Behavior of Adhesive Bonds

3.1 Introduction

In the previous chapter it has been shown that the degradation due to cyclic fatigue can be detected using a theoretical model in combination with experimental data. An external tensile load was employed to pull the bond into the nonlinear range of the traction-displacement $(Q - \Delta)$ curve. Detection of nonlinear behavior of fatigued specimen under static tensile loading by reflection of longitudinal waves was discussed. Most adhesive bond structures particularly in the aeronautical industry are lap joints that are subjected to shear loading. This chapter is, therefore, concerned with fatigued specimens that are statically loaded in shear. Results are presented in this chapter. Under shear loading, the nonlinear behavior should be more readily detectable by shear waves. In addition, shear and longitudinal wave

31

have both been used while the specimen is statically loaded in shear. A comparison is given for the different wave type inspections. It is also explored which loading method can more easily pull the bonds into the nonlinear range. The results suggest an optimal combination of the loading and the ultrasonic testing methods.

3.2   A superimposed shear wave

In Chapter 2 it was shown that a longitudinal ultrasonic wave can be used to detect the initiation of nonlinear behavior of a stressed adhesive bond. From the different load levels necessary for the detection of nonlinear behavior, degradation of the adhesive bond can be inferred. A detailed discussion of the theoretical model for use of longitudinal ultrasound for an adhesive bond under tensile loading has been presented in the previous chapter. In this chapter the approach is extended to the case that the adhesive bond is subjected to shear loading.

For a prestressed specimen under shear stress τ and relative shear displacement of two opposite points of the adhesive bond, Δ (see Fig. 3.1), an incident ultrasonic shear wave is considered as a small superimposed disturbance. The total stress and total displacement can be viewed as $\tau + \sigma_{yx}$ and $\Delta + \delta$, respectively, where σ_{yx} and δ are the stress and displacement due to the ultrasonic signal. Similarly as discussed in the previous chapter, the local slope at any point of the $\tau - \Delta$ curve can be approximated as

$$\frac{d\tau}{d\Delta} \approx \frac{\sigma_{yx}}{\delta} = \beta \tag{3.1}$$

From the local slope (β) of the $\tau - \Delta$ curve, it is convenient to define another parameter to describe the bond property. This parameter is called the effective
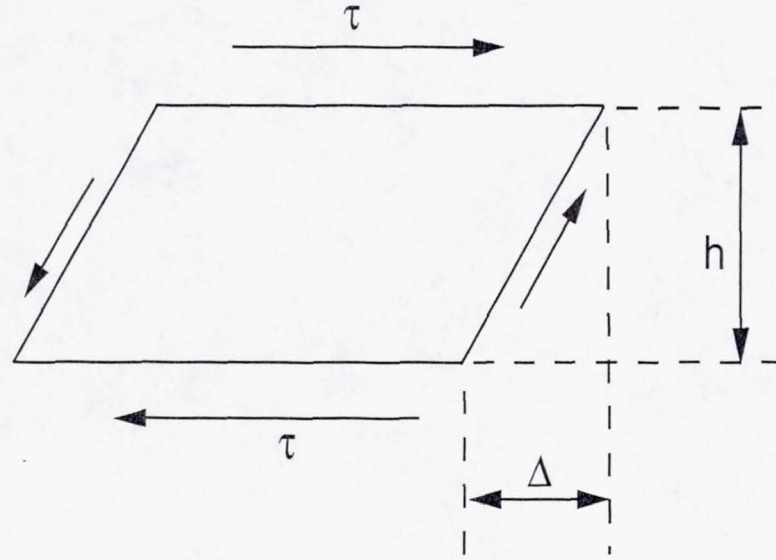
Figure 3.1: Shear deformation illustration (shear stress τ, deformation Δ, adhesive layer thickness h).

shear modulus $M_{eff,shear}$, where

$$M_{eff,shear} = \beta h \tag{3.2}$$

For the superimposed shear wave case, the derivation of the reflection coefficient, which is directly related to the bond property parameter, is completely analogous to the longitudinal case. Let us use u for the superimposed ultrasonic shear displacement, σ_{yx} denotes the shear stress, ρ is the density of the adhesive layer, $\bar{\sigma}_{yx}$ is the average stress in the interface layer, δ is the shear displacement across the layer. Figure 3.2 illustrates the incident, reflected and transmitted waves in the adherends. Both adherends are assumed to be of the same material.

Analogously to the longitudinal case, the three governing equations across the thin adhesive layer are

$$\sigma_{yx}|_{y=0^+} - \sigma_{yx}|_{y=0^-} = \frac{1}{2}\rho h[\ddot{u}|_{y=0^+} + \ddot{u}|_{y=0^-}] \tag{3.3}$$
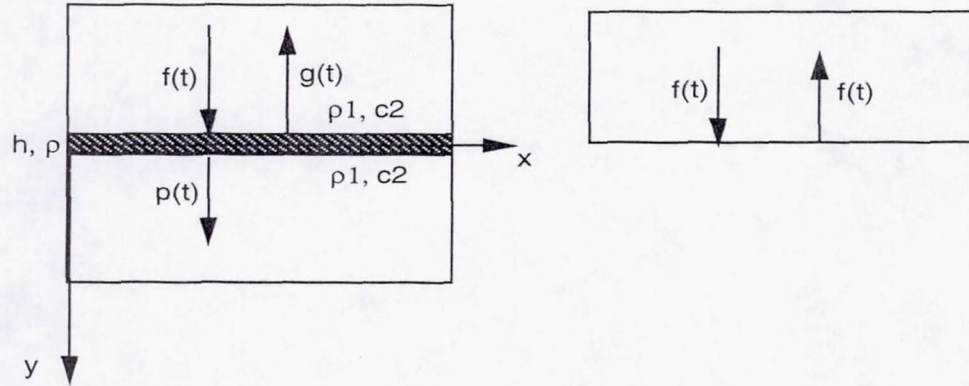
Figure 3.2: Illustration of wave motion. Left: Incident signal $f(t)$, reflected signal $g(t)$, transmitted signal $p(t)$. Right: 100% reflection at a free interface.

$$\bar{\sigma}_{yx} = \frac{1}{2}[\sigma_{yx}|_{y=0^+} + \sigma_{yx}|_{y=0^-}] \tag{3.4}$$

$$\delta = u|_{y=0^+} - u|_{y=0^-} \tag{3.5}$$

By virtue of Eq. 3.1, we can write

$$\bar{\sigma}_{yx} = \beta\delta \tag{3.6}$$

We define another parameter γ to simplify the final expression

$$\beta = \gamma\beta_0 \tag{3.7}$$

where

$$\beta_0 = \frac{\rho_1{}^2 c_2{}^2}{\frac{1}{2}\rho h} \tag{3.8}$$

Here ρ_1 is the density of aluminum and c_2 is the shear wave velocity of aluminum. If an unit incident harmonic wave is applied, the incident, reflected and transmitted waves can be written as follows

$$u^I(y,t) = e^{i(\omega t - ky)} \tag{3.9}$$

$$u^R(y,t) = Re^{i(\omega t + ky)} \tag{3.10}$$

$$u^T(y,t) = Te^{i(\omega t - ky)} \tag{3.11}$$

After some manipulations, Eqs. 3.3- 3.11 yield a simple expression for the reflection coefficient in the form

$$R(\omega) = \frac{i\bar{\omega}}{i\bar{\omega} + 2\gamma} - \frac{i\bar{\omega}}{i\bar{\omega} + 1} \tag{3.12}$$

where

$$\bar{\omega} = \frac{\rho h}{2\rho_1 c_2} \omega \tag{3.13}$$

For any known incident signal $f(t)$, an application of the Fast Fourier Transform (FFT) gives us $F(\omega)$. By the use of $R(\omega)$, the following expression for the simulated reflected signal $g^s(t)$ can be written

$$g^s(t) = \int_{-\infty}^{\infty} R(\omega)F(\omega)e^{-i\omega t}d\omega \tag{3.14}$$

By defining the deviation between simulated and experimental results as

$$Dev(\gamma) = \sum_{i=1}^{N}(g(t_i) - g^s(t_i, \gamma))^2 \tag{3.15}$$

the best parameter γ can be obtained by minimizing the deviation. Once best parameter γ is found, Eqs. 3.2, 3.7 and 3.8 can be used to calculate the effective shear modulus.

3.3 Configuration of experiment and specimen

The configuration of the experiment (see Fig. 3.3) consists of two units. One unit is a standard ultrasonic pulse-echo setup. The other unit is an Instron machine which enables us to apply a static shear load during the ultrasonic test. A Panametrics ultrasonic pulser/receiver (Model 5055PR) was used to excite the transducer and
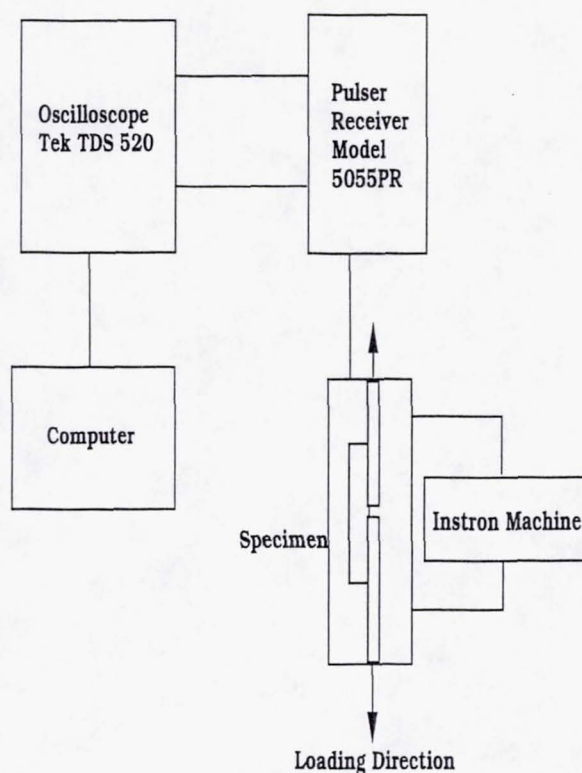
Figure 3.3: Experiment setup for the measurement of reflected signals from the adhesive bond under a static external shear loading.

to receive the signal. For the shear wave test, a longitudinal wave transducer with a central frequency of 5.0 MHz was used to generate shear waves through a specially designed angle-block (see Fig. 3.4(a)). For the longitudinal wave test, another transducer of $5.0MHz$ was used. Both transducers have an element diameter of 0.25 in. A Digital Oscilloscope (Tektronix TDS520) was used for data acquisition. Data from the oscilloscope were collected by a computer through a GPIB with a sampling frequency of 500 MHz. For better coupling conditions the water immersion method was used in both cases.

The angle-block is designed for ultrasonic wave mode conversion. In order to get maximum shear wave reflection from the adhesive bond, normal incidence of the
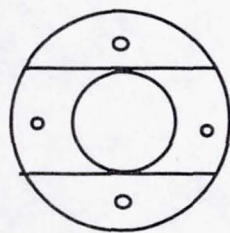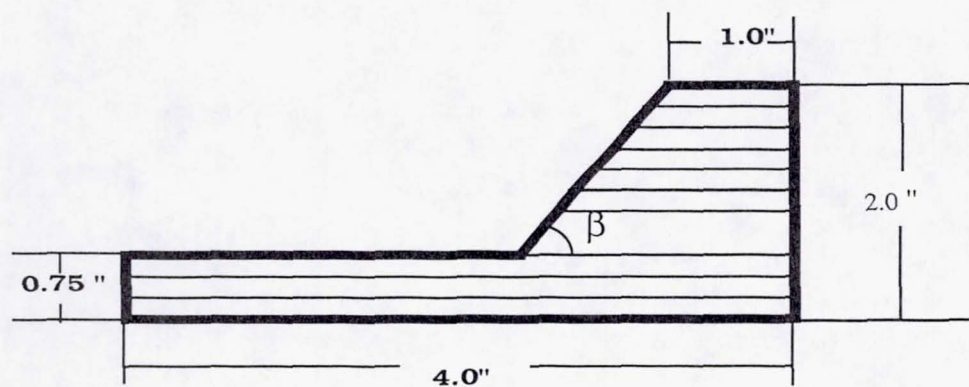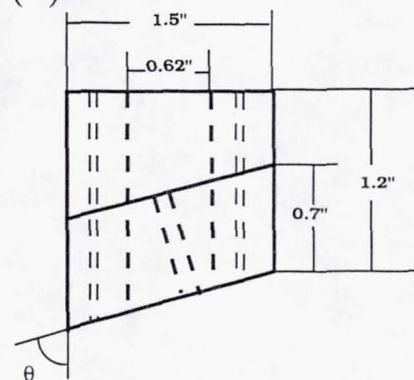
Figure 3.4: (a) Angle block to covert incident longitudinal wave to shear wave, (b) Fixture to hold the transducer and for mode conversion.

shear waves is strongly preferred. The angle block has an angle of $\beta = 45^0$. The incident longitudinal ultrasonic wave at the surface is converted to a 45^0 shear wave. Thus, the converted shear wave is incident normally to the bottom surface, which is the adhesive bond area. This is achieved by a specially designed fixture shown in Fig. 3.4(b).

The fixture is designed for two purposes. The first purpose is to hold the transducer for mode conversion. The second purpose is to be a water tank to immerse the transducer. Two screws are used for slightly adjusting the transducer to get a maximum reflection from the interface. The dimensions of the fixture is demonstrated in Fig. 3.4(b).

Figure 3.5 shows the assembled specimen. For a prescribed angle β, the incident angle α, and the angle θ in the fixture can be easily calculated using the following simple calculation:

$$\alpha = sin^{-1}[(c_w/c_t)sin\beta] \tag{3.16}$$

$$\theta = \frac{\pi}{2} - \alpha \tag{3.17}$$

where c_w and c_t are the ultrasonic wave velocity in water and the ultrasonic shear wave velocity in aluminum, respectively. For this experiment, $\alpha = 19.3^0$, hence angle $\theta = 70.7^0$.

Epoxy resins used for bonding the specimen are epoxi-patch provided by the Dexter Corporation. They contain two parts, part A resin and part B hardener. This epoxy has a full curing time of three days at room temperature and 24 hours at $140^0 F$. The epoxy was mixed 50% part A and 50% part B.

The adherend surface was carefully prepared. First, acetone is used to clean the
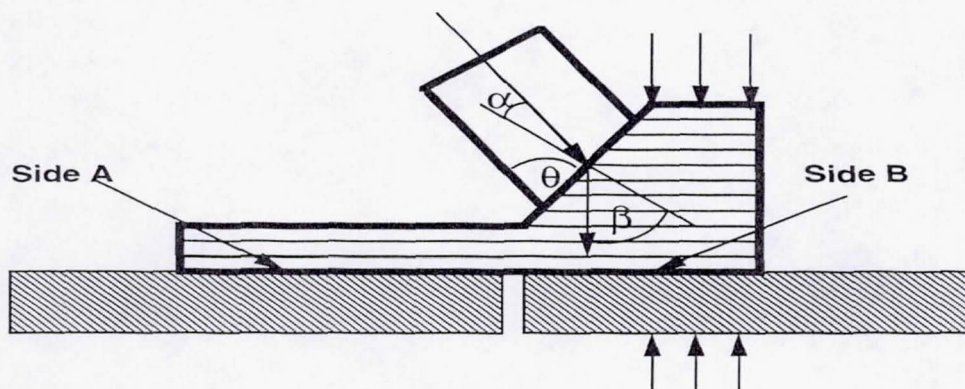
Figure 3.5: Assembly of adhesive bond specimen and the fixture for mode conversion.

surface, and then Methyl Ethyl Ketone (MEK) is used to clean the surface for an additional dozen of times. Air is used to dry the surfaces before placing the epoxy on the surfaces.

As discussed in the previous chapter, the thickness of the adhesive layer is an important parameter for the inverse problem calculation. Control of the thickness is achieved by a fixed uniform gap between the two adherends, namely, the angle-block and another aluminum piece. The adhesive layer thickness is $80 \mu m$.

As illustrated in Figure 3.5, the transducer is mounted at side B, which has a smaller bonding area (1.5 in × 1.5 in). Side A has a larger bonding area (1.5 in × 2.5 in). The cyclic fatigue load is only applied to side B. This guarantees that the nonlinear behavior will initiate at side B first when the specimen is under static shear loading.

An electronic switch is used when the simultaneous measurement of longitudinal and shear wave is conducted. The switch is connected to the pulser/receiver. it is convenient to switch back and forth to select either desired signal.

3.4   Experiment

3.4.1   Shear wave detection

The configuration that was considered first used a lap joint and shear wave transducers for normal incidence. The coupling of the transducers to the specimen presented, however, a great deal of trouble. It proved to be very difficult to maintain contact between the transducer and the specimen during testing. It was tried to use super glue to bond the transducer to the specimen. However, when the loading was increased, the contact condition changed at the transducer/aluminum interface. The contact was broken before the nonlinear behavior of the adhesive bond could be observed. To avoid these contact problems, it was decided to use mode conversion to generate normal incidence of the shear waves. This was achieved with the angle-block and the fixture shown in Figure 3.4.

For the shear wave test, three groups of specimen were prepared. One group of specimens were not subjected to any fatigue. The other two groups were subjected to 150 K and 300 K cycles fatigue, respectively. The cycling was done on the Instron machine. A Half-sine wave was used for the fatigue loading. The cyclic load was 200 to 2000 lbs compression. The loading frequency was 10 Hz.

During the shear static loading when the ultrasonic measurement is conducted, there was a slight change of the signal (see Fig. 3.6) at the beginning of loading. This change is negligible compared to the later nonlinear response. When the load was increased to the critical load level where the nonlinear behavior begins, the signal change (see Fig. 3.7) is much more pronounced than the initial change.

In calculating the effective modulus, the accuracy of the calculation depends on
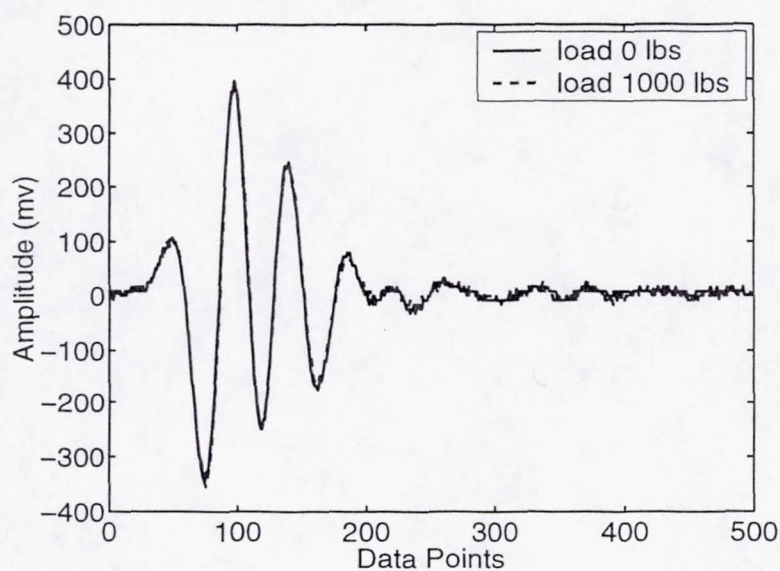
Figure 3.6: Very slight change for shear wave signals reflected from an adhesive bond which is in the linear range of the stress-strain behavior (Fatigued 300K cycles).
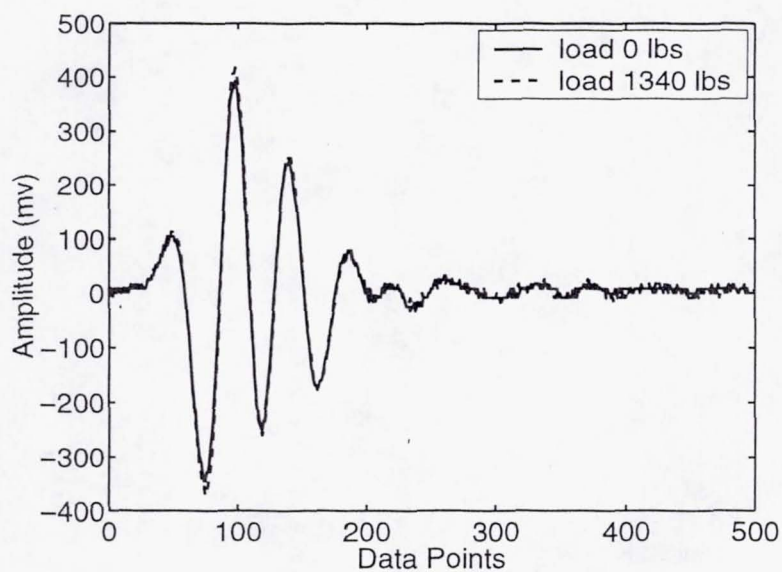
Figure 3.7: More pronounced change of shear wave signal reflected from an adhesive bond which is in the nonlinear range of the stress-strain behavior (Fatigued 300K cycles).

the accuracy of the experimental signal. In order to verify the consistency of the measured signal, two tests were done. Because of oblique incidence, signals cannot be picked up from the water/angle-block interface. One test is to obtain the same reflection from the angle-block/air interface. This can be easily done by maintaining the same water path from the transducer to the angle-block surface and the setup remains strictly the same. Another one was to test the consistency of the reflection from the bond interface. The accuracy and consistency of these signal measurements has a big influence on the inversion results. Our experiments show that the accuracy and consistency is good as long as the setup can be kept the same.

Using the inverse scheme, the simulated signal and effective shear moduli were calculated. Figure 3.8 shows a typical result for the measured signal versus the simulated signal. Figure 3.9 is the actual applied load versus the calculated effective shear moduli. From Fig. 3.9, we can see that for the nonfatigued specimen, the modulus has no change before 2500 lbs loading. For the 150 K cycle fatigued specimen, nonlinear behavior can be detected at 1950 lbs load level. For the 300K cycle fatigued specimen, the nonlinear starts even earlier, at around 1150 lbs load level. Figure 3.10 shows the stress-strain curve reconstructed from Fig. 3.9. From this graph, we can tell the clear difference of the adhesive bond stress strain relations of these three sets of specimens.

From these results, it may be concluded that the initiation of nonlinear behavior under shear loading can be determined by the analysis of the superimposed shear wave.
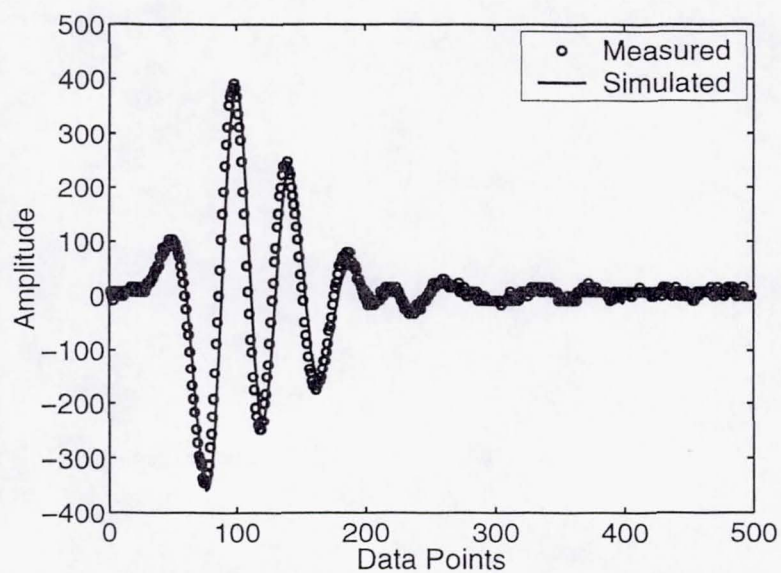
Figure 3.8: Measured signal versus simulated signal.
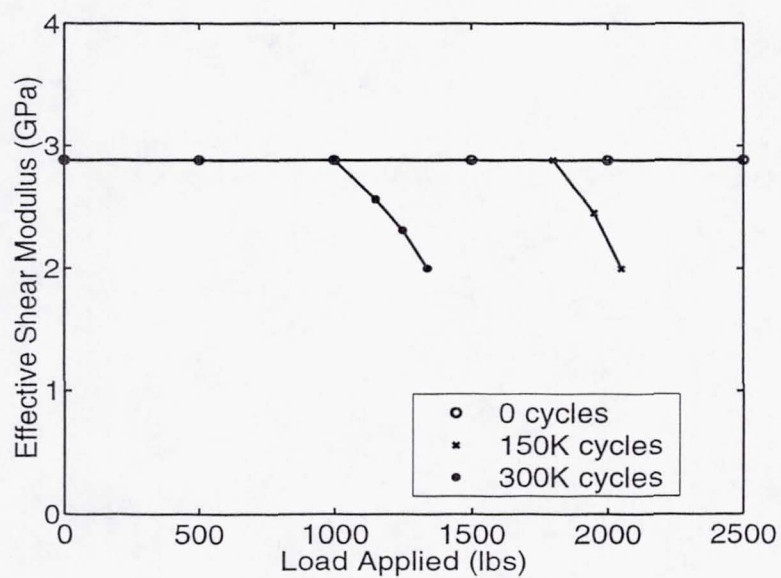
Figure 3.9: Actual applied load versus calculated effective shear modulus.
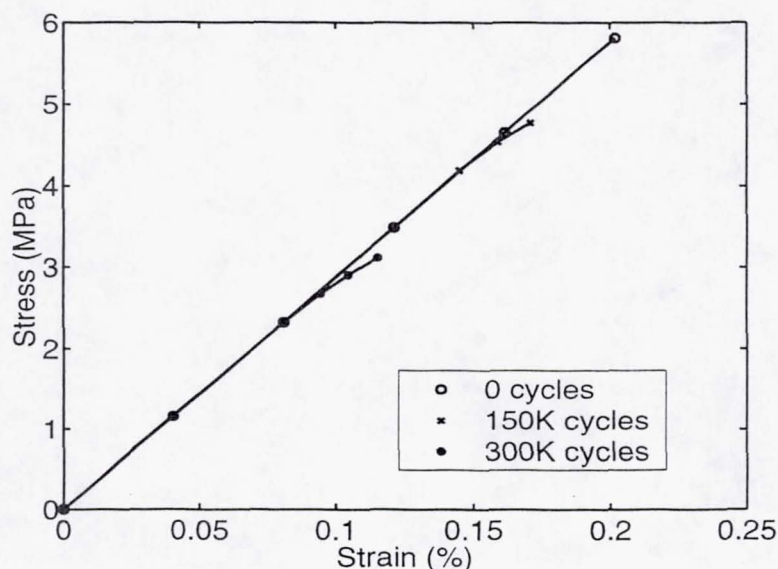
Figure 3.10: Reconstructed stress-strain relationship curve.

3.4.2 Simultaneous measurements

For practical applications, the shear wave measurement is not very convenient. As was discussed earlier, the coupling presents a problem. If a special fixture is designed to fulfill mode conversion, this will increase the difficulty of execution. A very reasonable question is if it is possible to detect the nonlinear response using a longitudinal wave while the specimen is loaded in shear. To investigate this question, the mode conversion fixture was mounted at one side of the specimen and the longitudinal transducer at the other side (see Fig. 3.11). The description of the fixture for the longitudinal wave test can be found in the previous chapter. Three groups of specimens with same bonding areas and fatigue history were prepared as in the shear wave test section.

For both the longitudinal wave and shear wave inspection, a single pulser is used. An electronic switch is connected to the pulser/receiver. The switch enables
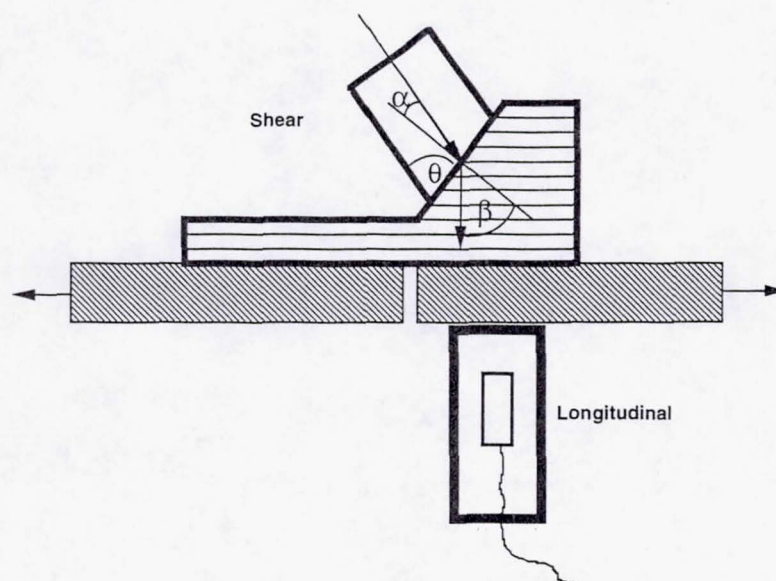
Figure 3.11: Simultaneous experiment specimen for both shear wave and longitudinal wave detection.

the convenient selection of the desired signal.

At the interface between the specimen and the longitudinal wave transducer holder, an interfacial stress exists when the specimen is loaded in shear. Thus the coupling condition variation yields a slight change in the reflected longitudinal wave signals when the stress-strain behavior is still in the linear range. However, this change is negligible compared to later changes in the nonlinear range (see Fig. 3.12)

It was interesting to observe that under shear loading the longitudinal wave can also detect the nonlinear response. Differences in reflected longitudinal and shear wave signals were observed at essentially the same critical shear load level. Thus, when the nonlinear behavior starts, both a shear wave and a longitudinal wave can detect the signal difference due to nonlinearity.

For the longitudinal case, the calculation of effective modulus can also be easily
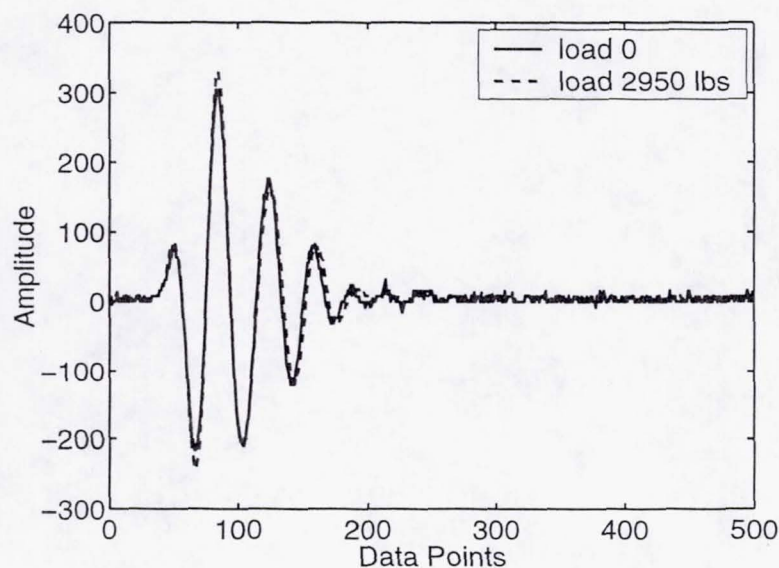
Figure 3.12: Longitudinal signal change in the nonlinear range of adhesive bond stress-strain relation (Fatigued: 150K).

carried out using the incident waveform and reflected waveform. The parameters needed in this calculation are the density of adhesive layer, the thickness of adhesive layer, and the longitudinal wave velocity of aluminum. The experimental results show that the effective modulus has changed under shear loading. The effective modulus versus the applied shear load has been plotted in Figure 3.13. If the tensile stress were known, the stress-strain curve for the longitudinal case would have been reconstructed directly from Figure 3.13. However, the reconstruction of the stress-strain curve is impossible due to lack of the information of tensile stress.

A separate bulk sample was prepared for the measurement of density, shear and longitudinal wave velocities. It was cured under the same procedure as in the bonding specimen. From these measurements, we can use the standard calculation to obtain the shear modulus of this epoxy as 2.35 GPa (ρc_t^2), and the Lame constant $\lambda + 2\mu$ as 6.72 GPa.
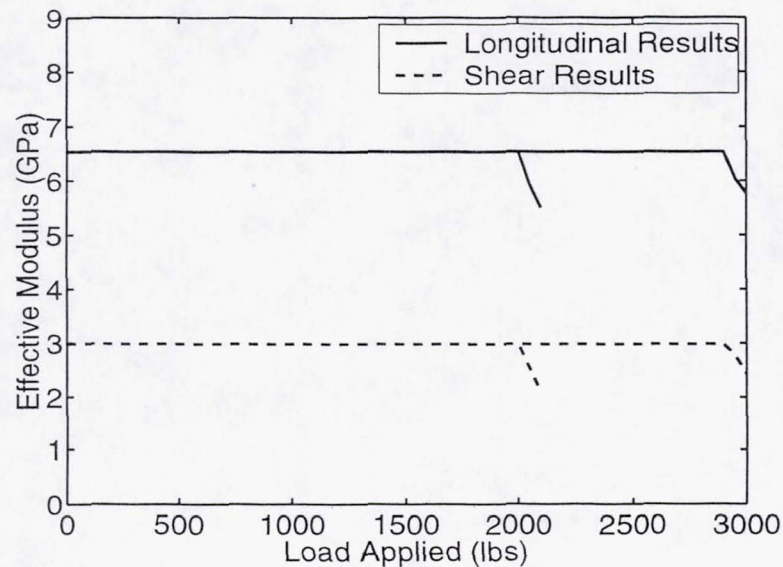
Figure 3.13: Longitudinal and shear wave detection results: Modulus vs. actual load applied.

It should be noted that the effective shear modulus (see Figure 3.13) obtained from the inverse calculation for specimens used for the simultaneous tests is a little higher than that for the previous specimens used for shear wave tests (see Figure 3.9). Another difference is that the nonlinear behavior critical load level for specimens used for the simultaneous tests is consistently higher than for the previous specimens for shear wave tests. These differences might be due to fatigue control. They also could be caused by small variation of the bond thickness. However, the results do not conflict with the conclusion that the initiation of nonlinear response can be ultrasonically detected.

3.4.3 Nonlinear behavior under shear loading and tensile loading

In the previous chapter it was shown that the nonlinear behavior of the adhesive bond under tensile loading can be detected using a longitudinal wave. In this chapter, It has been shown that a shear wave can be used to detect the nonlinear behavior of the adhesive bond under shear loading. It has also been shown that the nonlinear behavior of an adhesive bond under shear loading can be detected using a longitudinal wave. It remains to determine the best combination of loading and testing method. For that purpose, three sets of specimens with the same bonding area were prepared. One group of specimens for tensile loading is a circular bonding area with diameter 1.5" (the area is 1.766 in^2). Another group for shear loading has a bonding rectangular area of 1.5 in × 1.177 in (the area is 1.766 in^2). Each group of specimens was subjected to different fatigue cycles. They were: (1) no fatigue cycles, (2) 150 K fatigue cycles, and (3) 300K fatigue cycles. The fatigue load is -100 to -1000lbs compression. A longitudinal wave transducer was used to obtain the critical load. The critical load is the load at which nonlinear behavior starts, namely the load at which detectable changes in reflected longitudinal wave signals can be observed. Table 3.1 lists the critical load level for the specimens that have been subjected to 300K fatigue cycles. As might be expected, the shear loaded specimens display the nonlinear response much earlier than the tensile loaded specimens. For each different fatigue cycle case, the results are quite consistent. These results suggest that shear loading easier pulls the bond to the nonlinear range than tensile loading.

Table 3.1: Comparison of critical shear load and tensile load at which nonlinear behavior starts (when detectable change in longitudinal wave reflected signals can be observed)

Fatigued cycles (K)	Specimen number	shear (lbs)	tensile (lbs)
	1	1500	2700
300	2	1780	2090
	3	1370	2550

3.5   Discussion

It is shown that the shear wave can detect the nonlinearity induced by shear loading. It is also shown that the longitudinal wave can also be used to detect the nonlinearity induced by the shear loading. The critical shear load for longitudinal and shear wave detection is essentially the same. From the shear loading and tensile loading test, it is clear that the shear loading is easier to induce the nonlinearity. So, static shear loading and detection by longitudinal waves seem to be a better combination. However, in the case where shear modulus is desired, shear wave can also be used to serve this purpose.

3.6   Conclusions

In this chapter, it was first shown that a shear wave can be used for the detection of adhesive bond degradation generated by cyclic fatigue for a specimen under external static shear loading. Next it was shown that the nonlinear behavior of adhesive bond under shear loading can also be detected using a longitudinal wave. Differences in ultrasonic longitudinal and shear wave reflected signals are observed at essentially

the same external static shear loading level. For a best combination of loading and detection, a comparison of the onset of nonlinear behavior for tensile loading and shear loading was made. Experimental results show that specimens of the same numbers of fatigue cycles reach the nonlinear portion at a lower load level for shear loading than for tensile loading. Static shear loading and longitudinal wave detection thus provide a useful combination.

Chapter 4

Ultrasonic Nondestructive Evaluation of Adhesive Bond Degradation Using a Strain-Temperature Correspondence

4.1 Introduction

As an extension of the theoretical investigation of Ref. [32], experimental methods were developed in Chapters 2 and 3 to study the nonlinear behavior of a deteriorated adhesive bond through the introduction of an external load. Results on bond deterioration were obtained. However, the methods have not been implemented in field tests because a reliable method to apply a substantial amount of loading to the bond, when it is part of a structure, still has to be found.

For most materials a temperature change results in a wave velocity change.

51

Temperature effects on ultrasonic measurements of non-metallic coatings have been addressed before [39]. Adhesives are basically polymeric materials. The stress-strain behavior of polymeric materials strongly depends on the temperature [40]. On the other hand, as opposed to loading, it is easier to apply an increase in temperature to an adhesive bond. This chapter will introduce a sequence of temperature changes as an external factor, and take advantage of the temperature effects of the adhesive layer to determine the nonlinear stress-strain behavior of an adhesive as it may be induced by adhesive bond deterioration. The possibility of employing temperature measurements suggests a method that can be implemented in field tests.

This chapter starts with experimental observations of the ultrasonic signals reflected from adhesive bonds at different temperatures. It turns out that: 1) the signals reflected from adhesive bonds change with temperature in a certain pattern, 2) the reflected signals have a more severe change for a deteriorated specimen than for a non-deteriorated specimen and 3) the reflected signals can be completely recovered after heating and cooling cycles are applied to the specimen. These observations provide a motivation to relate stresses at a higher temperature to stresses at a larger strain. Thus, a strain-temperature correspondence principle is proposed. This principle provides a theoretical explanation of these observations. The heart of the idea is to predict the mechanical response at a larger strain from experimental data in the linear region as the temperature increases. The most important aspect of the principle is that the application of this principle yields nonlinear parameters nondestructively which can only be obtained destructively otherwise. Experimental verification of the principle will be given for a selected material. After the correspondence principle has been verified, it is applied to evaluate adhesive bond degradation.

Finally some conclusions are presented.

4.2   Experimental observations

Two adhesive bond specimens using AB epoxy as adhesive were used to show the preliminary experimental observations. One, referred to as sample #1, is a good bond without degradation. The second one was subjected to 2.3 million cycles compression fatigue loading, and is referred to as sample #2. After all measurements were carried out on sample #2, it was immersed in water for 15 days, and then referred to as sample #3.

The specimens were immersed in water. An electric heater was used to heat up the water tank to different temperatures. The ultrasonic signals reflected from the adhesive bonds were recorded to determine the temperature effects on adhesive bonds. It is clearly seen from Figure 4.1 that the signals reflected from the adhesive bond are quite different at different temperatures. Figure 4.2 shows the enlarged signal difference at different temperatures of sample #3. Figures 4.3 and 4.4 show the enlarged signal difference at different temperatures for samples #2 and #1, respectively.

A quantitative analysis of the reflected signals using the method described in next chapter shows that the signal change is due to the transit time increase through the thin bond line at an increased temperatures. The ultrasonic wave velocity in the thin adhesive layer decreases with increasing temperature. Another result obtained from the quantitative analysis of the reflected signals is that the degradation of the adhesive bond yields a more severe drop of the adhesive layer's velocity as the temperature increases. This means that, at a higher temperature, the modulus of
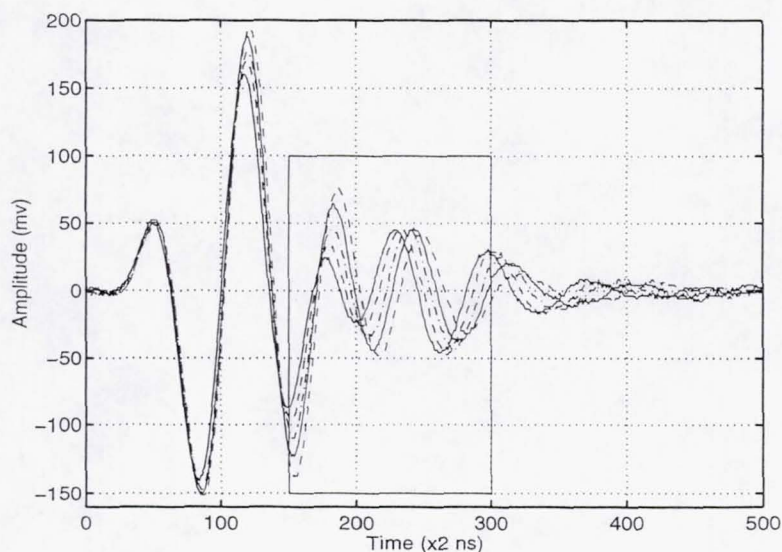
Figure 4.1: Signal difference of sample #3 at various temperatures.

adhesive layer in a deteriorated bond is smaller than the modulus of the adhesive layer in a non-deteriorated bond at the same temperature. If we had pulled the bond mechanically to a strain level in nonlinear range instead of using a temperature increase, we would also have expected the modulus of the deteriorated adhesive bond in to be smaller than that of the non-deteriorated bond at the same strain level. This observation provides the motivation to relate a larger strain to a higher temperature.

In addition to above observations, it was also observed that the ultrasonic signals from the adhesive bonds can be completely recovered after heating and cooling cycles. This means that no damage was done during the heating and cooling. Figure 4.5 indicates the complete recovery of the ultrasonic signal after a heating and cooling cycle.
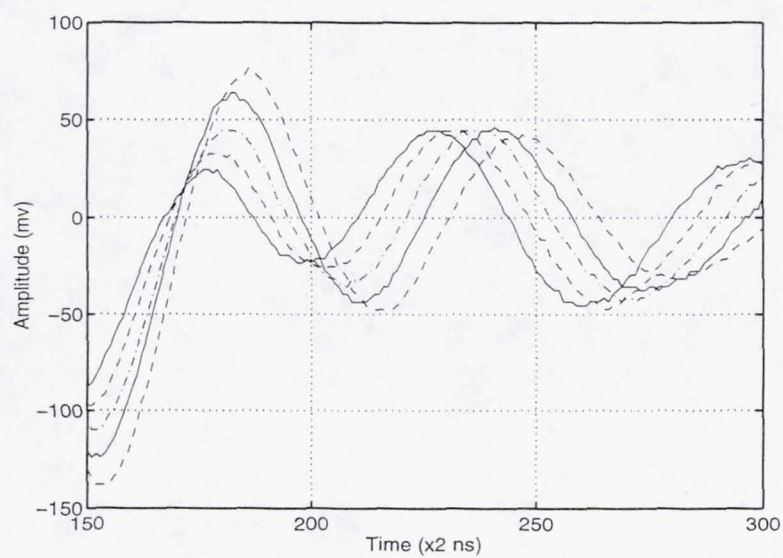
Figure 4.2: Enlarged signal difference at different temperatures of sample #3.
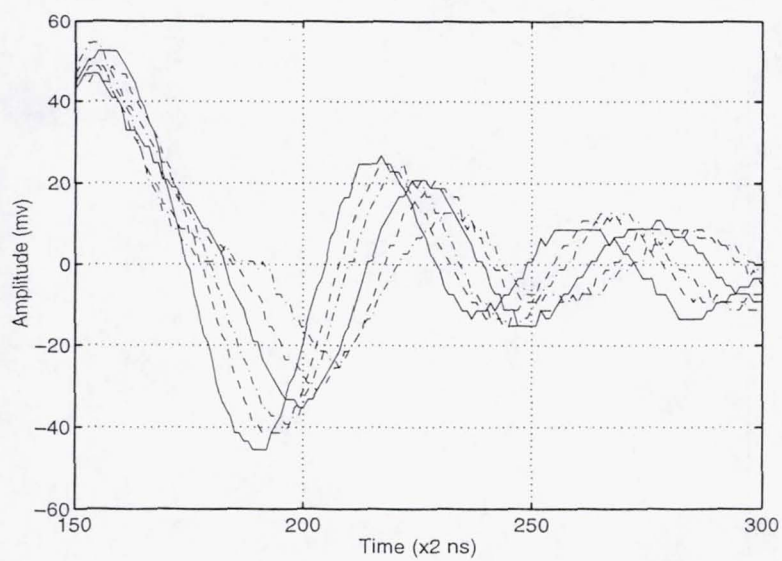
Figure 4.3: Enlarged signal difference at different temperatures of sample #2.
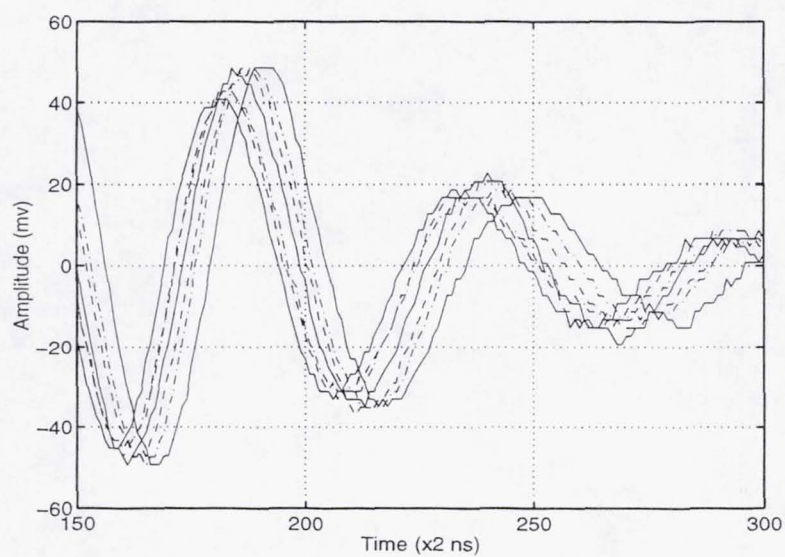
Figure 4.4: Enlarged signal difference at different temperatures of sample #1.
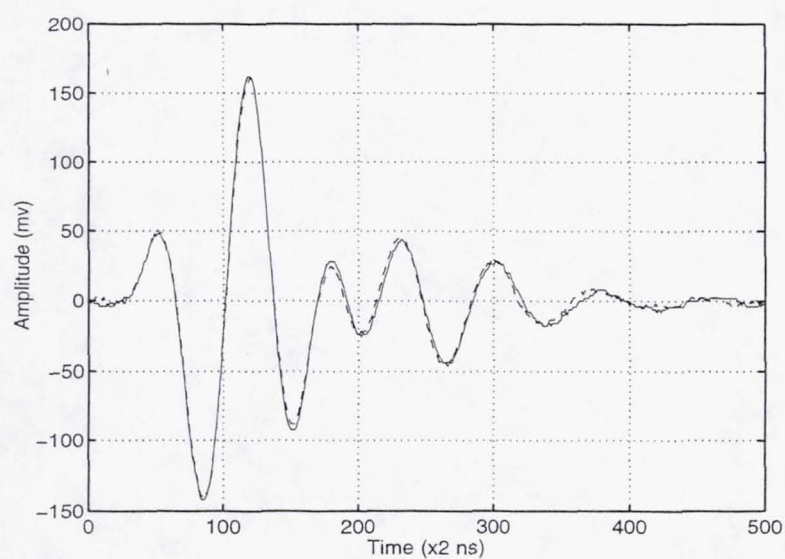
Figure 4.5: Complete recovery of ultrasonic signals after one cycle of heating of sample #3.

4.3 Strain-Temperature Correspondence

4.3.1 A general model

Suppose at reference temperature T_0 a stress-strain relation for characterizing an adhesive bond in tension or shear is given by

$$\sigma = C_0 \left[\epsilon - f(\epsilon) \right] \tag{4.1}$$

where C_0 is the initial slope of the curve, and $f(\epsilon)$ represents the nonlinear part of that curve with the obvious properties

$$\lim_{\epsilon \to 0} f(\epsilon) = 0, \qquad and \qquad \lim_{\epsilon \to 0} f'(\epsilon) = 0 \tag{4.2}$$

Experimental observations show that the temperature dependence of polymeric materials is very strong. At different temperature, a different stress-strain relation is obtained. If the stress-strain relation is expressed in a temperature dependent form, it can be written as

$$\sigma(T) = C(T) \left[\epsilon - g_T(\epsilon) \right] \tag{4.3}$$

where $C(T)$ is the initial slope of the stress-strain curve at different temperatures and $g_T(\epsilon)$ has the following properties

$$\lim_{\epsilon \to 0} g_T(\epsilon) = 0, \qquad \lim_{\epsilon \to 0} g_T'(\epsilon) = 0, \qquad and \qquad \lim_{T \to T_0} g_T(\epsilon) = f(\epsilon) \tag{4.4}$$

Differentiation of Eqs. 4.1 and 4.3 with respect to ϵ yields

$$\frac{d\sigma}{d\epsilon} = C_0 \left[1 - f'(\epsilon) \right] \tag{4.5}$$

$$\frac{d\sigma(T)}{d\epsilon} = C(T) \left[1 - g_T'(\epsilon) \right] \tag{4.6}$$

As discussed earlier, ultrasonic measurements at the reference temperature T_0 yields information on C_0. At a different temperature T, ultrasonic measurements yield information on $C(T)$. We are particularly interested in the ultrasonic measurements at different temperature T but at small strains, thus $g_T(\epsilon)$ is not relevant. We define the following relation

$$C(T) = C_0 \left[1 - h(T)\right] \tag{4.7}$$

Considering Equation 4.1, for a given reference temperature T_0, there must exist a strain, such that the slope of the stress-strain curve at the reference temperature and at that strain level equals the initial slope of the stress-strain curve at the temperature T. Thus mathematically this relation can be written as

$$h(T) = f'(\epsilon) \tag{4.8}$$

Equation 4.8 is called the strain-temperature correspondence relation. Once the strain-temperature correspondence is well established, the stress-strain curve at reference temperature T_0 can be conveniently obtained from the measurements of $h(T)$ at different temperatures, as follows

$$\sigma(\epsilon) = \int_{T_0}^{T(\epsilon)} C_0 \left[1 - h(\bar{T})\right] \epsilon'(\bar{T}) d\bar{T} \tag{4.9}$$

where $\epsilon'(\bar{T})$ means differentiation of $\epsilon(\bar{T})$ with respect to $\bar{T}$ and $T(\epsilon)$ can be inverted from Eq. 8 to obtain ϵ as a function of T.

Now, we will illustratively show how this principle works. Figure 4.6 shows different initial slopes of the stress-strain curve at two temperatures T_1 and T_2. The slopes at these two temperatures equal to the slopes of stress-strain curve at reference temperature T_0 at strain ϵ_1 and ϵ_2 respectively. Figure 4.7 shows a series
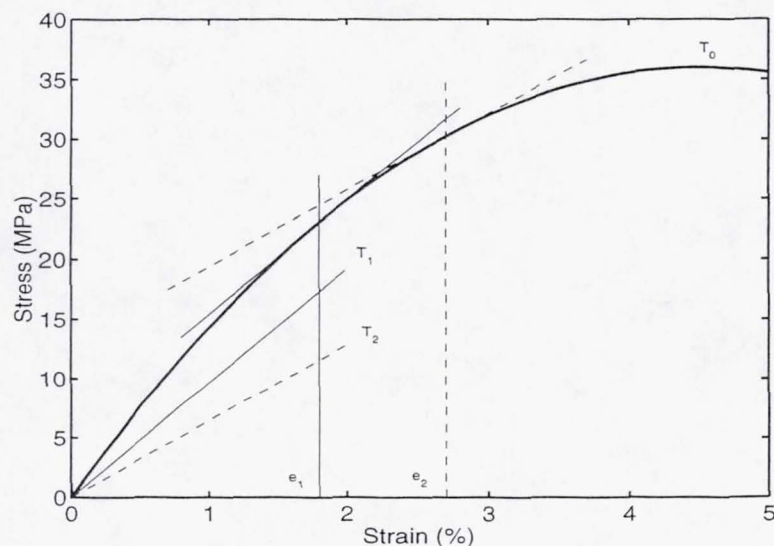
Figure 4.6: The initial slopes at temperature T_1 and T_2 and slopes at strain ϵ_1 and ϵ_2 are the same.

of different temperatures with different slopes of the stress-strain curve. Once the strain-temperature correspondence is established, Figure 4.8 can be plotted from Fig. 4.7 using the known correspondence. Then a stress-strain curve in the total regime (including the linear and the nonlinear regime) can be reconstructed. The reconstructed stress-strain curve will include the strength information of the adhesive bond.

From this illustration it is not difficult to conclude that the application of the strain-temperature correspondence makes it possible to predict the mechanical response in a larger strain regime from limited experimental data in the linear regime by increasing the temperature. Nonlinear parameters are obtained nondestructively. These obtained parameters define the strength of the adhesive bond.
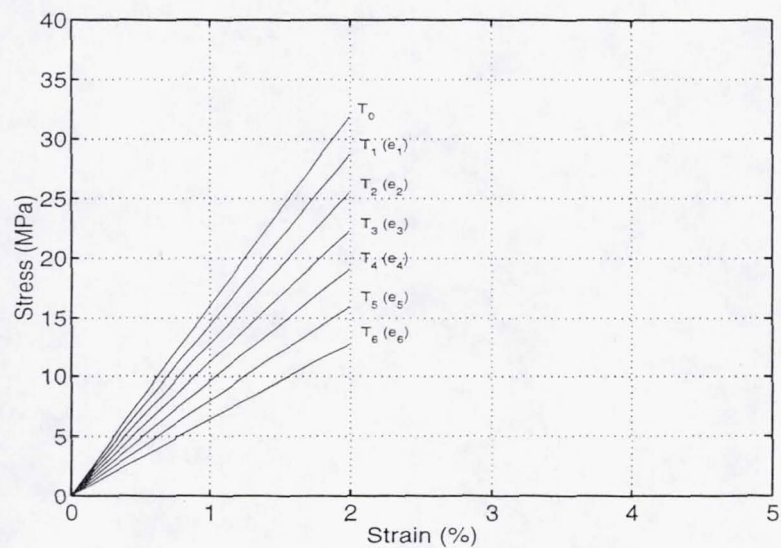
Figure 4.7: Initial slopes at different temperatures.
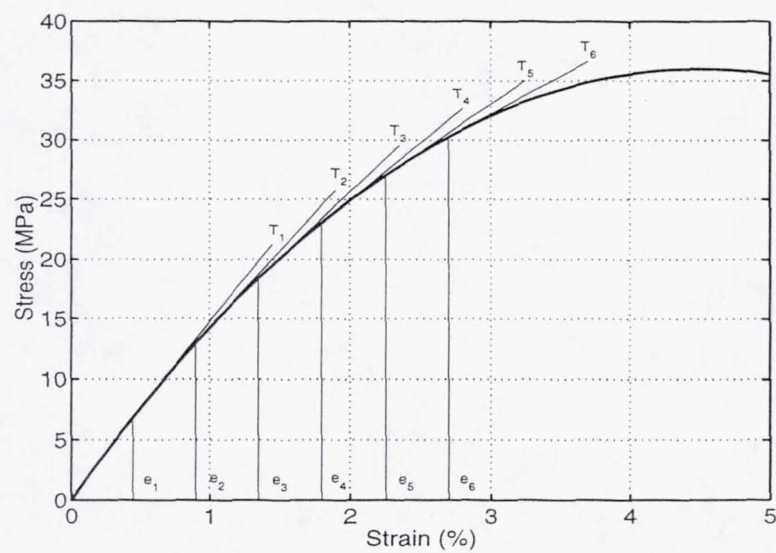
Figure 4.8: A reconstructed stress-strain curve [using Eq. 4.9] with the information of slopes at different temperatures [Fig. 4.7] and the strain-temperature correspondence relation [Eq. 4.8].

4.3.2   A simple model in tension

Specification of the form of $f(\epsilon)$ in Eq. 4.1 allows a more explicit analysis of the strain-temperature correspondence.

By defining $f(\epsilon)$ in a simple quadratic form, Equation 4.1 can be written as

$$\sigma = C_0 \left[\epsilon - \frac{\epsilon^2}{2\epsilon_0} \right] \tag{4.10}$$

where ϵ_0 denotes the ultimate strain (at $\epsilon = \epsilon_0$, the stress attains its maximum.).

On the other hand, experiments have shown that it is quite appropriate to assume a temperature dependence of the velocity in the form

$$\frac{dc(T)}{c_0 dT} = -\alpha_c \tag{4.11}$$

where c_0 is the wave velocity at reference temperature T_0, α_c is assumed to be a constant in a moderate temperature range where T doesn't deviate too much from the reference temperature T_0. The negative sign is to keep α_c positive [for most substances, the velocity decreases with a temperature increase (water is an exception)].

Ultrasonic measurements of the longitudinal wave velocity usually yield $\lambda + 2\mu$, where λ and μ are Lamé constants. For a given material at given temperature, we assume this quantity has a definite relation with the initial slope of the stress-strain curve [i.e. $C = \gamma(\lambda + 2\mu)$]. The experiment in next section will show that the parameter γ also changes with temperature. We can define a parameter η as the following

$$\gamma(T) = \gamma_0(1 - \eta \Delta T) \tag{4.12}$$

where γ_0 is for the reference temperature.

Then, the initial slope at temperature T can be expressed as

$$C(T) = \gamma(T)\rho(T)c(T)^2 \tag{4.13}$$

where $\gamma(T)$ is the factor which relates the Lamē constants and the initial slope at temperature T. Here, $\rho(T)$ and $c(T)$ are the density and velocity at temperature T. On the other hand, differentiation of Eq. 4.10 yields the slope at strain ϵ and at reference temperature T_0 as

$$\frac{d\sigma}{d\epsilon} = C_0 \left[1 - \frac{\epsilon}{\epsilon_0}\right] \tag{4.14}$$

Then, the following relation can be obtained by equating Eqs. 4.13 and 4.14

$$\gamma(T)\rho(T)c(T)^2 = C_0 \left[1 - \frac{\epsilon}{\epsilon_0}\right] \tag{4.15}$$

Linear approximations to $\rho(T)$ and $c(T)$ give the following relation (density is related to volume expansion, the volume expansion coefficient is 3β)

$$\gamma_0(1 - \eta\Delta T)\rho_0(1 - 3\beta\Delta T)c_0^2(1 - \alpha_c\Delta T)^2 = C_0 \left[1 - \frac{\epsilon}{\epsilon_0}\right] \tag{4.16}$$

where ρ_0 and c_0 denote the density and velocity at reference temperature T_0, $\Delta T = T - T_0$, β is the linear thermal expansion coefficient. As defined earlier, $C_0 = \gamma_0\rho_0c_0^2$. By omitting the higher order terms of ΔT, the above equation can be rewritten as

$$\frac{\epsilon}{\epsilon_0} = (3\beta + 2\alpha_c + \eta)\Delta T \tag{4.17}$$

Mechanical test can determine the ϵ_0 and η, and ultrasonic measurements can determine the α_c, then the strain-temperature correspondence is established. Measurements at a series of temperatures would be able to reconstruct a stress-strain curve as shown earlier using Eq. 4.9.

4.3.3 A simple model in shear and a parametric study

In the previous section, we have presented a simple model using the stress-strain relation in tension and the longitudinal wave velocity. The additional dependence of the initial slope (C) on a material constant (γ) results in the presence of the term η in the strain temperature correspondence for tension (Eq. 4.17). For the shear wave case, the shear wave velocity can be more directly related to the initial slope of the stress-strain relation in shear. Thus, a simpler form of a shear-strain temperature correspondence can be derived.

It has been shown [33] [41] that a stress-strain relation in shear to characterize an adhesive bond can be assumed in the simple form

$$\tau = \mu_0 \left[\epsilon - \frac{\epsilon^3}{3\epsilon_0^2} \right] \tag{4.18}$$

where $\epsilon > 0$ represents the shear strain, τ is the shear stress, μ_0 is the shear modulus at reference temperature T_0, and ϵ_0 is the ultimate shear strain.

On the other hand, a temperature shear-wave-velocity coefficient (α_{ct}) can be defined in a similar way as in Equation 4.11

$$\frac{dc_t(T)}{c_{0t}dT} = -\alpha_{ct} \tag{4.19}$$

where c_{0t} is the shear wave velocity at reference temperature T_0, $c_t(T)$ is the shear wave velocity at temperature T.

Following the same procedure as presented for the tension case, a shear-strain temperature relation can be derived in the following form

$$\left(\frac{\epsilon}{\epsilon_0} \right)^2 = (3\beta + 2\alpha_{ct})\Delta T \tag{4.20}$$

In this shear-strain temperature correspondence relation, we once again find that the velocity-temperature coefficient (α_{ct}) is directly related to the nonlinear parameter ϵ_0. For most polymeric materials, α_{ct} is usually much larger than β. So, α_c plays a dominant role in this relation. It is of interest to note that for this shear case the additional term η does not appear.

From Equation 4.18, the ultimate stress can be obtained as

$$\tau_{max} = \frac{2}{3}\mu_0\epsilon_0 \tag{4.21}$$

It is very obvious from Equation 4.21 that a higher shear modulus (μ_0) does not necessarily mean a higher ultimate stress, since the nonlinear parameter ϵ_0 also plays a major role in the equation. For example, a material with high stiffness at small strains but with a smaller ϵ_0 may have a lower ultimate stress than a material with lower initial stiffness but with a higher ϵ_0. Simple knowledge of μ_0 is not indicative of the ultimate stress or ultimate strength.

Now, we will show how the parameter α_{ct} is useful in the strength assessment, and how misleading the traditional simple measurement of c_{0t} can be. Suppose we have two different materials. Material 1 has a somewhat lower initial shear modulus than material 2, but material 1 has a much higher ultimate strain than material 2. Then, material 1 has a higher ultimate shear stress. The parameters for two materials are listed in Table 4.1. The shear stress-strain behavior for these two materials of this kind is shown in Figure 4.9. The shear modulus versus the shear strain for the two materials is shown in Figure 4.10. It is quite reasonable and probable that a higher α_{ct} value is expected for material 2. We consider the case that material 1 has a α_{ct} of 0.0023, and material 2 has a α_{ct} value of 0.0040. Then the shear wave velocity versus temperature can be plotted as shown in Figure 4.11.

Table 4.1: Parameters for material 1 and 2

Material	μ_0	ϵ_0	τ_{max}	α_{ct}	β
1	1.0	7.0	4.6667	0.0023	2.8×10^{-5}
2	1.2	4.0	3.2000	0.0040	5.5×10^{-5}
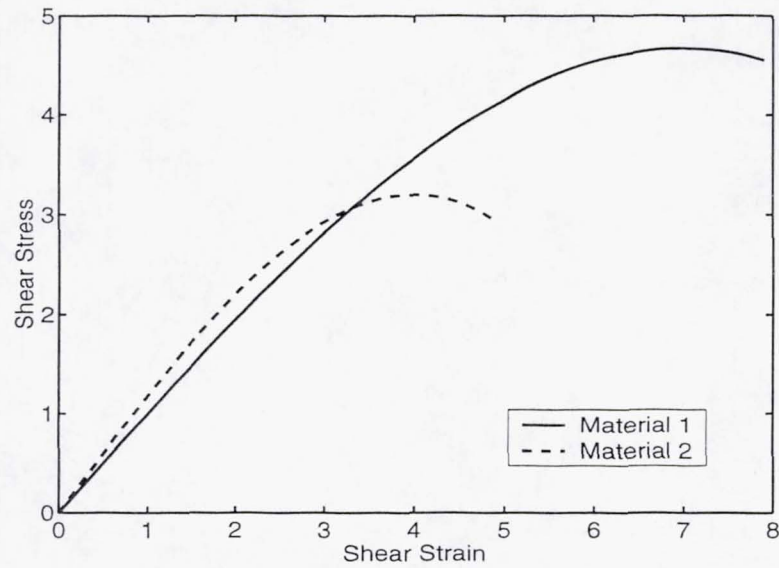
Figure 4.9: Shear stress-strain behavior for material 1 and 2.

It is not difficult to observe from this simple illustration that while the shear wave velocity c_{0t} can be indicative of the shear modulus μ_0 ($\mu_0 = \rho_0 c_{0t}^2$), α_{ct} is more indicative of the nonlinearity. The simple measurement of velocity would have concluded that material 2 is stronger than material 1. With the knowledge of α_{ct}, a more rational conclusion can be drawn instead. One more comment we would like to add is that material FM73 and material DER50-50 are similar in behavior to the case we have discussed here.
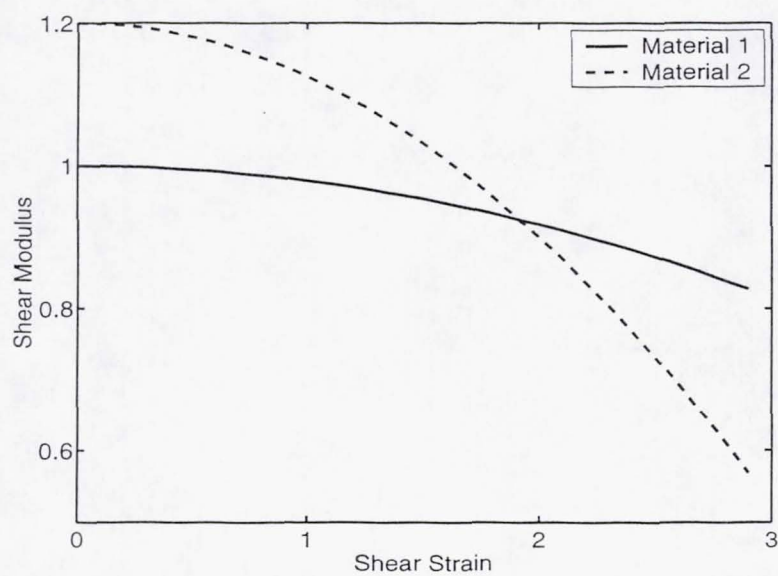
Figure 4.10: Shear modulus at different strains for material 1 and 2.
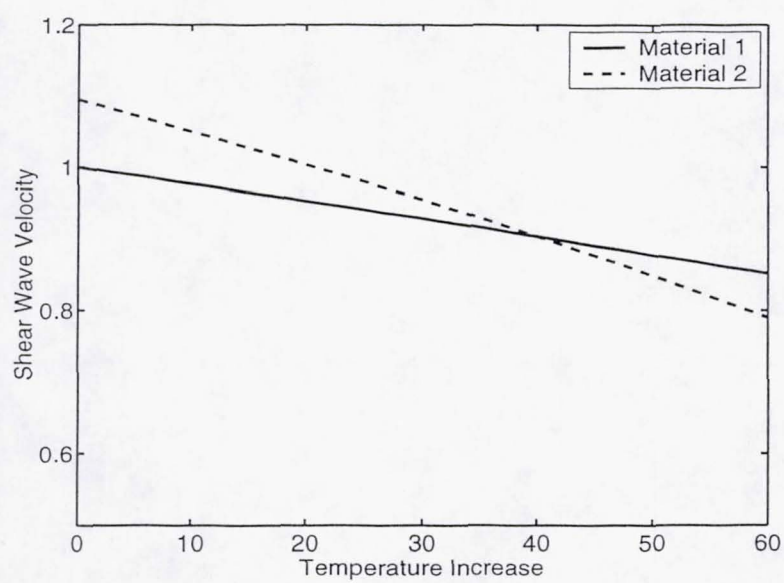
Figure 4.11: Shear wave velocity versus temperature increase for material 1 and 2.

4.3.4 Relation between the temperature shear-wave-velocity coefficient (α_{ct}) and the temperature longitudinal-wave-velocity coefficient (α_c)

Linear approximations to Eqs. 4.11 and 4.19 yield the following two equations

$$c(T) = c_0(1 - \alpha_c \Delta T) \tag{4.22}$$

$$c_t(T) = c_{0t}(1 - \alpha_{ct} \Delta T) \tag{4.23}$$

The longitudinal wave velocity (c) and the shear wave velocity (c_t) can be related to each other by Poisson's ratio [42]. The relation between the two velocities at temperature T can be expressed as

$$\left[\frac{c_t(T)}{c(T)}\right]^2 = \frac{1 - 2\nu(T)}{2[1 - \nu(T)]}, \tag{4.24}$$

where $\nu(T)$ is the Poisson's ratio at temperature T. For a very small temperature increase, we can define a parameter ζ to describe the Poisson ratio's change with temperature as

$$\nu(T) = \nu_0(1 + \zeta \Delta T) \tag{4.25}$$

where ΔT represents a small deviation from the reference temperature T_0.

Equation 4.24 can be rewritten as

$$c_t(T) = c(T)\sqrt{\frac{1 - 2\nu(T)}{2[1 - \nu(T)]}} \tag{4.26}$$

After Equation 4.25 is substituted into Equation 4.26, simple manipulation of Equation 4.26 yields

$$c_t(T) = c(T)\sqrt{\frac{1 - 2\nu_0}{2(1 - \nu_0)}}\sqrt{\frac{1 - \frac{2\nu_0 \zeta \Delta T}{1 - 2\nu_0}}{1 - \frac{2\nu_0 \zeta \Delta T}{2(1 - \nu_0)}}}, \tag{4.27}$$

where an infinitesimal increase of temperature ΔT has been considered. Also ζ is very small. We can apply linear approximations to the last term of the right-hand-side of the above equation. The linear approximations yield

$$c_t(T) = c(T)\sqrt{\frac{1 - 2\nu_0}{2(1 - \nu_0)}}\left(1 - \frac{\nu_0\zeta\Delta T}{1 - 2\nu_0}\right)\left(1 + \frac{\nu_0\zeta\Delta T}{2(1 - \nu_0)}\right) \tag{4.28}$$

If we neglect the $\zeta^2\Delta T^2$ terms and the higher order terms, the above equation can be approximated as

$$c_t(T) = c(T)\sqrt{\frac{1 - 2\nu_0}{2(1 - \nu_0)}}\left[1 - \nu_0\zeta\left(\frac{1}{1 - 2\nu_0} - \frac{1}{2(1 - \nu_0)}\right)\Delta T\right] \tag{4.29}$$

By defining χ as

$$\chi = \nu_0\zeta\left(\frac{1}{1 - 2\nu_0} - \frac{1}{2(1 - \nu_0)}\right), \tag{4.30}$$

and replacing $c(T)$ by Equation 4.22, the following equations can be obtained

$$\begin{aligned}
c_t(T) &= c_0(1 - \alpha_c\Delta T)\sqrt{\frac{1 - 2\nu_0}{2(1 - \nu_0)}}(1 - \chi\Delta T) & (4.31)\\
&= c_{0t}(1 - \alpha_c\Delta T)(1 - \chi\Delta T) & (4.32)\\
&\approx c_{0t}[1 - (\alpha_c + \chi)\Delta T] & (4.33)
\end{aligned}$$

From the above equation and Equation 4.23, we can see that α_c and α_{ct} can be directly related by

$$\alpha_{ct} = \alpha_c + \chi \tag{4.34}$$

where χ is defined by Equation 4.30. It is easy to check that χ is always positive. Thus, we can conclude that the temperature shear-wave-velocity coefficient (α_{ct}) is always greater than the temperature longitudinal-wave-velocity coefficient (α_c).

4.4 Experiments for tension case

A series of experiments was designed to take advantage of the temperature effects to evaluate adhesive bond degradation. The experiments were designed mainly for three purposes. The first purpose was to measure the temperature dependence of the longitudinal wave velocity in polymeric materials. The second purpose was to verify the strain-temperature correspondence principle. The third purpose was to use the temperature effects to evaluate the adhesive bond degradation. In the subsection that follows, the experimental procedure is explained in details.

4.4.1 Experimental procedure

First, experiments to show the temperature dependence of ultrasonic wave velocity in polymeric materials were conducted. The polymeric materials investigated included AB epoxy, DER epoxy system in two different compositions and FM73 adhesive films. Bulk samples in various dimensions were prepared for this study. As the most used couplant in immersion ultrasonic testing, temperature effects in water were also investigated.

After the parameters α_c and β in different polymeric materials were obtained from the above described tests, the second part of the experiments concentrated on the verification of the strain-temperature principle. In order to do so, mechanical testing was designed to obtain the stress-strain relation at reference temperature and obtain ϵ_0. The mechanical measurement at several temperatures was used to obtain η. After all the parameters were found, the strain-temperature correspondence was obtained.

The third part of the experiment applied the temperature effects to evaluate the adhesive bonds.

4.4.2 Experimental details

A. Fundamental experiments: Temperature dependence of ultrasonic wave velocity in water and polymeric materials

For all the experiments conducted in this section, both the transducer and specimen were immersed in water. Knowledge of the temperature dependence of the wave velocity in water is essential.

A target aluminum block was placed at a fixed distance from the transducer. The distance can be fixed at a known value. Because the water distance is known, the time of flight through the water path at different temperatures allows the calculation of the longitudinal wave velocity in water at different temperatures. The transducer used had a nominal center frequency of 5 MHz (Panametrics). The oscilloscope was a Tektronix $TDS520$.

An electric heater was used to heat up the water. A thermometer was used to measure the temperature. The experiment covered a temperature range from 20^0C to 50 ^0C. The temperature interval for each consecutive measurement was 5^0C.

For the moderate temperature range, it is also appropriate to assume that the velocity changes linearly with the temperature in water [43] [44]. A linear fit of the velocities at different temperatures yields the temperature-velocity coefficient in water. The α_c in water is $-1.5 \times 10^{-3} m/s/m/s/^0C$. As mentioned earlier, α_c in water is negative. This means that an increase in temperature is associated with an increase in wave velocity. At reference temperature $T_0 = 20^0C$, the velocity in
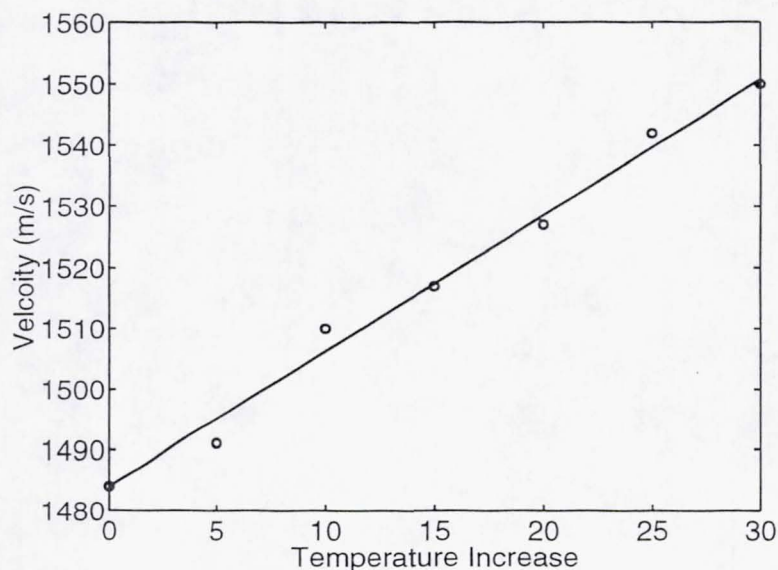
Figure 4.12: Velocity changes with temperature in water

water is $1484m/s$. At temperature 50^0C, it reaches $1550m/s$. Figure 4.12 shows the velocity in water at different temperatures as well as the best linear fit to those data. The velocity at given temperature T can be expressed as

$$c_w(T) = 1484[1 + 1.5 \times 10^{-3}(T - 20)] \qquad (4.35)$$

where the unit of $c_w(T)$ is in m/s. For a given water distance, the travel times can be calculated using the velocities obtained from above equation. Thus, by monitoring arrival time of the reflection from the the specimen front surface, the temperature can be determined. This provides a more convenient way to measure the temperature.

Now, we will turn our attention to the velocity measurement at different temperatures for polymeric materials. Consider that a bulk specimen is placed in water. The conventional method to obtain velocity information is to measure the time of flight through the specimen. Thickness information is obtained from another mea-

surement. The measurements become much more complicated when the sample is subjected to an additional factor, namely, temperature. The bulk sample will experience thermal expansion. If an extra measurement can be used to obtain the thermal expansion coefficient then appropriate corrections can be made. However, there will be cases where an extra measurement is not feasible. The question then is whether we can measure these two quantities simultaneously from ultrasonic data. If h_0 denotes the thickness of specimen at reference temperature T_0, the thickness at temperature T can be expressed as $h_0[1 + \beta(T - T_0)]$ after the thermal expansion is taken into account. Similarly, if c_0 represents the wave velocity of the specimen at reference temperature T_0, the wave velocity at temperature T can be obtained as $c_0[1 - \alpha_c(T - T_0)]$ by a linear approximation to Eq. 4.11. Thus the following equation can be obtained

$$\Delta t(T) = \frac{2h_0[1 + \beta(T - T_0)]}{c_0[1 - \alpha_c(T - T_0)]} \tag{4.36}$$

where $\Delta t(T)$ represents the time of flight at temperature T. We have discrete data for Δt at discrete temperatures. Through an error minimization, α_c and β can be simultaneously determined from a set of data obtained at different temperatures. So, the answer to the question stated above is in the affirmative.

The results obtained for $FM73$, AB Epoxy, DER Epoxy using this minimization are listed in Table 4.2.

The temperature dependence of the velocity for various materials is shown in Figure 4.13. The measurements were carried out using bulk samples. The transducer used was $2.25MHz$. Figure 4.13 has taken the thermal expansion into account. The

Table 4.2: α_c and β for three materials

Material	α_c $(10^{-3}km/s/km/s/^0C)$	β $(10^{-5}m/m/^0C)$
FM73	2.30	2.8
DER Epoxy (70-30)	3.40	5.2
DER Epoxy (50-50)	4.00	5.5
AB Epoxy	3.50	4.0

discrete values of the velocity are obtained from

$$c(T) = \frac{2h_0(1 + \beta\Delta T)}{\Delta t} \tag{4.37}$$

The lines are from

$$c(T) = c_0(1 - \alpha_c\Delta T) \tag{4.38}$$

where β and α_c were obtained by minimizing the error from the discrete data to fit Eq. 4.37.

It is clearly seen that the wave velocity in polymeric materials decreases with an increase of temperature. The dependence is different for different polymeric materials. For example, at 20^0C, both DER70-30 and DER50-50 have higher velocity values than FM73 has. However, when the temperature reaches 50^0C, FM73 has a higher velocity than both DER70-30 and DER50-50 have. Besides the usefulness of α_c in the strain-temperature correspondence, α_c itself can be used as an additional parameter to characterize the materials. It might yield more information of materials than the velocity can by itself.
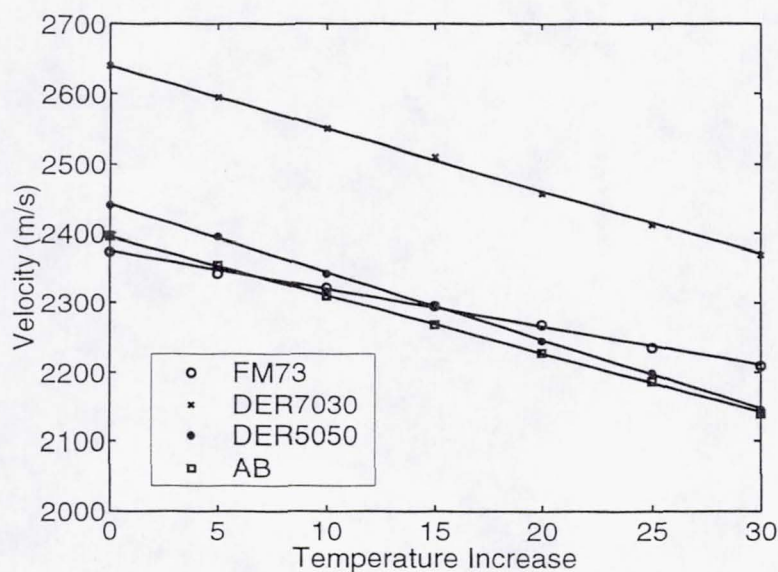
Figure 4.13: Temperature dependence of velocity for various materials. FM73 (circles), DER Epoxy 70-30 (x), DER Epoxy 50-50 (dots), AB Epoxy(squares)

B. Experimental verification of the strain-temperature correspondence principle

DER70-30 epoxy was selected for the experimental verification of the strain-temperature correspondence principle. Several dogbone specimens illustrated in Figure 4.14 were prepared to obtain the mechanical stress-strain relation. The dogbone specimens were made according to the recommended specification [45]. The dimensions of the specimens can be found in Figure 4.14. A strain-gauge method was implemented to measure the mechanical response. The strain rate was 0.02 in/min for the mechanical testing. Figure 4.15 shows the stress-strain relation for the DER70-30 specimen. A second order polynomial fit to that curve yields an ultimate strain of 3.26%.

In order to obtain the mechanical response at different temperatures, a dogbone specimen was used to obtain the stress-strain relation in the very initial linear region at different temperatures. The strain level was well under 0.3%. The reference
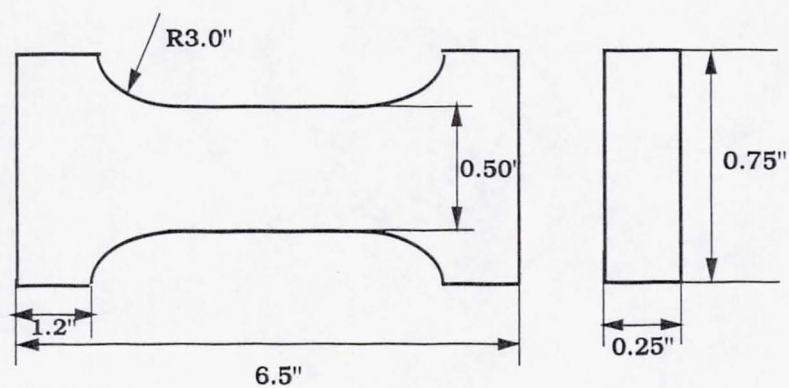
Figure 4.14: Dimensions of dogbone specimen
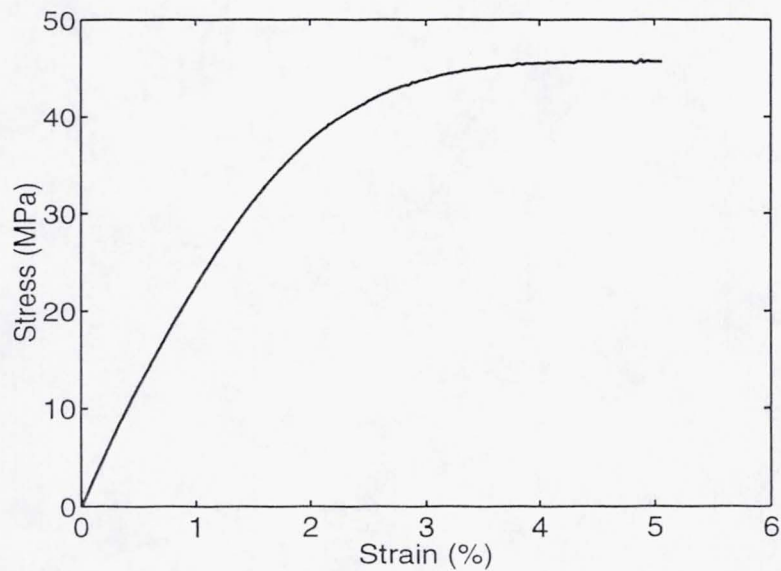
Figure 4.15: Stress-strain relationship at reference temperature 25^0 C for DER70-30 dogbone specimen
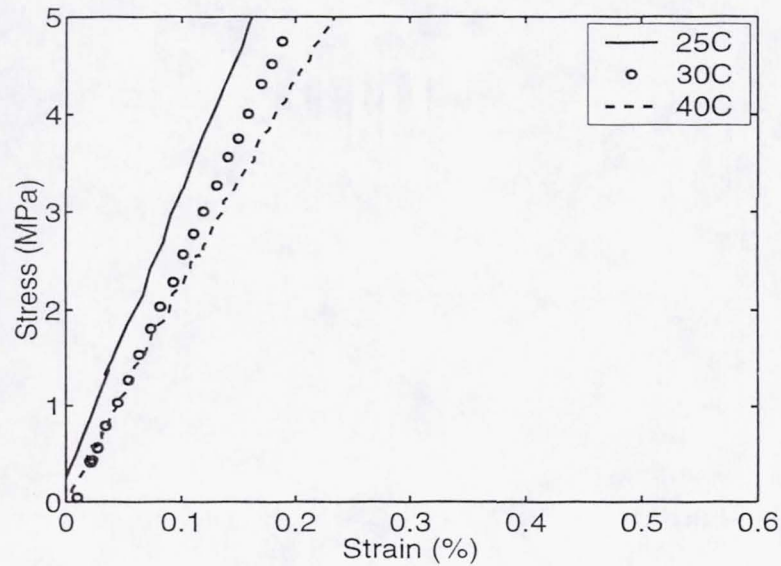
Figure 4.16: Different initial slopes of stress-strain relationship for DER70-30 dog-bone specimen

temperature was 25^0C. The other two temperatures were 30^0C and 40^0C. The experimental results for the DER70-30 Epoxy were plotted in Figure 4.16. After the very initial slopes were obtained at these three temperatures, the stress-strain curve in the full range (linear and nonlinear region) were obtained at the reference temperature.

Table 4.3 listed the measured initial slope of the stress-strain curve at different temperatures and the corresponding Lame constants calculated from the velocity values at the corresponding temperatures. The obtained parameter γ for each corresponding temperature is also listed in Table 4.3.

Figure 4.17 shows how the parameter γ changes with temperature. A linear fit according to Equation 4.12 yields the parameter η as 0.0096.

Now, we have all the parameters to define the strain-temperature correspondence

Table 4.3: Parameter γ at different temperatures

Temperature (^0C)	$\lambda + 2\mu$ (GPa)	C(T) (GPa)	Parameter γ (10^{-2} $1/^0C$)
25	7.5421	0.5727	7.59
30	7.2828	0.5386	7.40
40	6.7613	0.4407	6.52
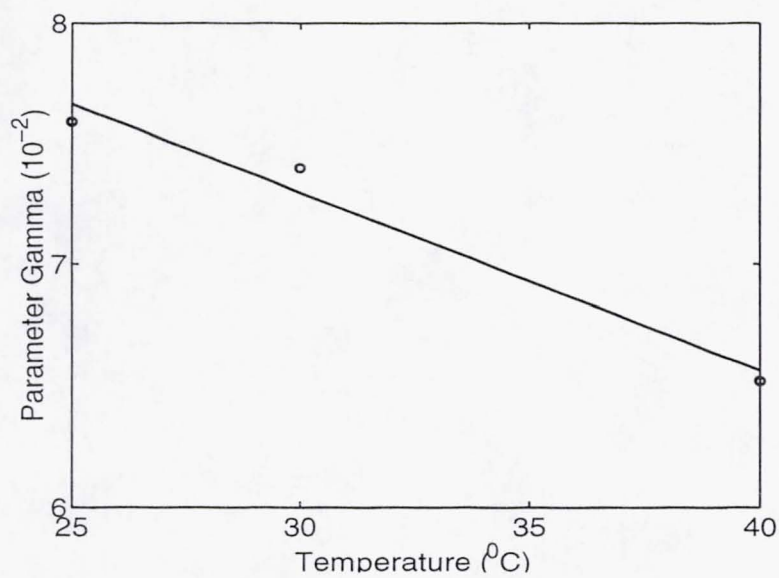
Figure 4.17: Parameter γ changes with temperature (circles: measured, line: best fit).
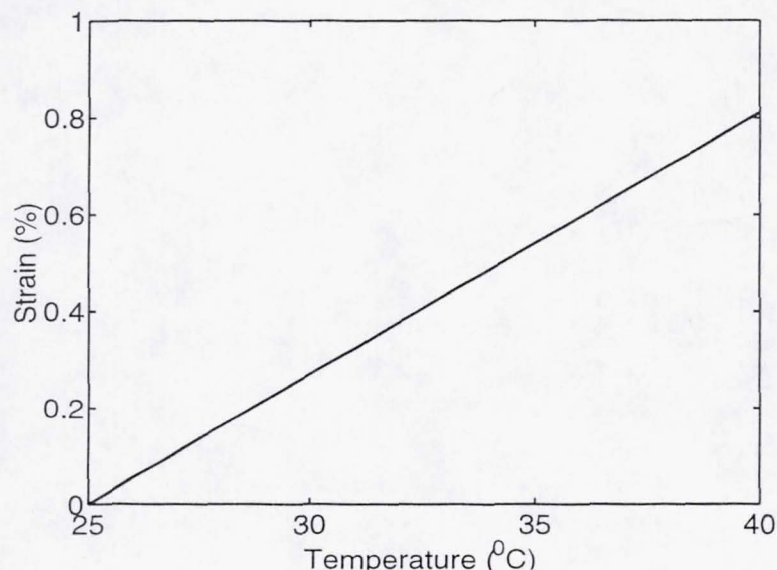
Figure 4.18: Measured strain-temperature correspondence relation (Using Eq. 4.17 and experimentally obtained parameters ϵ_0, α_c, and η.)

relation in Equation 4.17. The relation is plotted in Figure 4.18. By use of this relation, we can reconstruct the stress-strain relation using the ultrasonic data. A comparison of the mechanically obtained stress-strain curve and the reconstructed one is plotted in Figure 4.19. From Figure 4.19, we can see that two curves match well except for the very large strain region.

In this section, we have verified the strain-temperature correspondence and a stress-strain relation at reference temperature T_0 was obtained for DER70-30 epoxy.

C. Ultrasonic nondestructive evaluation of adhesive bond degradation

In order to simulate in-service fatigue, three-point-bending was selected to generate different severities of degradation in adhesive bond specimens. For some reason, DER epoxy adhesive bond specimens fail adhesively prior to the point when a change of α_c can be detected. Because the idea of the strain-temperature correspondence
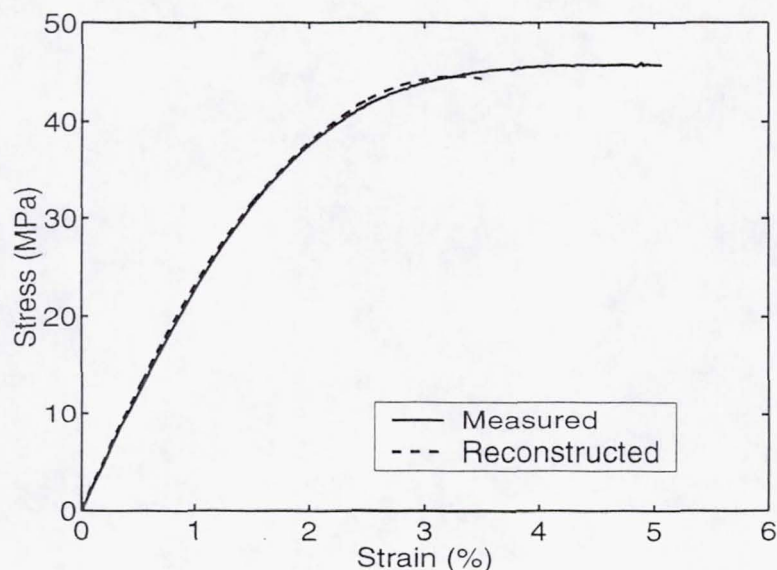
Figure 4.19: The comparison of the mechanically obtained stress-strain curve and the one reconstructed from the strain-temperature correspondence principle.

principle is to study the cohesive strength through the ultrasonic measurement of adhesive layer property, selection of this kind of adhesive bond is not appropriate for our study. Thus, we turned our attention to AB epoxy specimen.

The procedure of the experiment is as follows:

An AB adhesive bond specimen was cut into two pieces. One is kept as a reference specimen. The reference specimen was used to obtain the reference velocity-temperature relation (α_c). The other one was subjected to three-point-bending fatigue using a Instron machine. Prior to cycling, this specimen was also measured at different temperatures to make sure this specimen is comparable to the reference specimen. After that, a conventional C-Scan at room temperature was used to see if we can find any anomaly. Of course, if an original specimen is prepared, and it is in good condition, no anomaly is expected to be found. After a certain numbers of fatigue cycles, ultrasonic measurements were carried out again at different tem-

peratures for the fatigued specimen. After the ultrasonic measurements, we used a C-Scan to see if any damage can be detected. This loop continues until either we can find a change in α_c or the C-Scan can find an anomaly. The flowchart of this experiment is shown in Figure 4.20. In the flowchart, the **Temperature Effects** block contains two parts. The ultrasonic measurement at different temperatures for obtaining the α_c values at different fatigue stages is referred to as one part of the Temperature Effects block. The C-Scan at the elevated temperature to qualitatively observe the temperature effects is referred to the other part of the Temperature Effects block. The C-Scan at room temperature is referred to as the **Conventional Method**.

The specimens for this test were originally 2.25 by 1.5 in. The thickness was 0.75 in. They were cut into two pieces of the dimension of 2.25 by 0.75 in. If we select the maximum fatigue shear stress as 2.5 ksi, simple calculations [46] yield that the maximum load is around 3000 lbs. For the fatigue cycling, we used a half-sine waveform. The amplitude was -300 to -3000 lbs and the frequency was 5Hz.

The C-Scan system used was the Sonix Flexscan-C system. The transducer used for the C-Scan was a focused transducer with center frequency of 10MHz and diameter of 0.5 in.

For the ultrasonic measurements at different temperatures, a non-focused transducer of 5 MHz was used. In order to avoid edge effects in the ultrasonic measurements, the measurements were restricted to the middle region of the specimen.

Due to stress concentration at the edge of the specimens, most of the specimens failed at the edge before ultrasonic measurements at different temperatures can detect a change in α_c in the middle region.

First, we present a result when the damage was initiated at the middle region of the specimen (close to the long edge). Before 600K fatigue cycles, the methods described above could not detect any anomaly. After 600K fatigue cycles, the α_c value for the fatigued specimen was still the same as for the reference specimen. However, the C-Scan at 30^0C could spot some anomalies in the middle region (Figure 4.21(a)) of this specimen. After another 86K fatigue cycles, the reflected signal from the fatigued specimen at 20^0C was still essentially the same as from the reference specimen. However, at higher temperature, a change of the reflected signal was detected. This change yielded a larger α_c value of 0.0038 (compared to 0.0032 for the reference specimen). The elevated temperature C-Scan at this stage revealed an additional area of anomaly in the middle region (Figure 4.21(b)). At both 600K and 686 K fatigue cycles, the C-Scan at room temperatures did not indicate damage in the middle region. This was expected, because the waveforms from the deteriorated bond and non-deteriorated bond are the same at reference temperatures. After another 50K fatigue cycles, the specimen completely failed.

For both of the other two specimens, no change in α_c could be detected in the middle region before a C-Scan at room temperature could detect the failure at the edge. However, the results are still encouraging and show the utility of the temperature effects.

Figure 4.22 shows the waveform obtained from an adhesive bond that was not subjected to any fatigue. Figure 4.23 shows the waveforms obtained from an adhesive bond that was subjected to 612K fatigue cycles. From those waveforms, we may see that the deteriorated bond's waveform has a larger change from 20^0c to 40^0C. The α_c value in the middle region is 0.0043 for the deteriorated bond. The velocity versus
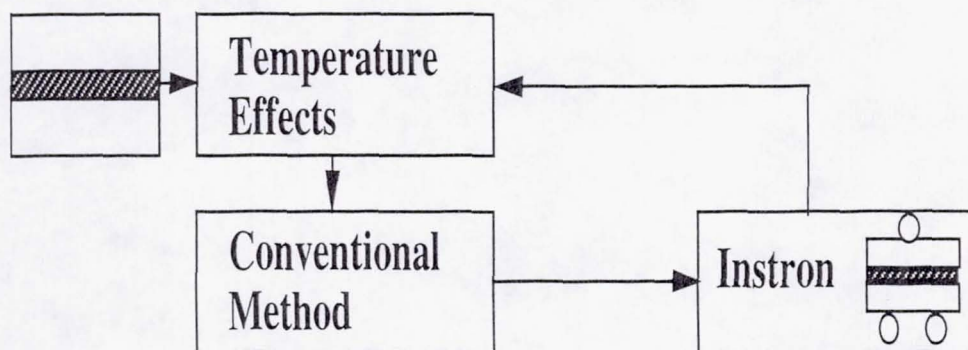
Figure 4.20: Flowchart of experiment to evaluate the adhesive bond degradation using temperature effects

temperature in the adhesive layer is plotted in Figure 4.24. The C-scan images at room temperature and an elevated temperature are shown in Figure 4.25. We can see that the elevated temperature can bring out the middle area which cannot be shown at room temperature.

For another adhesive bond specimen, no methods could detect any anomaly at 600 K fatigue cycles. After 806 K fatigue cycles, C-Scan images at both room temperature (Figure 4.26(a)) and elevated temperature (Figure 4.26(b)) show that the adhesive bond failed. It is of interest that the C-Scan image at an elevated temperature revealed an additional layer area of anomaly than the C-Scan at the room temperature.

Now, let us summarize and analyze the experimental results. First of all, before the C-Scan at room temperature can detect the damage in the middle region, an α_c increase was detected. The effective modulus versus temperature for different α_c values is plotted in Figure 4.27. If we relate a temperature to a strain, then the effective stress-strain curve can be plotted as shown in Figure 4.28. It is clearly seen that the larger the α_c value, the smaller the residual strength is. Thus, α_c can serve
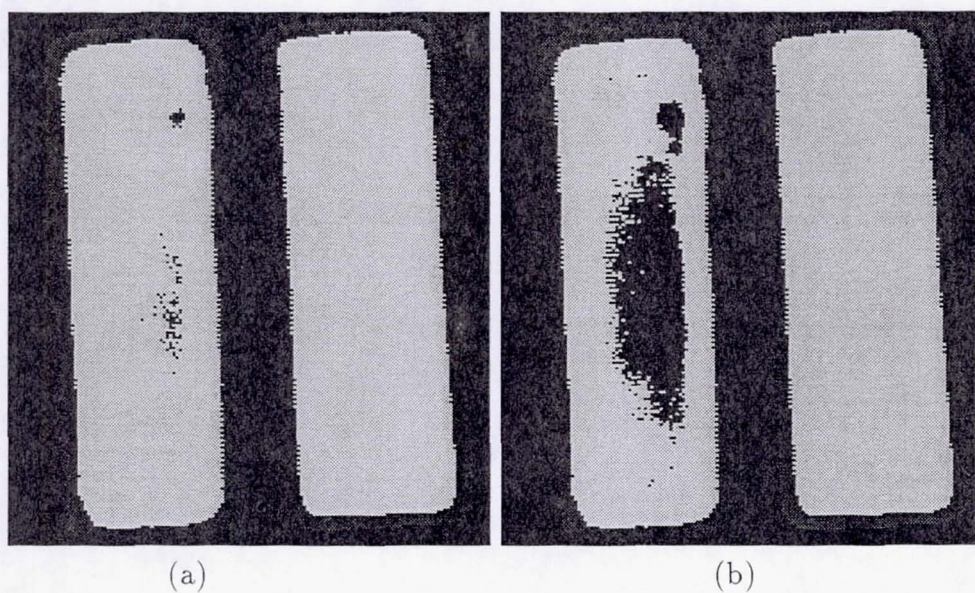
Figure 4.21: Ultrasonic C-Scan image comparison at an elevated temperature(30⁰C) at different fatigue cycles (a) 600K, (b) 686K.
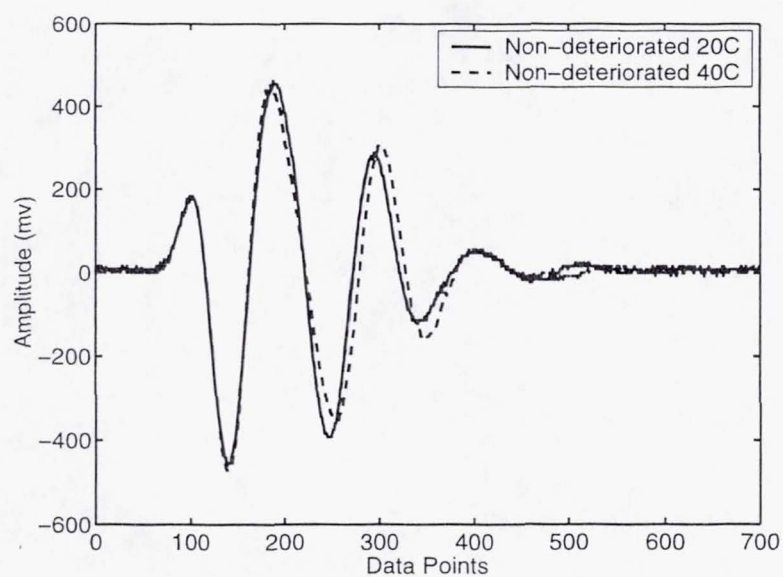
Figure 4.22: Adhesive bond's waveforms at different temperatures for non-deteriorated specimen
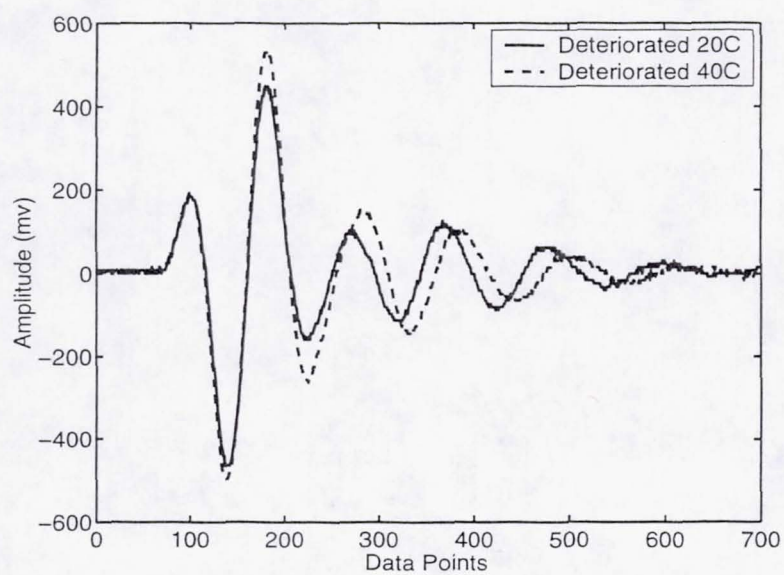
Figure 4.23: Adhesive bond's waveforms at different temperatures for deteriorated specimen
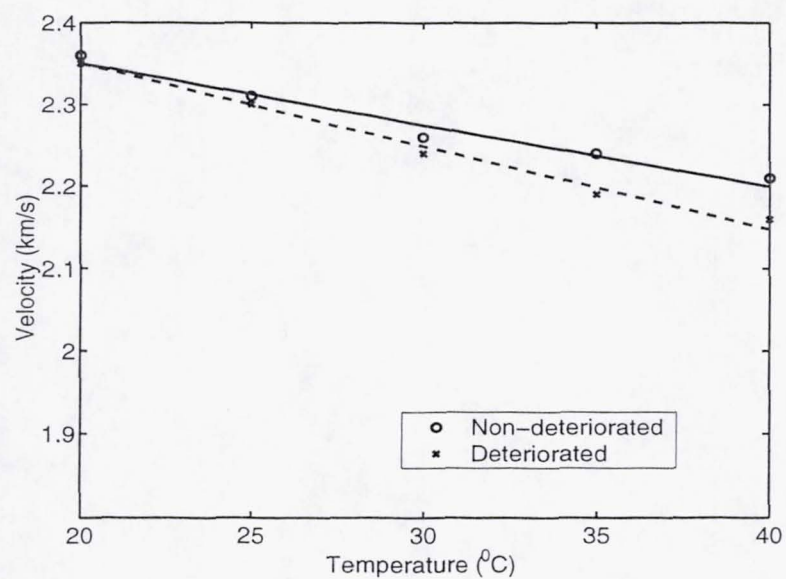
Figure 4.24: Adhesive layer's velocity temperature dependence (comparison for deteriorated and non-deteriorated specimen)

85
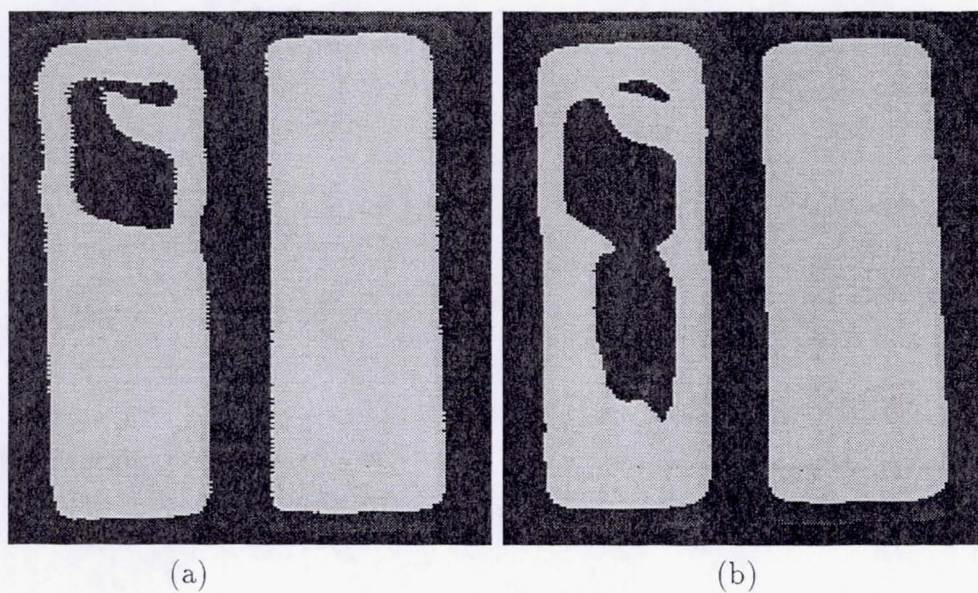
Figure 4.25: Ultrasonic C-Scan image comparison at (a) room temperature(20⁰C) and (b) an elevated temperature (30⁰C) for a specimen subjected to 612K fatigue cycles
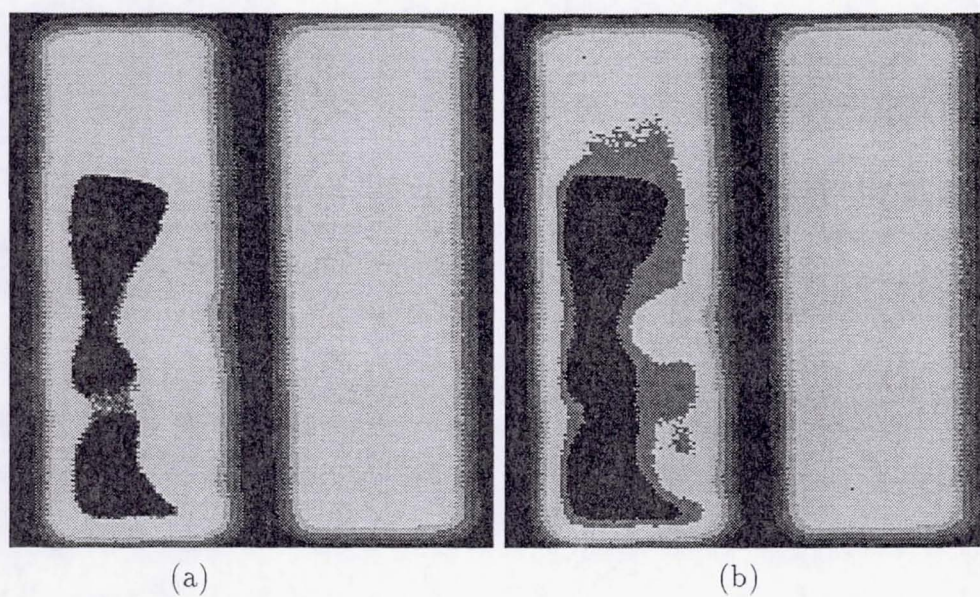
Figure 4.26: Ultrasonic C-Scan image comparison at room temperature(20⁰C) and an elevated temperature (30⁰C) for a specimen subjected to 806K fatigue cycles
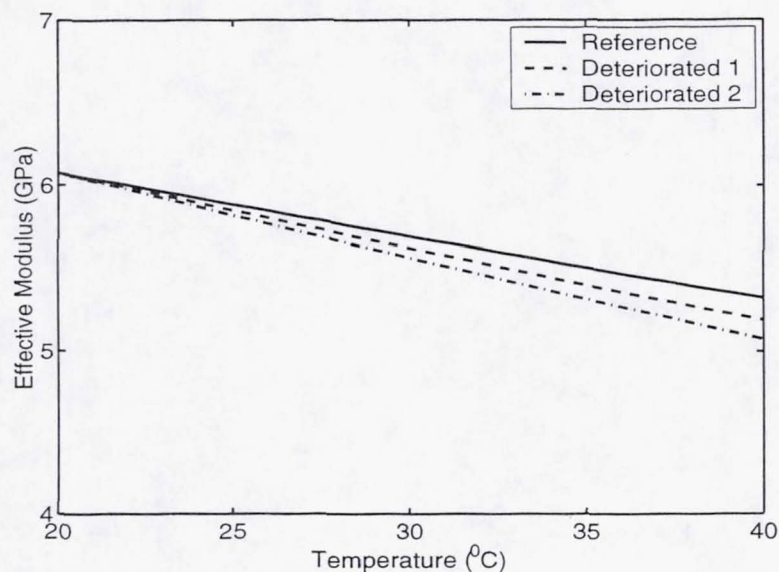
Figure 4.27: Effective modulus versus temperature for three different adhesive bonds with three different α_c values: Reference $\alpha_c = 0.0032$, Deteriorated 1: $\alpha_c = 0.0038$, Deteriorated 2: $\alpha_c = 0.0043$.

as a quantitative indicator for adhesive bond degradation evaluation. Qualitatively, the results are also encouraging. The C-Scan at an elevated temperature obviously yields more information than the C-Scan at room temperature. This is due to the fact that at an elevated temperature, the deteriorated bond's adhesive layer has a smaller velocity value, consequently has a larger acoustic impedance to contrast with the adherend. The C-Scan at elevated temperature can qualitatively display the temperature effects.

From this section, we may conclude that the α_c is a good indicator of the degradation. The C-Scan at elevated temperature can be applied to reveal more information regarding adhesive bond degradation than the conventional method can. The advantage of using the temperature increase can be schematically represented in Figure 4.29.
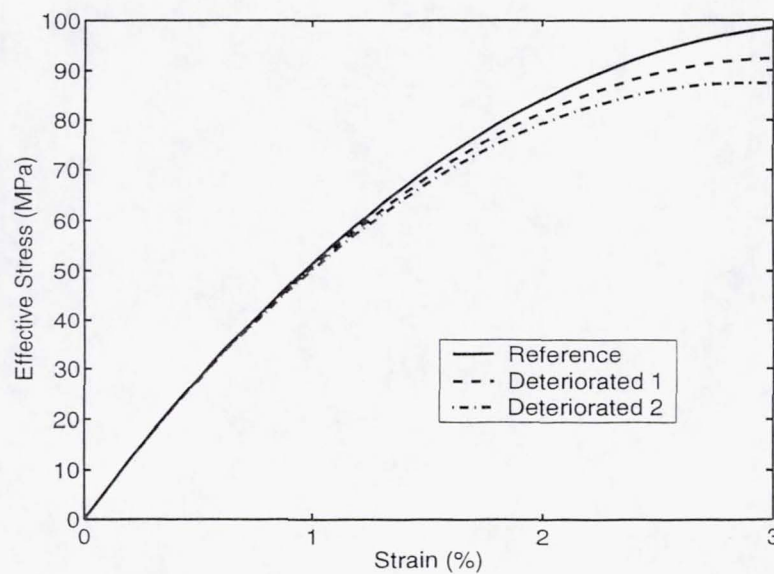
Figure 4.28: Effective stress-strain relation for three adhesive bonds with three different α_c values: Reference $\alpha_c = 0.0032$, Deteriorated 1: $\alpha_c = 0.0038$, Deteriorated 2: $\alpha_c = 0.0043$.
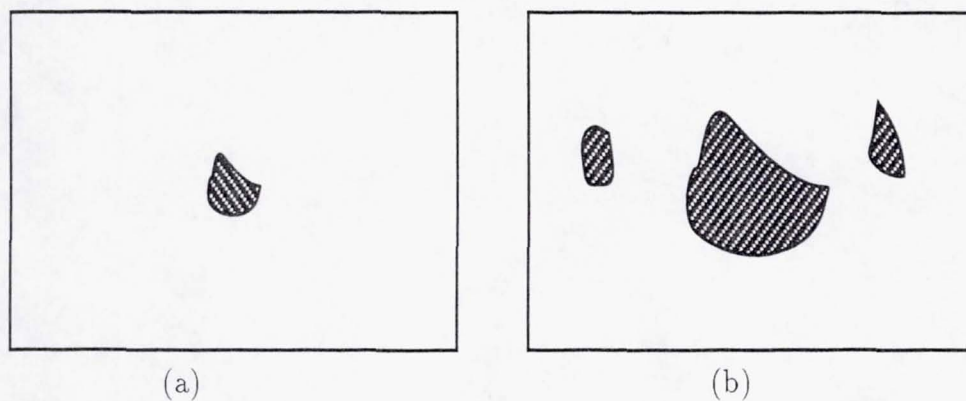
Figure 4.29: Advantage of elevated temperature C-Scan. (a) C-Scan image at room temperature, (b) C-Scan image at an elevated temperature.

4.5   Discussion

Based on experimental observations, a general strain-temperature correspondence principle has been proposed. This principle establishes a quantitative relation between the temperature and the mechanical strain. It can be used to study the adhesive bond degradation by increase of temperature at small strains instead of applying an external static loading. This principle shows potential in predicting the larger strain behavior from experimental data at increasing temperature in the linear region. By specifying particular forms of nonlinear stress-strain relations, explicit strain-temperature correspondences for both the tension and the shear case were established. It has been shown that the parameter α_c (α_{ct}) is more indicative of nonlinear stress-strain behavior. The wave velocity more appropriately characterizes the material stiffness at small strains.

It was indicated in Ref. [32] that the real and largely unanswered challenge to ultrasonic NDE for adhesive bond strength assessment is to define a single parameter or a set of parameters which determine the bond strength and which can be measured by an ultrasonic technique. Thus, the goal of the ultrasonic nondestructive assessment of adhesive bond strength becomes a matter of successfully finding parameters that are directly related to the nonlinear parameters of adhesive bonds. In earlier theoretical work, some degree of success has been achieved in Refs. [32] [33]. The principle presented in this chapter offers another step toward the realization of that goal. More importantly, the ultrasonic parameters that have to be determined, can conveniently be obtained by experimental measurements. It is possible that the principle has a more general applicability, and may be useful in other wave type formulations. It may be possible to find other wave parameters directly related to

nonlinear parameters of adhesive bonds.

A specific material was used to prove the principle. For other polymeric materials, the strain-temperature correspondences for both tension and shear case can be established in the same fashion. As long as the stress-strain behavior of the adhesive bond under investigation can be modeled in the form specified here, a deviation of α_c (α_{ct}) from the reference value should be an indication of a deviation of the adhesive bond nonlinear parameters, since theoretical relations showing that α_c (α_{ct}) is inversely proportional to ϵ_0 (ϵ_0^2) have been established.

In addition to the applicability of this principle to ultrasonic nondestructive evaluation of adhesive bonds, the principle should be useful in ultrasonic material characterization in general, especially when polymeric materials which are sensitive to temperature change are under consideration. The experiments in this chapter studied the temperature dependence of the longitudinal wave velocity of various polymeric materials. It was found that the temperature dependence is different for different materials, which means that different materials have different α_c values. A comprehensive survey of ultrasonic parameters that were used for NDE was given in [47]. It is worth noting that α_c itself may add another parameter to the ultrasonic NDE of materials in general (not particularly for adhesive bonds), especially when nonlinear behavior information is desired. For another particular example, α_c could provide a nondestructive measure to study the hygrothermal property of epoxy film adhesives in addition to the destructive testing described in [48]. Also, quantitative measurement of α_c may provide useful information for heat damage assessment of composite materials, which is still a very difficult problem to do.

The theoretical investigation of Section 4.3.4 concludes that the temperature

shear-wave-velocity coefficient (α_{ct}) is always greater than the temperature longitudinal-wave-velocity coefficient (α_c). A bigger α_{ct} means the drop with temperature of the shear wave velocity is bigger than the drop for the longitudinal wave velocity at a same elevated temperature. So, the approach will be more sensitive if the shear wave is used. In addition, for the shear wave case the additional term η is absent from the strain-temperature correspondence. The parameter α_{ct} is more directly related to shear strength which is more desirable for real applications. An obliquely incident longitudinal wave can be converted into a shear wave, thus a pitch-catch mode may be well suited for adhesive bond evaluation. In addition, by simultaneous application of longitudinal and shear waves, information regarding η can be derived, because η is essentially a function of Poisson's ratio [49].

From the practical point of view, it is interesting to see that even a 10^0C increase in temperature can yield some additional useful information regarding adhesive bond degradation. If a uniform heating method is implemented, by simply increasing the temperature, a C-Scan at an elevated temperature can be used to the real application. Due to the presence of air bubbles on the specimen surface at higher temperatures, the elevated temperature C-Scan was limited to a maximum temperature of 30^0C. If a suitable couplant free of air bubbles is used, better results can be expected at higher temperatures. Furthermore, based on the fact that the temperature shear-wave-velocity coefficient (α_{ct}) is always greater than the temperature longitudinal-wave-velocity coefficient (α_c), the application of shear waves at an elevated temperature should yield even better results.

4.6　Conclusions

For both the tension and shear cases, the nonlinear parameters of an adhesive bond have been quantitatively related to ultrasonic parameters through a strain-temperature correspondence principle. It has been shown that the temperature velocity coefficients which quantify the relations between the wave velocities and the temperature are a quantitative measure of the wave velocity change with temperature are indicative of nonlinearity. While the strain-temperature correspondence principle shows the potential to quantitatively evaluate the residual strength of adhesive bonds, the safest conclusions we can make at this point are: 1) the temperature change has been proven to be a good alternative to static loading as the external factor to evaluate the adhesive bond degradation, 2) the α_c is a quantitative measure of nonlinearity, and consequently a good indicator of adhesive bond degradation, and 3) the results presented in this chapter suggest that the C-Scan at an elevated temperature can be used to reveal more information on adhesive bond degradation.

Chapter 5

Determination of Ultrasonic Parameters of an Adhesive Bond Using Reflected Waveform Data

5.1 Introduction

An ultrasonic signal reflected from a material or a structure contains a lot of useful information. In addition to the inherit transducer and couplant responses, the nature of the material or structure that the ultrasound traverses determines the signal. Thus, quantitative evaluation of material properties through a correlation of received signals and the properties of materials is in many cases possible. Indeed, a lot of information of a received signal can be utilized to characterize a material. The time of flight is used to determine the wave velocity and then this velocity is correlated to material properties [11,50-51]. The velocity measurement is also used in the curing monitoring of epoxy resins [51-54]. The transit time of a signal through a thin adhesive layer can serve as an important parameter in the evaluation

92

of the bond cohesive strength [55-57]. The change of amplitude of the signal is also a commonly used parameter to study the interface of two joined materials such as adhesive bonds, diffusion bonds and welding. Attenuation is used to evaluate properties of materials such as the porosity [58-59]. When ultrasound is traveling through a layered structure, spectrum analysis is used to characterize the thicknesses by analyzing the resonance frequency [12,56,60-61].

In this chapter, determination of the ultrasonic parameters of an adhesive bond using the reflected waveform data is investigated. For an adhesive bond, the reflected signals are very complicated due to the fact that 1) the ultrasonic signals experience multiple reflections inside the thin layer, 2) the multiple reflections can not be separated because the transit time of the layer is very small, and the observed reflected signal is the superposition of multiple reflections. Because the layer is very thin, there will be no resonance frequency observed for the moderate range of frequency (5-10MHz). Thus, conventional spectrum analysis is not applicable in this case. In this chapter, we first establish a theoretical relation between the incident pulse and reflected waveform from an adhesive bond. This relation is then used to show how the parameter changes affect the reflected waveform. Then an error minimization scheme is proposed to extract the parameters that characterize an adhesive bond. In the last sections of this chapter, the error minimization scheme is applied to real applications.

5.2 The formation of the complicated waveform reflected from an adhesive bond

In order to extract the ultrasonic parameters that characterize an adhesive bond, it is essential to understand how the complicated waveform from an adhesive bond is formed. From this understanding we can define the parameters that can fully characterize an adhesive bond. We know that a complicated waveform is formed because of the multiple reflections at the thin layer; however, it would be useful to establish a theoretical relation between the incident pulse and the reflected waveform.

5.2.1 Relation between the incident pulse and the waveform reflected from an adhesive bond

If a pulse $f(t)$ is incident on an adhesive bond, a complicated signal $g(t)$ will be returned due to the multiple reflections from the adhesive layer. The purpose of this section is to establish a theoretical relation that can quantitatively relate $g(t)$ to $f(t)$. We first use an incident harmonic wave to study the multiple reflections at the layer to obtain the reflection function. This function can be later used to relate the complicated waveform reflected form an adhesive bond to the incident pulse.

A unit plane harmonic wave propagating in the positive x direction in a nonattenuating purely elastic medium can be represented by

$$u(x,t) = e^{i(\omega t - kx)}, \tag{5.1}$$

where u represents the displacement, ω represents the angular frequency, k is the wave number, and x and t specify the coordinates in space and time.

Consider a layered structure as shown in Figure 5.1, where layer 2 is an adhe-
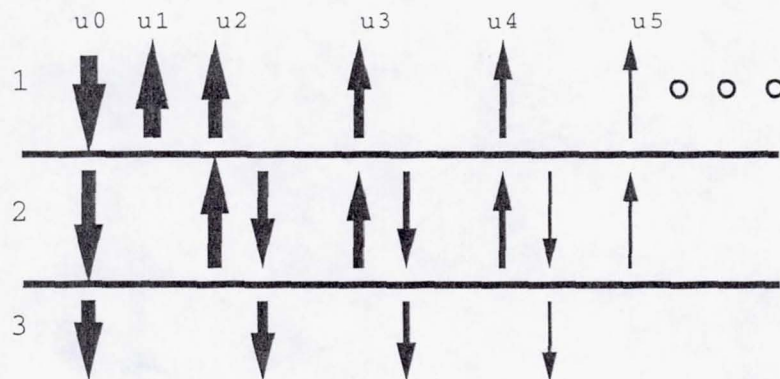
Figure 5.1: Schematic of ultrasonic wave multiple reflections at a thin layer

sive layer. For an incident harmonic wave from material 1, a number of reflected harmonics come back. The individual reflections can be expressed by the following infinite series

$$u_1(x,t) = R_{12}e^{i(\omega t + k_1 x)} \tag{5.2}$$

$$u_2(x,t) = T_{12}R_{23}T_{21}e^{i(\omega t + k_1 x - 2k_2 h)} \tag{5.3}$$

$$u_3(x,t) = T_{12}R_{23}R_{21}R_{23}T_{21}e^{i(\omega t + k_1 x - 4k_2 h)} \tag{5.4}$$

$$\cdots \qquad \cdots$$

$$u_n(x,t) = T_{12}R_{23}{}^{n-1}R_{21}{}^{n-2}T_{21}e^{i(\omega t + k_1 x - 2(n-1)k_2 h)} \tag{5.5}$$

$$\cdots \qquad \cdots$$

where $R_{ij}(i=1,2, j=1,2,3)$ denotes the reflection coefficient at the ij interface for waves incident from the i side. T_{12} denotes the transmission coefficient at interface 12 for waves incident from material 1, and k_i $(i=1,2)$ is the wave number in material i. The total reflected displacement caused by the incident harmonic wave

is

$$u^r(x,t) = \sum_{n=1}^{\infty} u_n(x,t) \tag{5.6}$$

This infinite series can be summed by virtue of

$$|e^{i(\omega t - kx)}| \leq 1 \tag{5.7}$$

It follows that Equation 5.6 can be rewritten as

$$u^r(x,t) = \left[R_{12} - \frac{T_{12}T_{21}R_{23}e^{-2ik_2h}}{1 - R_{12}R_{23}e^{-2ik_2h}} \right] e^{i(\omega t + k_1 x)} \tag{5.8}$$

For the simple case where materials 1 and 3 are identical, the above equation can be simplified as (by noting that $R_{21} = -R_{12}$ and $T_{12}T_{21} = 1 - R_{12}^2$)

$$u^r(x,t) = \left[R_{12} - \frac{(1 - R_{12}^2)R_{12}e^{-2ik_2h}}{1 - R_{12}^2 e^{-2ik_2h}} \right] e^{i(\omega t + k_1 x)} \tag{5.9}$$

As far as the attenuation in the adhesive layer is concerned, we can replace k_2 by a complex number $k_2 = k_2'(1 - i\alpha)$, where α is the attenuation per wavelength. Taking into account that $k_2' = \omega/c$, $\Delta t = 2h/c$ (c is the wave velocity in the thin adhesive layer, h is the thickness of the adhesive layer, and $\Delta t/2$ is the **transit time**) and replacing R_{12} by r, R can be expressed as a function of ω, Δt, and α as

$$R(\omega, r, \alpha, \Delta t) = r - \frac{(1 - r^2)re^{-(i+\alpha)\omega\Delta t}}{1 - r^2 e^{-(i+\alpha)\omega\Delta t}} \tag{5.10}$$

Now we can relate the reflected signal $g(t)$ to the incident pulse $f(t)$ by the following relation in terms of the discrete Fourier transform and the discrete inverse Fourier transform

$$g(t_i) = DIFT[R(\omega_i)DFT(f(t_i))] \tag{5.11}$$

For the case that is discussed here (material 1 and material 3 are identical), we can write down the reflection coefficients for different arrivals as follows

$$R_1 = r \tag{5.12}$$

$$R_n = -r^{2n-3}(1-r^2)e^{-(n-1)(i+\alpha)\omega\Delta t}, n > 1 \tag{5.13}$$

The arrival of signals in the time domain can be calculated using the discrete inverse Fourier transform

$$g_n(t_i) = DIFT[R_n(\omega_i)DFT(f(t_i))], n = 1, 2, 3, ... \tag{5.14}$$

From this theoretical analysis, it can be seen that if the three parameters [reflection coefficient (r), attenuation coefficient (α) and transit time $(\Delta t/2)$] are defined, the reflected signal will be defined. Thus the three parameters characterize an adhesive bond.

5.2.2 A Gaussian pulse incident on a fictitious thin layer

This section will show how a complex waveform is generated when a Gaussian pulse is incident on a thin layer. Figure 5.2 shows a Gaussian-modulated sinusoidal pulse. It is considered an acceptable simulation of a real pulse. This Gaussian RF pulse with a 10.0 MHz center frequency and 90% bandwidth is sampled at a rate of 1 GHz (the sampling interval is 1 ns). The pulse is truncated when the envelope falls $50dB$ below its peak. The fictitious adhesive layer has a reflection coefficient for the first reflection of r of 0.72. The reflection coefficient for an aluminum/epoxy interface is close to this value. The attenuation coefficient is assumed to be 0.03. Three transit times are considered: 30, 35 and 40ns, respectively. With designated r, α and transit time values, the reflection function in Equation 5.10 is defined. By the application of Equation 5.11, the reflected signal can be generated. Figure 5.3 plots three reflected signals for the three above described adhesive bonds. As illustrated in Figure 5.3, the waveform features can be quite different for the three transit
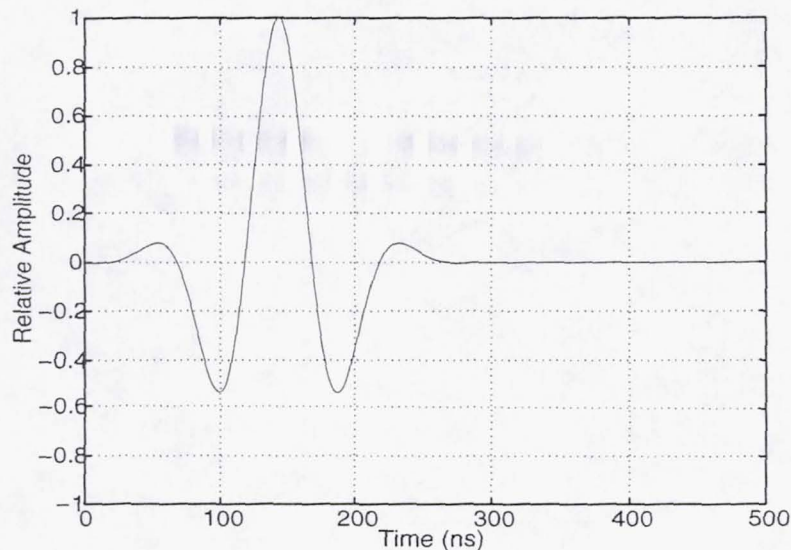
Figure 5.2: An incident Gaussian pulse with center frequency $10MHz$ and 90 % bandwidth

times. Figure 5.4 shows that a very small variation in transit time (40 and 41 ns) can result in a small change of reflected waveform. These illustrations suggest that a further understanding of the waveforms is desirable.

As discussed earlier, with the knowledge of the ultrasonic parameters we can simulate different arrivals in the time domain by application of Equation 5.14. For the fictitious adhesive layer with a transit time of 40 ns, the simulated first three arrivals are plotted in Figure 5.5(a) to (c). Figure 5.5(d) shows the comparison of the complete signal and the summation of the first three arrivals. The first arrival is the direct reflection from the top adherend/adhesive interface. The second arrival is the one after the ultrasonic wave is transmitted at the top interface, travels through the whole layer thickness, then reflects at the bottom interface, and then is transmitted into the top adherend. The third arrival has experienced one more reflection at the top interface and the bottom interface. The first three arrival approximation of the
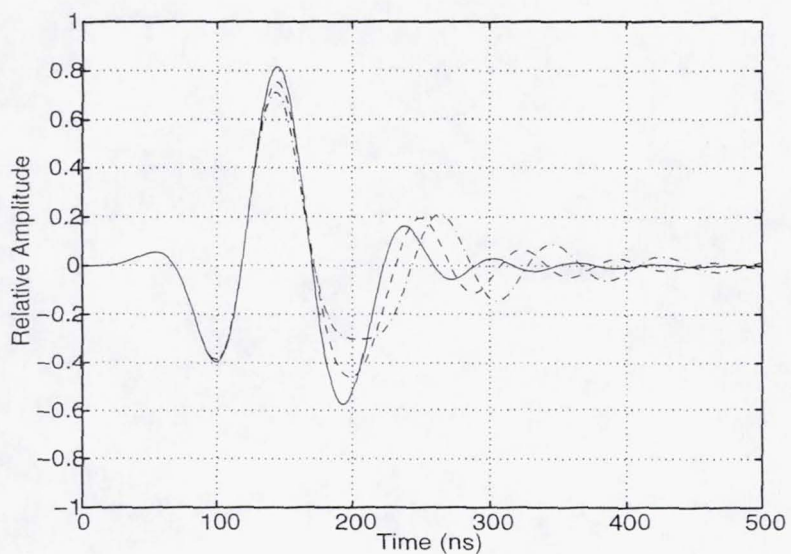
Figure 5.3: Signals reflected from different fictitious layers which have the same reflection coefficient ($r = 0.72$), the same attenuation coefficient ($\alpha = 0.03$), and different transit time (solid line $30ns$, dashed line $35ns$, dotted line $40ns$)
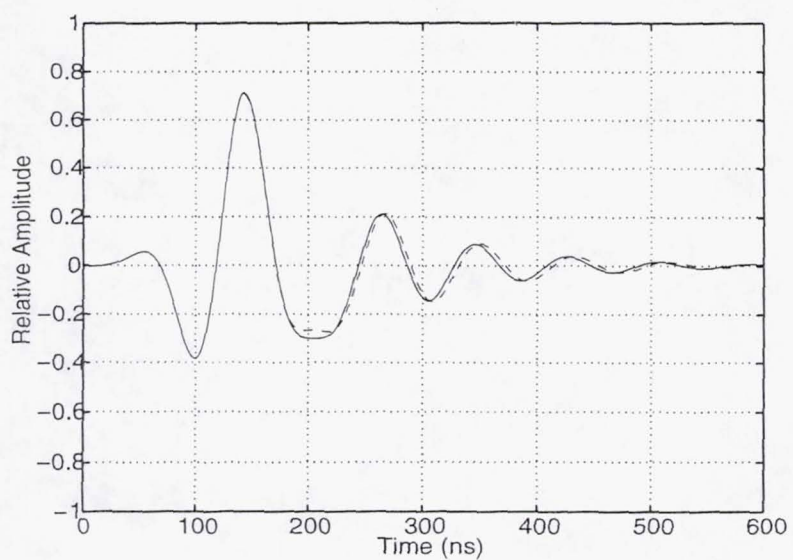
Figure 5.4: Signals reflected from two different fictitious layers with a very small variation of the transit time (solid line $40ns$, dashed line $41ns$)
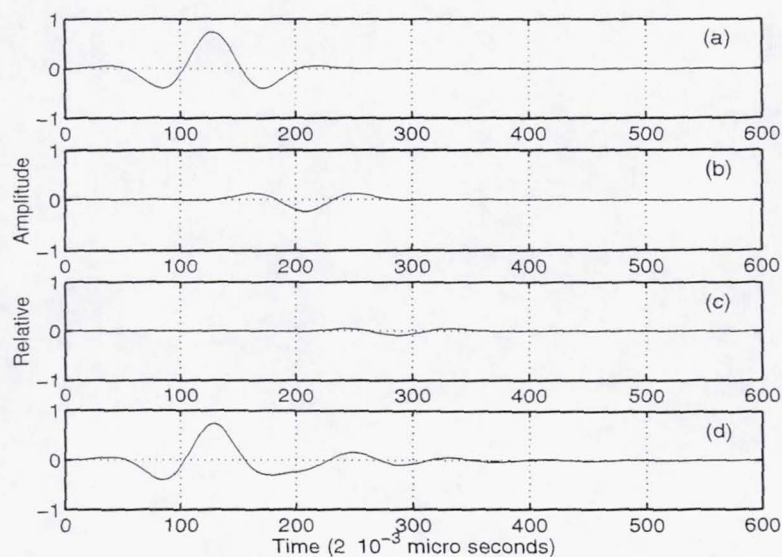
Figure 5.5: Individual reflected signals of different arrivals superimpose to a complex waveform. (a) first arrival, (b) second arrival, (c) third arrival, (d) comparison of complete waveform and the summation of the first three arrivals (solid: complete signal, dashed: summation of the first three arrivals)

total waveform can be very accurate by noting that the third arrival has a very small amplitude (the fourth is even smaller). The time delay of each consecutive arrival is clearly shown in the figure. The time delay that appears in this figure is twice the transit time we defined earlier. In this case, the time difference for each consecutive plot is 80 ns.

Using a Gaussian incident pulse, we have shown in this section that the three parameters (r, α, transit time) define the reflected waveform feature. It has been shown that the complicated waveform is the result of superposition of different arrivals that can not be separated.

5.3   Determination of ultrasonic parameters

In the previous section, it has been demonstrated that the three parameters can define complicated waveform features. It is shown that the different arrivals super-impose to a complicated waveform. In actual applications we do have a received complicated waveform. The question then is: can we obtain parameters from the measured waveform? The solution to this question is important. In the remainder of this section, we propose an error minimization algorithm to extract the useful parameters and then discuss some detailed examples.

5.3.1   The parameter determination algorithm

The algorithm for the parameter determination adopted here is the standard Simplex multiple parameter minimization algorithm [62]. In the multiple parameter minimization, the error function definition is crucial. The error function is in a normalized form in the frequency domain. The error function is defined as

$$\epsilon(r, \alpha, \Delta t) = \frac{1}{N} \sum_{i=1}^{N} |G(\omega_i) - R(\omega_i, r, \alpha, \Delta t) F(\omega_i)| \qquad (5.15)$$

where $G(\omega_i)$ and $F(\omega_i)$ represent the discrete Fourier transforms of the reflected signal $g(t)$ and incident signal $f(t)$, respectively. This form of the error function has an obvious advantage over comparing the absolute spectra, since this particular form also takes the phase into account.

Given a physically meaningful initial guess of the three parameters, the iteration algorithm generates a set of parameters (r, α and the transit time) that characterize the adhesive bond. Once the parameters are obtained, we can use Equation 5.11 to simulate the reflected signal and compare it with the measured one to check the

accuracy of the obtained results. In cases where different arrivals need to be known, different arrivals can be calculated by the application of Equation 5.14 using the parameters that have been obtained.

5.3.2   Detailed examples of parameter determination

We will use two adhesive bond specimens as examples to show how the error minimization scheme works. The adhesive bond studied in this section is made of FM73 thin adhesive film which is widely used in the aerospace industry because of its many attractive properties. The adherend used was 6061 aluminum sheet that was 1.5×1.5 in in size with uniform thickness of 0.5 in. The aluminum surfaces were cleaned using acetone and MEK solvent was used to remove the grease and dirt. The joints were cured in a vacuum at $250^0 F$ and 35 psi for 2.5 hours. The adhesive layer of sample #1 was made of 5 layers of FM73 adhesive thin film. The adhesive layer in sample #2 was made of one layer of the thin film.

The ultrasonic signals were digitized in a specified sampling interval by a digitizing oscilloscope. The signals were acquired using a transducer with nominal center frequency of $10 MHz$. For the measurement of sample #1, the sampling frequency was 0.5 GHz (sampling interval is 2 ns). The reflected signal from the aluminum/air interface is a most straightforward choice of the incident signal.

First, we will present the results for sample #1. Figure 5.6 shows three measured signals reflected at three different positions in sample #1. It is evident that the signals are quite different.

The optimized parameters (r, α and transit time) for each position using the optimization algorithm are listed in Table 5.1.
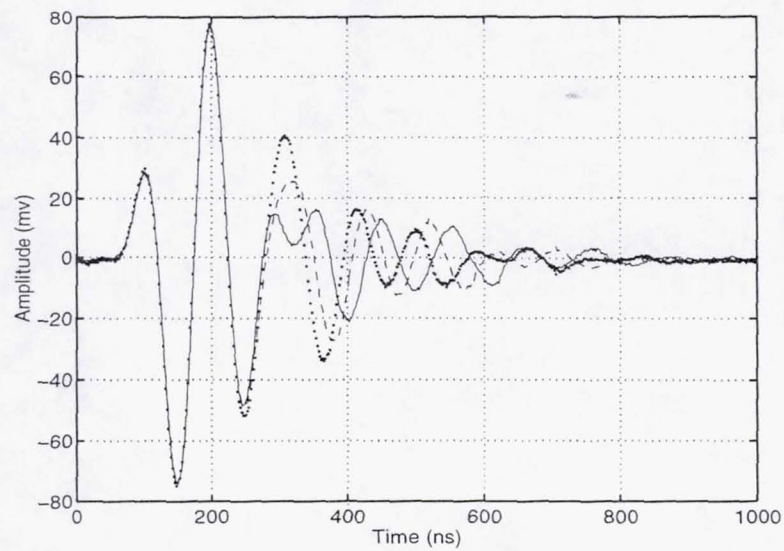
Figure 5.6: Reflected signals for sample #1 at three different positions with different thicknesses

Table 5.1: Optimized parameters and deduced quantities for sample #1.

Location	r	α	transit time (ns)	$h(\mu m)$	$h_m(\mu m)$
#1 − 1	0.720	0.0324	102	242.76	240.56
#1 − 2	0.723	0.0304	92	218.96	212.80
#1 − 3	0.724	0.0229	86	204.68	201.98

Figure 5.7: Reconstructed results for reflected signal for position 1. Top: Comparison of the measured and the calculated signal. Bottom: First three arrivals.

After the parameters are obtained, we can reconstruct the simulated signals and different arrivals using Equation 5.14.

Figures 5.7- 5.9 show the reconstructed results for the three signals. For each signal, the top plot shows the comparison of the total reflected signal (solid line) and the calculated complete signal using the obtained parameters. The three plots that follow show the first, second and third arrivals, respectively. For these three positions, good agreement of the measured signal and the calculated signal has been achieved.

Figures 5.10- 5.12 show the frequency spectra for the three total signals with corresponding simulated spectra. In the three cases, the simulated spectrum and the measured spectrum match very well. The resonant frequency is exactly the same for the simulated spectrum and the measured spectrum. These results verify that the parameters have been accurately determined.
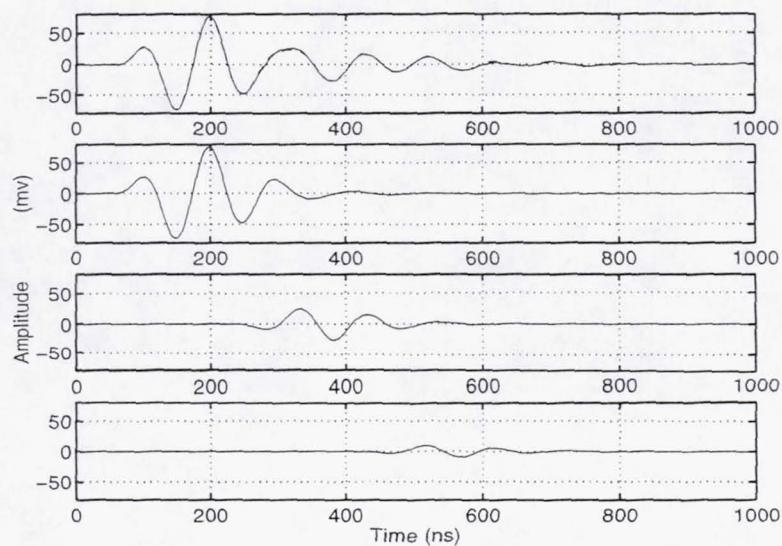
Figure 5.8: Reconstructed results for reflected signal for position 2. Top: Comparison of the measured and the calculated signal. Bottom: First three arrivals.
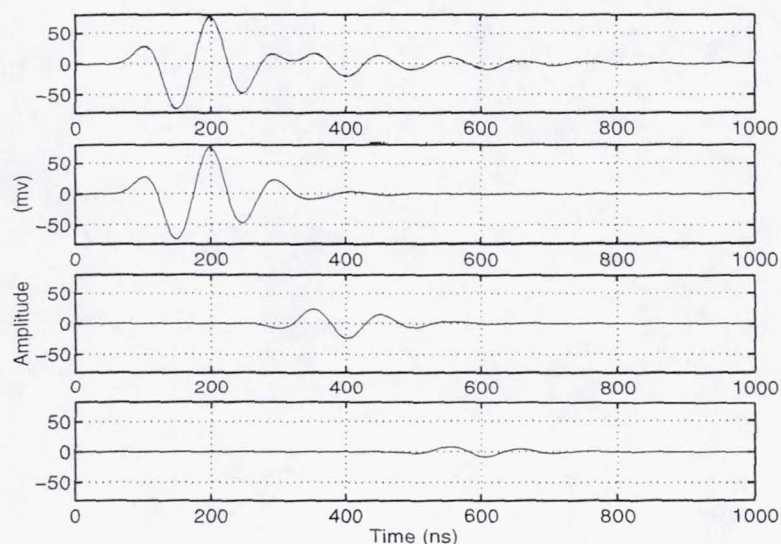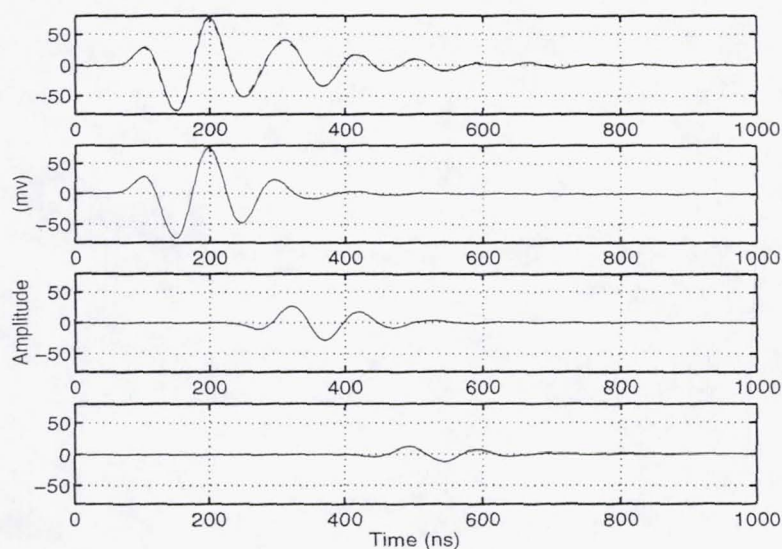

Figure 5.9: Reconstructed results for reflected signal for position 3. Top: Comparison of the measured and the calculated signal. Bottom: First three arrivals.
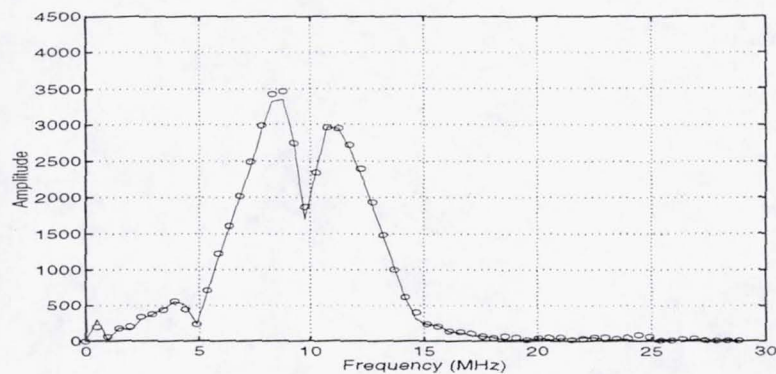
Figure 5.10: Simulated spectrum (solid line) versus the measured spectrum (circle points) for position 1.
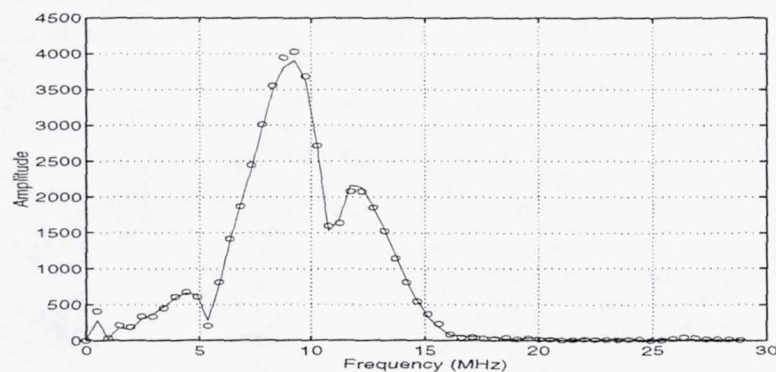
Figure 5.11: Simulated spectrum (solid line) versus the measured spectrum (circle points) for position 2.
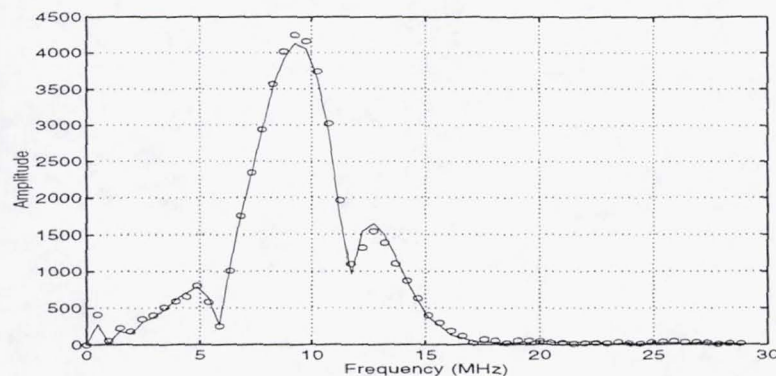
Figure 5.12: Simulated spectrum (solid line) versus the measured spectrum (circle points) for position 3.

Table 5.2: Different arrival times for different transit times (all units in ns).

Transit time	Δt	First arrival	Second arrival	Third arrival	Fourth arrival
51	102	0	102	**204**	306
102	204	0	**204**	408	**<u>612</u>**
153	306	0	306	<u>**612**</u>	918

Now let us look at the error behavior. Figure 5.13 is the error surface for two parameters: transit time and reflection coefficient (r). From that error surface several observations can be made. First, the convergence in the transit time direction is very good. Secondly, there is more than one minimum in the error surface. Only the strongest minimum corresponds to the optimized parameter set.

Figure 5.14 is the contour plot using the same data for which Figure 5.13 is generated. The figure clearly shows that the three minima are associated with three evenly spaced transit times. These three minima have different values of r. The explanation for these three minima seems simple. The middle minimum which has the smallest error in the error surface is the strongest minimum. It is associated with the optimal parameter set. The expected different arrival times for different transit times are listed in Table 5.2. From that table, it is not difficult to see that: 1) for the transit time $51ns$, the third arrival ($204ns$) matches the "true" second arrival ($204ns$), and 2) for the transit time $153ns$, the third arrival ($612ns$) matches the "true" fourth arrival ($612ns$).

Figure 5.15 plotted the comparisons of the measured signal and the reconstructed signal using the parameters corresponding to the other two error minima. From Figure 5.15, it is seen that if we use the parameter values that correspond to the other two minima, the simulated signal deviates too much from the measured signal.
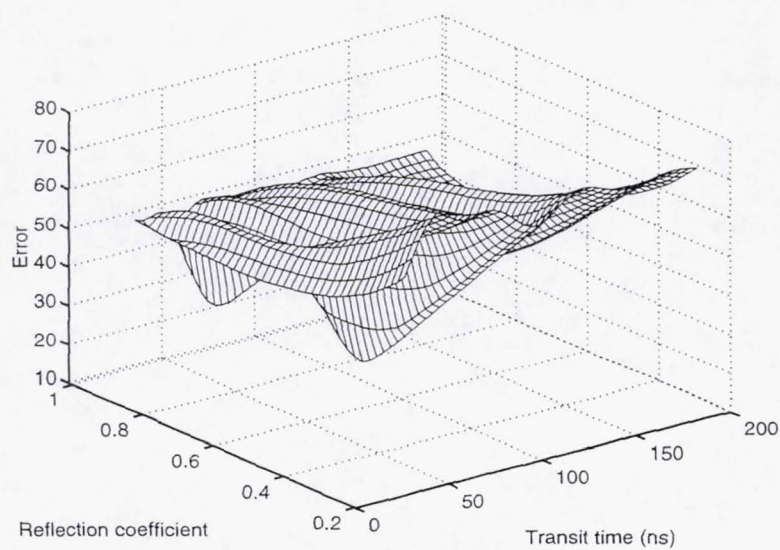
Figure 5.13: Error surface for reflection coefficient and transit time, generated using signal from position 1.
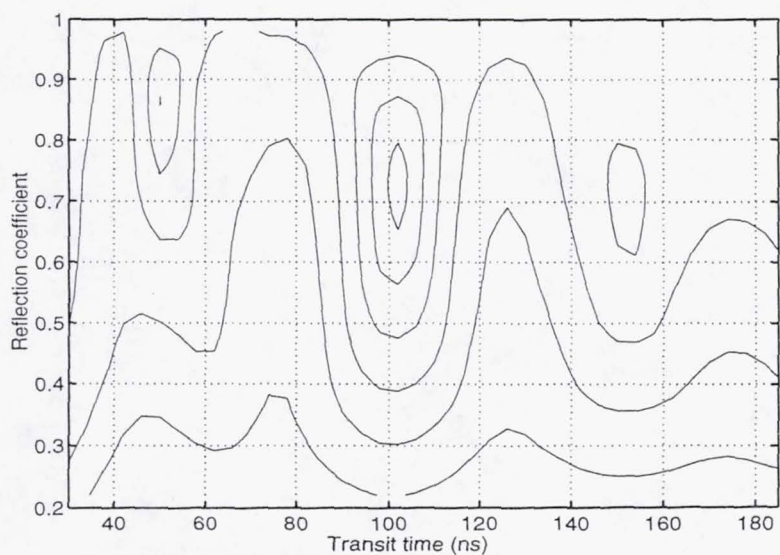
Figure 5.14: Contour plot of error function for reflection coefficient and transit time, generated using signal from position 1.
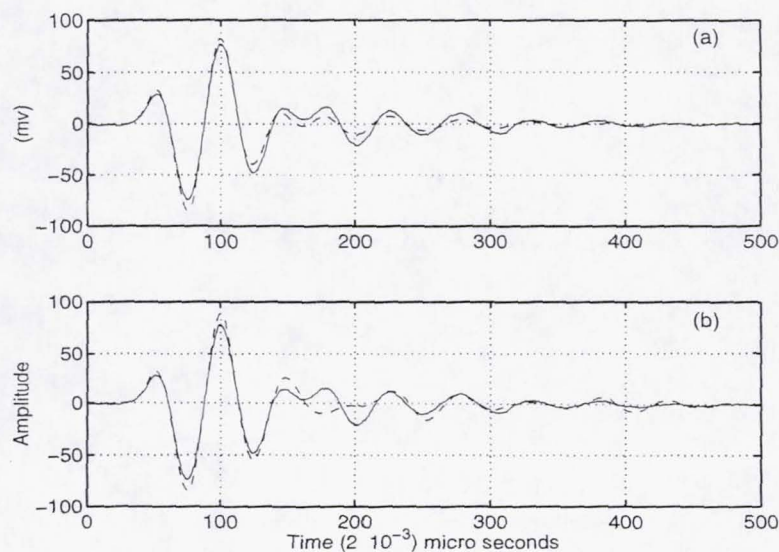
Figure 5.15: Comparisons of measured (solid lines) and simulated signals (dashed lines) for other two error minima. (a) r=0.84, $\alpha = 0.025$, transit time $51ns$. (b) r=0.7, $\alpha = 0.025$, transit time $153ns$

Thus, it is not difficult to obtain the optimized parameter set.

We used the obtained transit time to calculate the layer thickness by assuming uniform wave velocity in the thin adhesive layer. Very good results are obtained as verified by the optical microscopy measurement. The calculated results (h) and the optical measurement results (h_m) are listed in Table 5.1. The discrepancy of the measured results and the calculated results is within 3%.

Now, we will present the results for sample #2. For the very thin adhesive layer, a twice as large sampling frequency was used ($f_s = 1GHz$, the sampling interval 1 ns). In order to avoid experimental error, 5 acquisitions of the reference signal and the reflected signal were obtained at every point. The calculated results were obtained from the averaged signal of these 5 acquisitions.

The parameters obtained are listed in Table 5.3. Following the same procedure

Table 5.3: Optimized parameters and deduced quantities for specimen #2.

Location	r	α	transit time (ns)	$h(\mu m)$	$h_m(\mu m)$
#2 − a	0.769	0.0176	31	73.83	71.30
#2 − b	0.758	0.0050	23	54.74	52.60

described earlier, we can reconstruct the different arrivals and the simulated total signal. Figures 5.16 and 5.17 show the comparison of the reconstructed results for points a and b in the time domain. Figures 5.18 and 5.19 show the comparison of the measured and simulated frequency spectra. Once again, the match between the measured and calculated results both in the time domain and the frequency domain is exceptionally good. From the frequency spectrum, it is clearly seen that no single resonant frequency exists. The traditional method using resonance frequency to deduce adhesive bond parameters would be unable to produce results for this case.

We note from Table 5.3 that the transit times are quite different for these two positions. By assuming a uniform wave velocity, this means that the thicknesses at these two positions are different. The calculated thicknesses (h) using the obtained transit times are listed in Table 5.3. Figure 5.20 is the optical microscopy results for these two points. The standard ruler is $1/500$ in for each consecutive white/black separation. The measured results (h_m) from the microscopy observation are 71.30 and 52.60 μm for points a and point b respectively. The discrepancy is less than 5%.

As previously stated, reflection from an aluminum/air interface was selected as the incident pulse for the above calculation. While this was a very natural choice, there are cases where this choice is inconvenient or unavailable.

Figure 5.16: Reconstructed results for point a signal. Top: Comparison of the measured signal (solid) and the simulated signal (dashed), Bottom: the first three arrivals.
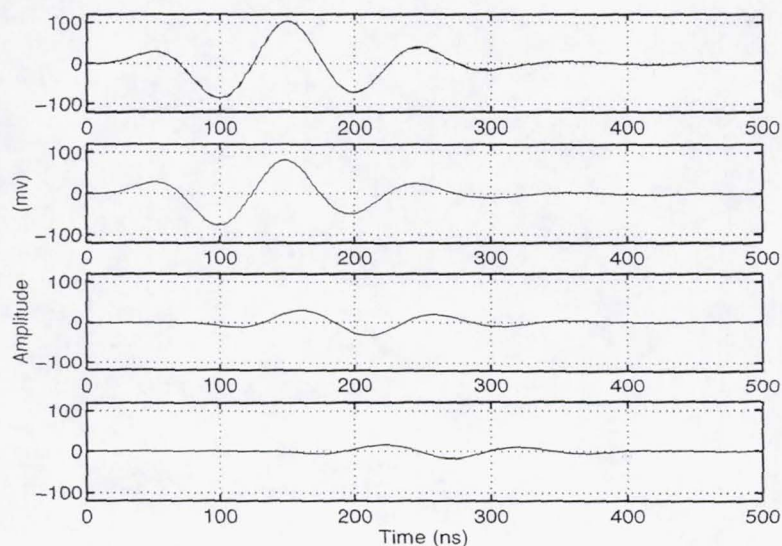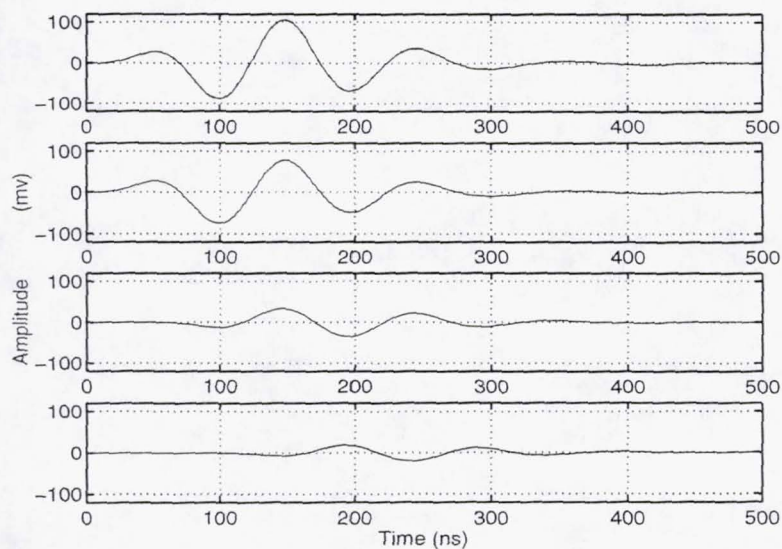

Figure 5.17: Reconstructed results for point b signal. Top: Comparison of the measured signal (solid) and the simulated signal (dashed), Bottom: the first three arrivals.
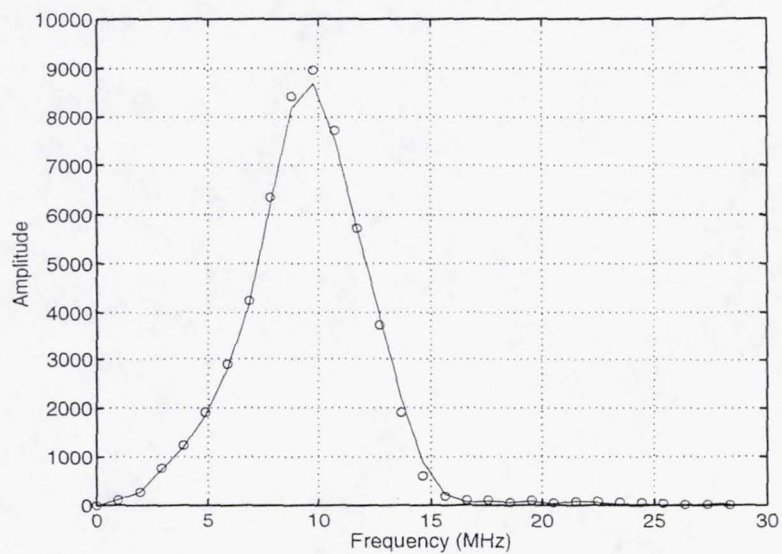
Figure 5.18: Frequency spectrum for point *a* signal. Solid: simulated, Circle: measured.
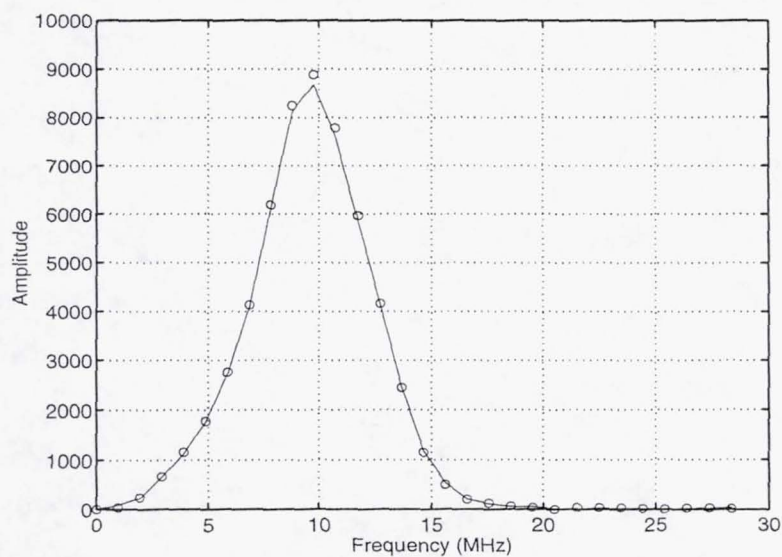
Figure 5.19: Frequency spectrum for point *b* signal. Solid: simulated, Circle: measured.
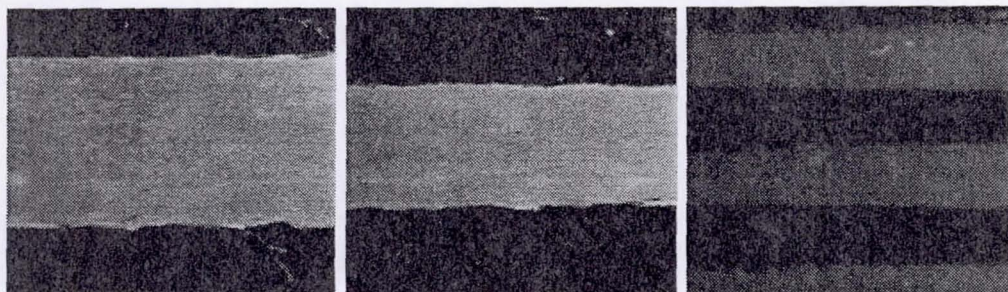
Figure 5.20: Optical microscopy photo of the cross sections of the thin adhesive layer at different positions and standard/reference scale.

For reasons of convenience or in the absence of the availability of the adherend/air interface signal to obtain the reference incident signal, a reasonable replacement for the reference signal would be the signal reflected from the couplant/top adherend interface. In this case, a phase shift close to π of the real incident signal should be used. As observed in experiments, these two signals are essentially of the same shape after the phase shift of π is taken into account. The only difference is the amplitude. A strongly dispersive or dissipative medium certainly distorts the shape of the pulse [63]. Here the adherend material is aluminum, which is not dispersive.

A slight effort is needed to acquire the useful parameters. Suppose the reflected signal from the couplant/top aluminum interface is $f_0(t)$, then the real incident signal can be obtained by multiplying a factor

$$f(t) = -\xi f_0(t) \tag{5.16}$$

where ξ is a constant factor, the negative sign takes care of the phase shift and guarantees a positive factor ξ. In the frequency domain, it follows that

$$F(\omega) = -\xi F_0(\omega) \tag{5.17}$$

Table 5.4: Optimized parameters and deduced quantities using couplant/top adherend reflected signal as reference signal.

Location	ξ	r	α	Transit time (ns)	$h(\mu m)$
$\#1-1$	0.340	0.708	0.0299	102	242.76
$\#1-2$	0.342	0.705	0.0306	92	218.96
$\#1-3$	0.348	0.700	0.0299	86	204.68
$\#2-a$	0.350	0.700	0.0249	31	73.83
$\#2-b$	0.349	0.699	0.0198	23	54.74

Then the error function can be reformulated as

$$\epsilon(\xi, r, \alpha, \Delta t) = \frac{1}{N}\sum_{i=1}^{N} |G(\omega_i) + \xi R(\omega_i, r, \alpha, \Delta t)F(\omega_i)| \tag{5.18}$$

It is not difficult to observe that the constant factor ξ is not coupled with r by looking at the first few terms of $\xi R(\omega, r, \alpha, \Delta t)$: ξr, $-\xi r(1-r^2)e^{-(i+\alpha)\omega\Delta t}$, $-\xi r^3(1-r^2)e^{-2(i+\alpha)\omega\Delta t}$. Thus, the solution of ξ should be unique. Experiments conducted using this alternative choice of the reference signal showed this approach to be correct. The obtained results are listed in Table 5.4.

First, let us take a look at the parameter ξ. For the five positions, the values of ξ are in the range of 0.340 to 0.349. They are very close to each other. ξ is approximately a constant. The reflection coefficients are even closer to each other, ranging from $0.699-0.708$. The attenuation coefficients are also close to the previous results using the reflection from aluminum/air interface as the reference signal. The most accurate results are for the transit time. The transit time is exactly the same as before. This once again supports our previous conclusion that the transit time measurements are very accurate.

5.4   Applications

5.4.1   Epoxy curing monitoring

A thorough investigation of ultrasonic wave velocity changes and the attenuation variations during the epoxy curing process can be found in [59]. From [59] it is seen that during the curing process, the epoxy resins undergo a tremendous change in moduli and consequently a tremendous change in ultrasonic parameters. However, those results were obtained from thick samples of epoxy and each consecutive arrivals from the epoxy could be clearly separated. The information obtained there relied on the amplitude and the arrival time of each separated arrival. For the thin layer case, it is impossible as shown earlier that the different arrival can be separated. It has been shown earlier that the method discussed in this chapter does not need the arrival times to be separated, even without the presence of a single resonant frequency. We can take advantage of our method for this thin adhesive layer curing monitoring case.

A DER732 and DER331 epoxy system in between aluminum adherends was used for the experiment. The curing agent is DEH26. The composition is 30% DER733, 70% DER331 and 12% in weight of curing agent. The epoxy was observed to be in a gel state between 1.5 to 2.5 hours. A reflected signal was recorded every half hour during the initial 5 hours and every hour thereafter. The fully curing time is 24 hours at room temperature. After 5.5 hours, no significant changes in ultrasonic signals were observed. After 5.5 hours only two measurements were taken. Both adherends are 6061 aluminum cylinders with diameters of 1.5 in. The thickness of the aluminum block is 1.00 in. A transducer with a nominal center frequency

of 10 MHz was used. The sampling interval was 2 ns. The reference signal was recorded after the the transducer was aligned and before the epoxy was poured into the uniform gap in between the two adherends. So the reference signal was the reflection from the aluminum/air interface.

The error minimization scheme yields directly the reflection coefficient r, the attenuation coefficient α and the transit time at different curing stages. It was observed that the maximum attenuation occurs at 1.5 hour (gel state). The optimized α at this stage is 0.034. Each measurement was converted to a normalized attenuation coefficient by dividing by the maximum value of α. Thickness variations resulting from cure shrinkage can be shown to be second-order effects [51]. By assuming that there is no change in the thickness, we can calculate the wave velocity for every measurement from the optimized transit time. The maximum velocity was achieved at the fully cured stage. The thickness of the adhesive layer was designed to be 60 μm. If this thickness is used to calculate the velocity, the final stage velocity was determined as $2609m/s$. This is close to the fully cured state velocity obtained using a bulk sample ($2650m/s$).

Figure 5.21 shows how the reflection coefficient, the normalized velocity and the normalized attenuation change with the curing time. The reflection coefficient is monotonically decreasing until the final stage. This is mainly because the acoustic impedance increases with the curing time. The velocity is monotonically increasing until it reaches the final stage value. The physical explanation is that the elastic moduli increase with increased curing time and approach the highest value at the fully cured stage. The results obtained here for a thin epoxy layer are consistent with previous work on thick specimens [50-51,53-54]. The interesting part is the
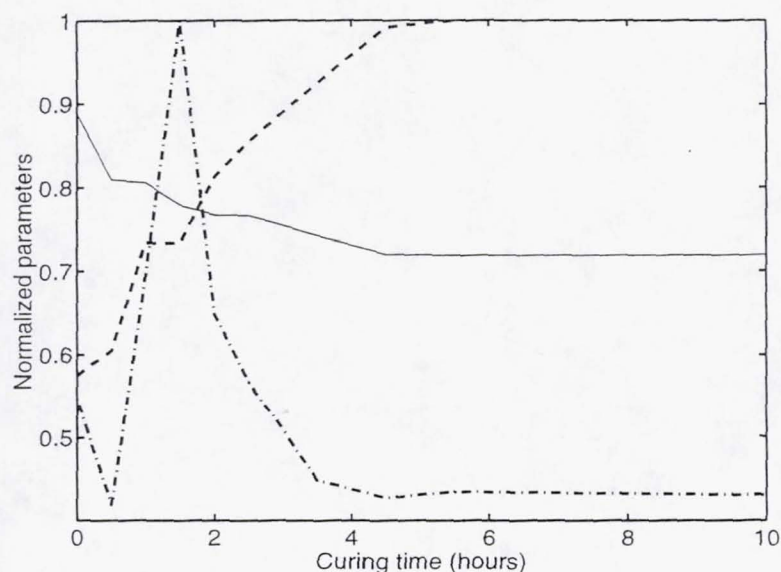
Figure 5.21: Reflection coefficient (solid line), normalized velocity (dashed line) and normalized attenuation coefficient (dash-dotted line) vs. curing time.

attenuation. It reaches its highest value at 1.5 hour (gel state). Similar results for the attenuation coefficient were reported in an experiment for thick epoxy specimens in Ref. [51].

The most interesting aspect of the results is that this information was derived from the ultrasonic data reflected from a very thin layer ($60\mu m$). The signal change from the very beginning (0 hour) to the fully cured state is quite small (see Figure 5.22). It is impossible to derive so much useful information from this rather small change if the present method would not be used.

5.4.2 Temperature-velocity coefficient measurement in adhesive bonds

In Chapter 4, we used temperature effects to evaluate the adhesive bond degradation. It was shown that the temperature-velocity coefficient (α_c) can be used as an
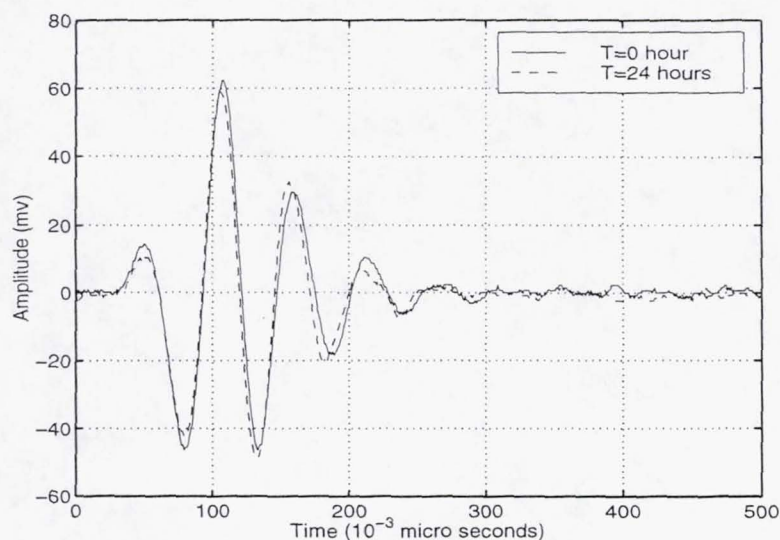
Figure 5.22: Comparison of signals reflected from an adhesive layer at the initial stage and the final stage of the curing process.

indication of degradation. The α_c was obtained from a quantitative analysis of the reflected signals from adhesive bonds at different temperatures.

At different temperature, a different waveform was obtained. By using the error minimization scheme, we can obtain the transit time in the adhesive layer at each temperature. The transit time allows us to obtain the velocity at each temperature and then the temperature-velocity coefficient can be obtained.

Figure 5.23 shows the comparison of the ultrasonic signals reflected from the non-deteriorated bond at 20^0C and 40^0C. Figure 5.24 shows the comparison of the signals reflected from an adhesive bond that has been subjected to 686K cycle three-point-bending fatigue. If we compare the signals from the deteriorated and the non-deteriorated adhesive bond at 20^0C, little difference is seen. However, the reflected signals from these two bonds at 40^0C have a observable difference. The difference at the negative peak of the main lobe can be seen. Following the procedures described
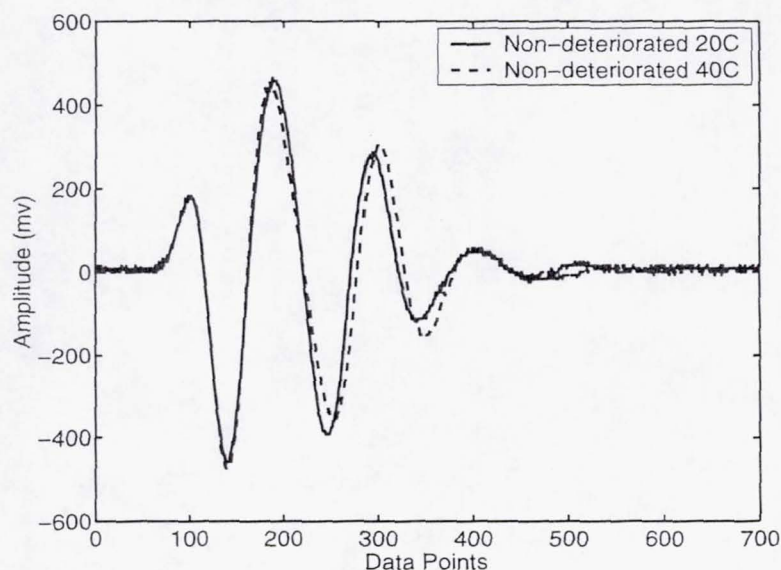
Figure 5.23: Waveform reflected from an adhesive bond that has not been subjected to fatigue.

above, we obtain the velocity versus the temperature for both bonds. The results are plotted in Figure 5.25. It is clearly seen that the velocity's temperature dependence is different for these two bonds. The α_c value is 0.0038 for the deteriorated bond compared to 0.0032 for the non-deteriorated bond. If we use the reflection coefficient r to plot the first arrival signals for these two bonds at 40^0C, a much clearer difference can be observed (Figure 5.26).

5.5   Discussion

It has been shown that the application of the error minimization scheme yields very accurate results for the transit time. In addition, the reflection coefficient and the attenuation coefficient can be derived simultaneously.

The most obvious advantage is that this method requires much lower frequencies
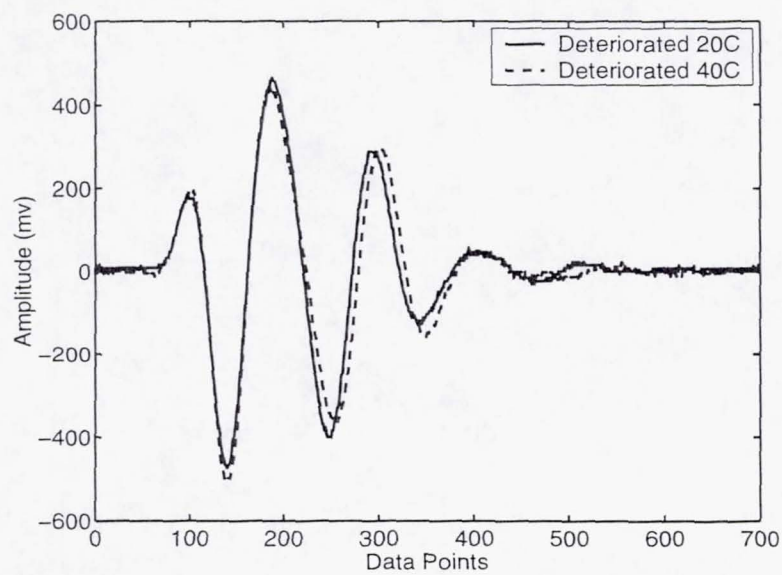
Figure 5.24: Waveform reflected from an adhesive bond that has been subjected to 686 K fatigue cycles.
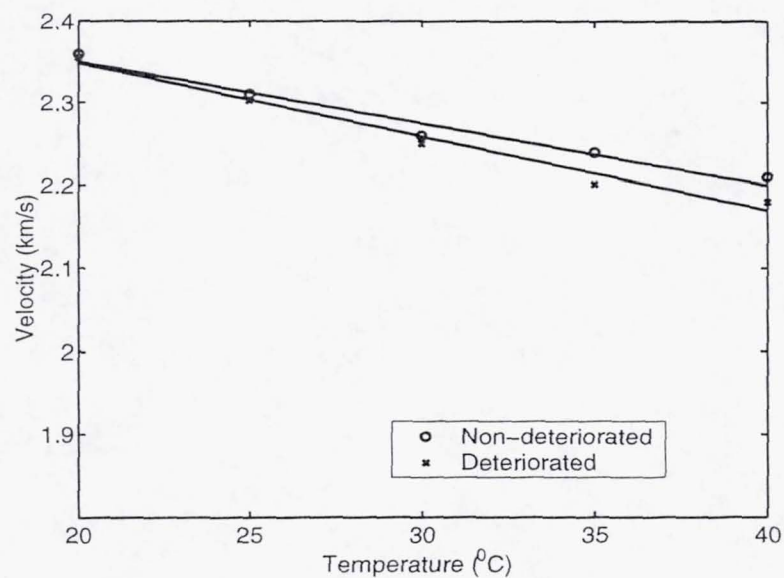
Figure 5.25: Velocity change versus temperature. Different α_c value.
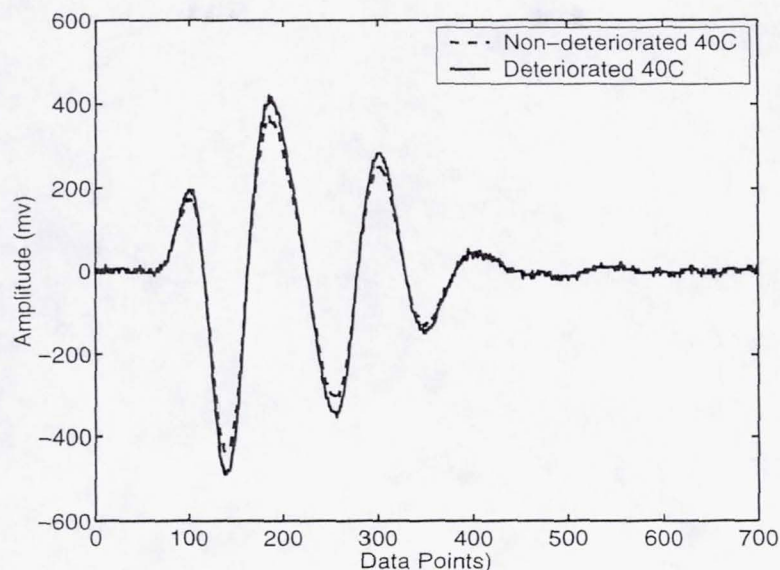
Figure 5.26: The first arrival comparison for a deteriorated bond and non-deteriorated bond.

than reported elsewhere, which simplifies the procedure, reduces cost and improves efficiency. For the results reported in Ref. [50], frequencies of $30\text{-}100MHz$ had to be used for the resolution of a 50-200 μm layer. The transducers used were specially designed short pulse transducers with a pulse rise and fall time of $0.7ns$. For our method, a commercially available $10MHz$ transducer is good enough to obtain the important parameters that can be related to adhesive bond properties. This method does not require the presence of a resonant frequency in the spectrum.

Because this method uses a reflected waveform, it has the advantage that only one side access to the specimen is needed. In case the transmitted waveform is required for analysis, a transmission function can be derived in the same fashion as the reflection coefficient.

This chapter only considered a special case, where the adherends are thick and both adherends are of the same materials. For cases where the adherend is thin

and multiple reflections from the adherend cannot be resolved, multiple reflections from the adherends have to be considered. In this case, the reflection function still can be derived in a more complicated form. For cases where the adherends are of different materials, two different reflection coefficients at the interface and two different transmission coefficients will enter the reflection function.

5.6 Conclusions

The method discussed in this chapter can accurately obtain the transit time in a thin adhesive layer. The reflection coefficient and the attenuation coefficient can be simultaneously obtained. This method provides a powerful tool to study the adhesive bond properties by obtaining ultrasonic parameters from reflected waveform data.

Chapter 6

Summary of Conclusions

In this work, ultrasonic techniques to detect adhesive bond degradation generated by cyclic fatigue loading have been explored. The experimental results show that the introduction of external factors (static loading or temperature changes) with simultaneous application of ultrasonic techniques is a productive and promising approach. As a result of the application of the appropriate external factors, ultrasonic measurements yield information on the onset of nonlinearity of an adhesive bond, and therefore on the onset of strength reduction due to adhesive bond degradation. Thus, the beginning of adhesive bond strength reduction due to degradation was detected using the ultrasonic techniques with the aid of external factors.

It was shown that a superimposed longitudinal wave can be used to detect the onset of the nonlinear behavior of an adhesive bond when it is subjected to tensile loading. By analyzing the reflected longitudinal wave signals at different load levels, the effective moduli of the adhesive layer can be obtained. The load, at which an observable change of the reflected signal is detected, is indicative of the nonlinearity,

123

and therefore of adhesive bond degradation. The results show that degradation due to cyclic loading fatigue can be detected by the reduction of the linear portion of the stress-strain curve in which the slope in the linear range remains unchanged.

It was shown theoretically that the effective shear moduli at different stress levels can be obtained from ultrasonic shear wave measurement data with the aid of external shear loading. Experiments verified that the initiation of nonlinear behavior under shear loading can be detected by a superimposed shear wave. It turned out, however, that the onset of nonlinear behavior under shear loading can also be detected by a longitudinal wave. Both detectable changes in reflected longitudinal wave and shear wave signals were observed at essentially the same shear load level for a given severity of degradation. Static shear loading and longitudinal wave detection provide a useful combination for the detection of the onset of nonlinear behavior of adhesive bonds.

A strain-temperature correspondence principle was also presented. A sequence of temperature changes with ultrasonic measurements in the linear range was shown to be a convenient and productive alternative to static loading. The temperature-velocity coefficient which quantifies the relation between the wave velocity and the temperature is a quantitative measure of nonlinearity and consequently a good indicator of adhesive bond degradation. A theoretical investigation suggests that for this case the application of shear waves may be more productive than the application of longitudinal waves. A C-Scan at an elevated temperature was also used to reveal more information on adhesive bond degradation.

Finally, a technique to obtain the ultrasonic parameters from reflected waveform data has proven to be a useful tool to study the onset of nonlinear adhesive bond

properties.

Bibliography

[1] C. V. Cagle. *Adhesive Bonding: Techniques and Applications*. McGraw-Hill, New York, 1968.

[2] J. L. Cotter and M. G. D. Hocky. Metal joining with adhesives. *International Metallurgical Reviews*, 19:19, 1974.

[3] E. M. Petri. Plastics and elastomers as adhesives. *Handbook of Plastics and Elastomers*, 1975.

[4] MIL-HDBK-691B. *Military Standardization Handbook: Adhesive Bonding*. 1987.

[5] R.B. Thompson and D.O. Thompson. Past experiences in the development of tests for adhesive bond strength. *Journal of adhesion science and technology*, 5(8):583–599, 1991.

[6] *Metals Handbook, Ninth Edition, Volume 17: Nondestructive Evaluation and Quality Control*. ASM International, 1989.

[7] *Nondestructive Testing Handbook, 2nd Edition, Volume Seven: Ultrasonic Testing*.

[8] G.M. Light and H. Kwun. *Nondestructive Evaluation of Adhesive Bond Quality*. Nondestructive Testing Information Center, Southwest Research Institute, San Antonio, TX, 1989.

[9] P. A. Meyer and J. L. Rose. Ultrasonic determination of bond strength due to surface preparations in aluminum to aluminum adhesive bond systems. *J. Adhes.*, 8:145–153, 1976.

[10] J. L. Rose, M. J. Avioli, and R. Bilgram. A feasibility study on the nde of an adhesively bonded metal to metal bond: An ultrasonic pulse echo approach. *Brit. J. Nondestr. Test*, pages 67–71, 1983.

[11] G.A. Alers, P.L. Flynn, and M.J. Buckley. Ultrasonic techniques for measuring the strength of adhesive bonds. *Materials Evaluation*, 3/4:77–84, 1977.

[12] F.H. Chang, P.L. Flynn, D.E. Gordon, and J.R. Bell. Principles and applications of ultrasonic spectroscopy in nde of adhesive bonds. *IEEE Trans. Sonics Ultrason*, SU-23:334–338, 1976.

[13] J. W. Raisch and J. L. Rose. Computer controlled ultrasonic adhesive bond evaluation. *Materials Evaluation*, 37(6):55–64, 1979.

[14] F. H. Chang, J. C. Couchman, J. R. Bell, and D. E. Gordan. Correlation of nde parameters with adhesive bond strength in multi-layered structures. 1975.

[15] G. A. Alers and R. K. Elsley. Measurement of metal to adhesive bond quality using digital signal analysis. 1977.

[16] G. H. Thomas and J. L. Rose. An ultrasonic evaluation and quality control tool for adhesive bonds. *J. Adhes.*, 10:293–316, 1974.

[17] A. I. Lavrentyev and S. I. Rokhlin. Ultrasonic study of environmental damage initiation and evolution in adhesive joints. *Res Nondestr Eval*, 10(1):17–41, 1998.

[18] D. O. Thompson, R. B. Thompson, and G. A. Alers. Nondestructive measurement of adhesive bond strength in honeycomb panels. *Mater. Eval.*, 32(4):81–85, 1974.

[19] S. I. Rokhlin, M. Hefets, and M Rosen. An ultrasonic interface wave method for predicting the strength of adhesive bonds. *J. Appl. Phys.*, 52(4):2847–2851, 1981.

[20] S. I. Rokhlin, M. Hefets, and M Rosen. An elastic interface wave guided by a thin film between two solids. *J. Appl. Phys.*, 51(7):3579–3582, 1980.

[21] A. Pilarski. Ultrasonic evaluation of the adhesion degree in layered joints. *Mater. Eval.*, 43:765–770, 1985.

[22] S. I. Rokhlin. Diffraction of lamb waves by a finite crack in an elastic layer. *J. Acoust. Soc. Am.*, 67(4):1157–1165, 1980.

[23] A. K. Mal, P. C. Xu, and Y. Bar-Cohen. Analysis of leaky-lamb waves in bonded plates. *Inter. J. Engin. Sci.*, 27(7):770–791, 1989.

[24] P. C. Xu, A. K. Mal, and Y. Bar-Cohen. Inversion of leaky lamb wave data to determine cohesive properties of bonds. *Inter. J. Engin. Sci.*, 28(4):331–346, 1990.

[25] Y. Bar-Cohen and A. K. Mal. Characterization of adhesive bonding using leaky lamb waves. *Rev. Prog. QNDE*, 9B:1271–1277, 1990.

[26] D. Rois, L. A. Bergman, and J. H. Bucksbee. Adhesive bond quality assurance using the acousto-ultrasonic technique. *Brit. J. Nondest. Test*, pages 375–358, 1986.

[27] C. H. Yew. Using ultrasonic sh waves to estimate the quality of adhesive bonds: A preliminary study. *J. Acoust. Soc. Am.*, 76(2):525–531, 1984.

[28] S. I. Rokhlin and D. Marom. Study of adhesive bonds using low frequency obliquely incident ultrasonic waves. *J. Acoust. Soc. Am.*, 80(2):585–590, 1986.

[29] A. Pilarski and J. L. Rose. A transverse-wave ultrasonic oblique-incidence technique for interfacial weakness detection in adhesive bonds. *J. Appl. Phys.*, 63(2):300–307, 1988.

[30] L. Singher. Bond strength measurement by ultrasonic guided waves. *Ultrasonics*, 35(4):305–315, 1997.

[31] J. N. Barshinger J. L. Rose. Development of guided waves for adhesive bond inspection. *Int. SAMPE Symp Exhib (Proceedings)*, 41(1):615–624, 1996.

[32] J.D. Achenbach and O.K. Parikh. Ultrasonic analysis of nonlinear responses and strength of adhesive bonds. *Journal of Adhesion Science and Technology*, 5(8):601–618, 1991.

[33] O.K. Parikh and J. D. Achenbach. Analysis of nonlinearly viscoelastic behavior of adhesive bonds. *Journal of Nondestructive Evaluation*, 13(3/4):221–226, 1992.

[34] J.M. Baik and R.B. Thompson. *Journal of Nondestructive Evaluation*, 4:177–196, 1984.

[35] P. McGowan and L. Adler. ultrasonic assessment of adhesive joint degradation using stress induced non-linearity. *Review of progress in Quantitative Nondestructive Evaluation*, 13:1547–1554, 1994.

[36] D. Jiao and J. L. Rose. An ultrasonic interface layer model for bond evaluation. *Journal of adhesion science and technology*, 5(8):631–646, 1991.

[37] T. Chernobelskaya, S. Kovnovich, and E.Harnik. The testing of adhesive-bonded joints by a very high resolution ultrasonic probe. *Journal of Physics D: Applied Physics*, 12, 1979.

[38] N.J. DeLollis. *Adhesives for Metals Theory and Technology*. Industrial Press Inc., 1970.

[39] *http : //www.ndt.net/wshop/forum/forum.htm*. NDT.net Discussion Forum. 1999.

[40] F. W. Billmeyer Jr. *Textbook of Polymer Science*. New York, Interscience Publishers, 1962.

[41] P. McGowan P. B. Nagy and L. Adler. Acoustic nonlinearities in adhesive joints. *Review of Progress in Quantitative Nondestructive Evaluation*, 9B:1685–1692, 1990.

[42] J. D. Achenbach. *Wave Propagation in Elastic Solids*. North Holland, 1973.

[43] Z. Sun and H. Ying. A multi-gate time of flight technique for estimation of temperature distribution in heated tissue: theory and computer simulation. *Ultrasonics*, 37:107–122, 1999.

[44] F. A. Duck. *Physical Properties of Tissue-A Comprehensive Reference Book*. Academic Press, New York, 1990.

[45] ASTM Standard Designation D638-89. Standard Test Methods for Tensile Properties of Plastics. 1989.

[46] I. M. Daniel and O. Ishai. *Engineering Mechanics of Composite Materials*. New York, Oxford, 1994.

[47] L. Yang and A. Fatemi. Cumulative fatigue damage and quantifying parameters: a literature review. *Journal of Testing and Evaluation*, 26(2):89–100, 1998.

[48] G. Sharon, H. Dodiuk, and S. Kenig. Hygrothermal properties of epoxy film adhesives. *J. Adhesion*, 30:87–104, 1989.

[49] J. Krautkramer and H. Krautkramer. *Ultrasonic Testing of Materials, 4th ed.* Springer-Verlag, 1990.

[50] R.E. Challis, T Alper, A.K. Homes R.P. Cocker, and J.D.H. White. Ultrasonic absorption ans velocity dispersion measurements in thin adhesive layer. *Ultrasonics*, 29:22–28, 1991.

[51] Albert M. Lindrose. Ultrasonic wave and moduli changes in a curing epoxy resin. *Experimental Mechanics*, 18:227–232, 1978.

[52] B. Mitra and D.J. Booth. Remote cure monitoring of epoxy materials using optical techniques. *Ultrasonics*, 34:569–572, 1998.

[53] H.T. Hahn. Application of ultrasonic technique to cure characterization of epoxies. *Nondestructive Methods for Material Property Determination, Plenum Press, New York by C.O. Rudd and R.E. Green*, 1984.